Evaluation of polycyclic amines as modulators of calcium homeostasis in models of neurodegeneration

Lois-May Young, B.Pharm., M.Sc.

Dissertation submitted in partial fulfillment of the requirements for the degree *Doctor of Philosophy* in Pharmaceutical Chemistry at the North West University Potchefstroom Campus

Supervisor: Prof. C.J. van der Schyf
Co-supervisor: Prof. S.F. Malan
Co-supervisor: Dr. W.J. Geldenhuys

2012

Potchefstroom

CONTENTS

ABSTRACT

Compromised calcium homeostasis in the central nervous system (CNS) is implicated as a major contributor in the pathology of neurodegeneration. Dysregulation of Ca^{2+} homeostasis initiates downstream Ca^{2+}-dependent events that lead to apoptotic and/or necrotic cell death. Increases in the intracellular free calcium concentration ($[Ca^{2+}]_i$) may be the result of Ca^{2+} influx from the extracellular environment or Ca^{2+} release from intracellular Ca^{2+} stores such as the endoplasmic reticulum (ER). Influx from the extracellular environment is controlled predominantly by voltage gated calcium channels (VGCC), such as L-type calcium channels (LTCC) and ionotropic glutamate receptors, such as the N-methyl-D-aspartate (NMDA) receptors. Ca^{2+} release from the ER occurs through the inositol-1,4,5-triphosphate receptors (IP_3Rs) or ryanodine receptors (RyRs) *via* IP_3-induced or Ca^{2+}-induced mechanisms. Mitigation of Ca^{2+} overload through these Ca^{2+} channels offers an opportunity for pharmacological interventions that may protect against neuronal death.

In the present study the ability of a novel series of polycyclic compounds, both the pentacycloundecylamines and triquinylamines, to regulate calcium influx through LTCC was evaluated in PC12 cells using calcium imaging with Fura-2/AM in a fluorescence microplate reader. We were also able for the first time to determine IC_{50} values for these compounds as LTCC blockers. In addition, selected compounds were evaluated for their ability to offer protection in apoptosis-identifying assays such as the lactate dehydrogenase release assay (LDH-assay), trypan blue staining assay and immunohistochemistry utilizing the Annexin V-FITC stain for apoptosis. We were also able to obtain single crystal structures for the tricyclo[6.3.0.$0^{2,6}$]undecane-4,9-dien-3,11-dione (**9**) and tricyclo[6.3.0.$0^{2,6}$]undecane-3,11-dione (**10**) scaffolds as well as a derivative, *N*-(3-methoxybenzyl)-3,11-azatricyclo[6.3.0.$0^{2,6}$]undecane (**14f**). We also evaluated the possibility that the polycyclic compounds might be able to modulate Ca^{2+} flux through intracellular Ca^{2+} channels.

Computational methods were utilized to accurately predicted IC_{50} values and develop a QSAR model with marginal error. The linear regression model delivered $r^2 = 0.83$, which indicated a favorable correlation between the predicted and experimental IC_{50} values. This model could thus serve as valuable predictor for future structural design and optimization efforts. Data obtained from the crystallographic analysis confirmed the NMR-data based structural assignments done for these compounds in previous studies. Obtaining structural information gave valuable insight into the differences in size and geometric constrains, which are key features for the LTCC activity of these compounds.

In conclusion, we found that all of the compounds evaluated were able to attenuate Ca^{2+} influx through the LTCC, with some compounds having IC_{50} values comparable with known LTCC blockers such as nimodipine. Representative compounds were evaluated for their ability to afford protection against apoptosis induced by 200 μM H_2O_2. With the exception of compound **14c** (the most potent LTCC blocker in the series, $IC_{50} = 0.398$ μM), most compounds were able to afford protection at two or more concentrations evaluated. Compound **14c** displayed inherent toxicity at the highest concentrations evaluated (100 μM). We concluded that compounds representing both types of structures (pentacycloudecylamines and triquinylamines) have the ability to attenuate excessive Ca^{2+} influx through the LTCC. In general the aza-pentacycloundecylamines (**8a-c**) were the most potent LTCC blocker which also had the ability to offer protection in the cell viability assays. However, NGP1-01 (**7a**) had the most favorable pharmacological profile overall with good activity as an LTCC blocker ($IC_{50} = 86$ μM) and the ability to significantly attenuate cell death in the cell viability assays, exhibiting no toxicity. In addition to their ability to modulate Ca^{2+} influx from the extracellular environment, these compounds also displayed the ability to modulate Ca^{2+} flux through intracellular Ca^{2+} channels. The mechanisms by which they act on intracellular Ca^{2+} channels still remains unclear, but from this preliminary study it would appear that these compounds are able to partially inhibiting Ca^{2+}-ATPase activity whilst possibly simultaneously inhibiting the IP_3R. In the absence of extracellular Ca^{2+} these compounds showed the ability in inhibit voltage-induced Ca^{2+} release (VICaR), possibly by modulating the gating charge of the voltage sensor being the dihydropyridine receptors.

In future studies it might be worthwhile to do an expanded QSAR study and evaluate the aza-pentacycloundecylamines. To clarify the mechanisms by which the polycyclic compounds interact with intracellular Ca^{2+} channels we should examine the direct interaction with the individual Ca^{2+} channels independently. The polycyclic compounds evaluated in this study demonstrate potential as multifunctional drugs due to their ability to broadly regulate calcium homeostasis through multiple pathways of Ca^{2+} entry. This may prove to be more effective in diseases where perturbed Ca^{2+} homeostasis have devastating effects eventually leading to excitotoxicity and cell death.

Keywords: Neurodegeneration, voltage gated calcium channels (VGCC), L-type calcium channel (LTCC) blockers, multifunctional drugs, polycylic compounds, pentacycloundecylamines, triquinylamines.

UITTREKSEL

Gekompromiteerde kalsium homeostase in die sentrale senuweestelsel (SSS) is een van die hoof faktore in die patologie van neurodegenerasie. Wanregulering van Ca^{2+} homeostase inisieer Ca^{2+}-afhanklike prosesse wat lei tot apoptotiese en/of nekrotiese seldood. ‘n Verhoging in die intrasellulêre vrye kalsium konsentrasie ($[Ca^{2+}]_i$) is die gevolg van Ca^{2+} influks vanaf die ekstrasellulêre omgewing of Ca^{2+} vrystelling vanuit intrasellulêre Ca^{2+} store soos die endoplasmiese retikulum (ER). Ekstrasellulêre Ca^{2+} influks word hoofsaaklik beheer deur spanningsafhanklike kalsiumkanale soos die L-tipe kalsiumkanale en die ionotropiese glutamaatreseptore soos die *N*-metiel-D-aspartaat reseptorkanale (NMDA-kanale). Ca^{2+} word vrygestel vanuit die ER deur inositol-1,4,5-trifosfaat reseptore (IP_3Rs) of rianodien reseptore (RyRs) deur middel van IP_3- of Ca^{2+}-geïnisieerde meganismes. Moderering van die Ca^{2+} oorlading deur hierdie Ca^{2+} kanale bied geleenthede vir farmakologiese intervensie wat beskerming kan bied teen neuronale seldood.

In die huidige studie het ons die vermoë van hierdie unieke reeks polisikliese verbindings, pentasiklo-undekielamiene en trikwinielamiene, om kalsium influks te reguleer deur die L-tipe spanningsafhanklike kalsiumkanale geëvalueer. PC12 selle is gebruik en kalsium fluks is gemeet deur fluoressensiemeting van geaktiveerde Fura-2/AM in ’n mikroplaatleser. Ons het ook daarin geslaag om vir die eerste keer IC_{50}-waardes van hierdie verbindings te bepaal as L-tipe kalsiumkanaal blokkers. Addisioneel, het ons verskeie verbindings geëvalueer vir hul vermoë om beskerming te bied teen apoptosemeganismes insluitende die vrystelling van laktaat dehidrogenase (LDH-studie), verkleuring van Trypan-blou, en in ’n immunohistochemie-studie waarin Annexin V-FITC verkleuring ’n positiewe aanduiding van apoptose is. Ons was ook daartoe in staat om ’n enkelkristal X-straalstruktuurbepaling te doen vir twee trikwinaan-moederverbindings: trisiklo[6.3.0.$0^{2,6}$]undekaan-4,9-dieen-3,11-dioon (**9**) en trisiklo[6.3.0.$0^{2,6}$]undekaan-3,11-dioon (**10**) asook ’n derivaat, *N*-(3-metoksiebensiel)-3,11-asatrisiklo[6.3.0.$0^{2,6}$]undekaan (**14f**). In hierdie studie het ons ook die moontlikheid

ondersoek dat die polisikliese verbindings die vermoë besit om Ca^{2+} fluks deur intrasellulêre kalsiumkanale te reguleer.

Rekenaarmodellering is gebruik ter ontwikkeling van kwantitatiewe struktuur-aktiwiteitsverwantskapsmodelle om die IC_{50}-waardes vir verbindings as L-tipe kalsiumkanaal blokkers te voorspel. Die ontwikkelde lineêre regressiemodel het akkurate voorspellings gelewer van die IC_{50}-waardes (r^2 = 0.83) vergeleke met eksperimenteel-bepaalde IC_{50}-waardes. Hierdie model kan dus dien as ’n waardevolle hulp in die voorspelling van aktiwiteit in toekomstige ontwikkeling en optimalisering van nuwe reekse verbindings. X-straal kristallografiese analise het ons daartoe in staat gestel om die KMR-struktuurbepalings wat in vorige studies gedoen is, te verifieer. Die inligting verkry van die struktuuranalises het waardevolle insig gebied rakende die grootte en geometriese oorwegings van die verbindings wat van belang is vir aktiwiteit as L-tipe kalsiumkanaalblokkers.

Ten slotte het ons gevind dat al die verbindings wat geëvalueer is in hierdie studie, daartoe in staat was om Ca^{2+} influks deur die L-tipe kalsiumkanale te verminder, met IC_{50}-waardes by sekere verbindings wat vergelykbaar is met dié van bekende L-tipe kalsiumkanalblokkers soos nimodipien. Verteenwoordigende verbindings is geëvalueer vir hul vermoë om beskerming te bied in sel-lewensvatbaarheidstudies wat aanduidend is vir apoptose geïnduseer deur 200 μM H_2O_2. Met die uitsondering van verbinding **14c** (die mees potente L-tipe kalsiumkanaalblokker in die reeks, IC_{50} = 0.398 μM), was die meeste verbindings daartoe in staat om beskerming te bied. Verbinding **14c** het inherente seltoksisiteit getoon by die hoogste konsentrasie geëvalueer (100 μM). Ons kon die afleiding maak dat verbindings verteenwoordingend van beide moederstrukture (pentasiklo-undekielamiene en die trikwinielamiene) daartoe instaat was om oormatige Ca^{2+} influks deur die L-tipe kalsiumkanale te verminder. Oor die algemeen was die asa-pentasiklo-undekielamiene (**8a-c**) die mees potente L-tipe kalsiumkanaalblokkers wat ook die vermoë getoon het om beskerming te bied in sel-lewensvatbaarheidstudies. NGP1-01 (**7a**) het die mees gunstige farmakologiese profiel getoon met goeie L-tipe kalsiumkanaalblokkeringsaktiwiteit (IC_{50} = 86 μM), asook die vermoë om sel lewensvatbaarheid aansienlik te verhoog. Hierdie verbinding het ook geen inherente

seltoksisiteit getoon nie. Addisioneel tot hul vermoë om Ca^{2+}-fluks vanaf die ekstrasellulêre omgewing te reguleer, toon die verdindings ook die vermoë om Ca^{2+}-fluks deur intrasellulêre kalsiumkanale te reguleer. Die meganisme waardeur die verbindings op intrasellulêre kalsiumkanale inwerk is steeds nie seker nie, maar vanuit hierdie voorlopige studie wil dit blyk dat die verbindings daartoe in staat is om Ca^{2+}-ATPase aktiwiteit gedeeltelik te inhibeer terwyl hulle ook moontlik daartoe in staat is om die IP_3R gelyktydig te inhibeer. In die afwesigheid van ekstrasellulêre Ca^{2+}, toon hierdie verbindings die vermoë om aksiepotensiaal-geïnduseerde Ca^{2+} vrystelling te inhibeer. Dit geskied moontlik deur modulering van die polarisasiesensor, in hierdie geval die sensor van die dihidropiridienreseptor.

In toekomstige studies mag dit van waarde wees om die asa-pentasiklo-undekielamiene te evalueer in ’n uitgebreide kwantitatiewe struktuur-aktiwiteits verwantskaps studie. Die voortgesette evaluering van die meganismes waardeur die polisikliese verbindings interaksies uitoefen op die intrasellulêre kalsiumkanale is ook van belang in toekomstige studies. ‘n Moontlike benadering sou wees om direkte interaksie met die verskillende kanale betrokke, in afsonder te ondersoek. Die polisikliese verbindings geëvalueer in hierdie studie toon potensiaal as multi-funksionele verbindings gebaseer op hul vermoë om op ‘n breë basis Ca^{2+}-homeostase te reguleer deur verskeie aanknopingspunte van Ca^{2+}-fluks. Hierdie benadering mag meer effektief wees in die behandeling van toestande waar wanregulering van Ca^{2+}-homeostase verwoestende gevolge het en uiteindelik lei tot eksitotoksisiteit en seldood.

Sleutelwoorde: Neurodegenerasie, spanningsafhanklike kalsiumkanale, L-tipe spanningsafhanklike kalsiumkanale blokkers, multi-funksionele verbindings, polisikliese verbindings, pentasiklo-undekielamiene, trikwinielamiene.

CHAPTER 1

INTRODUCTION

1.1 The role of calcium in neurodegenerative disease

Perturbation of calcium (Ca^{2+}) homeostasis and subsequent Ca^{2+} overload have been implicated in conditions such as physiological ageing,[1] as well as acute neurological disorders such as ischemia, trauma and epilepsy; and chronic neurological disorders such as Alzheimer's disease, Parkinson's disease and Huntington's disease.[2-5] For these conditions one common key mediator in neuronal death is Ca^{2+}. Although physiological elevation of in intracellular Ca^{2+} is part of normal cell function and homeostatic mechanisms exist to maintain the intracellular Ca^{2+} concentration ($[Ca^{2+}]_i$), excessive Ca^{2+} influx of together with Ca^{2+} release from intracellular compartments can overwhelm Ca^{2+}-regulatory mechanisms and lead to cell death.[6] Cell death caused by Ca^{2+} overload is referred to as excitotoxicity, and the excessive elevation of $[Ca^{2+}]_i$ leads to the over activation of proteases, lipases, phosphatases, and endonucleases that can either damage the structural integrity of the cell membrane or induce oxidative stress.[5, 7]

Neurons possess specialized homeostatic mechanisms to control $[Ca^{2+}]_i$ by regulating Ca^{2+} influx, Ca^{2+} efflux, Ca^{2+} buffering, and internal Ca^{2+} storage. These regulatory mechanisms will be discussed in further detail in chapter 2. Apart from the *N*-methyl-D-aspartate (NMDA) receptor, α-amino-3-hydroxy-5-methylisoxazole-4-propionic (AMPA) receptor, and kainate receptor subtypes; voltage-gated Ca^{2+} channels (VGCCs), such as the L, N, T and P/Q-type Ca^{2+} channels have also been implicated as a major gateway for Ca^{2+} entry from the extracellular environment.[4, 8] During traumatic brain injury, it has been shown that anoxic depolarization has a biphasic effect: first, pre-synaptic Ca^{2+} entry triggering the release of glutamate (a major excitatory neurotransmitter); and second, depolarization in the post-synaptic neuron will cause opening of the VGCC with subsequent influx of Ca^{2+}, whilst also acting as

a trigger to remove the Mg^{2+} block of the NMDA receptor (NMDAR).[9] Activation of the NMDAR leads to alterations in the concentration of intracellular ions, especially those of Ca^{2+} and Na^{+}. The additional influx of Na^{+} causes osmotic swelling and damage to cells. Choi and colleagues suggested that glutamate toxicity is primarily dependent on Ca^{2+} influx and because of its large Ca^{2+} conductance, the NMDAR has been a focus point of many research initiatives concerning excitotoxicity and neurodegenerative diseases.[10-12] Studies with NMDAR antagonist, such as MK-801 have shown that blocking Ca^{2+} entry through this receptor could be neuroprotective,[13, 14] however most of these drugs have failed clinical trails due to side effects associated with blocking the normal function of glutamate mediated processes and $[Ca^{2+}]_i$ depletion.[15] This problem has been overcome with a drug such as memantine which acts as an uncompetitive, low-affinity open-channel blocker of the NMDAR.[15, 16] Memantine is well-tolerated due to its fast on-off binding kinetics and uncompetitive antagonism which means that it only blocks Ca^{2+} influx when the channel is in the open state, regulating excessive Ca^{2+} influx and not resulting in $[Ca^{2+}]_i$ depletion. Memantine has a polycyclic structure and is currently the only drug, under the trade name Namenda®, clinically used to treat Alzheimer's disease.[17, 18] Another approach in the treatment of neurodegenerative diseases would be to block Ca^{2+} influx through the L-type Ca^{2+} channels (LTCCs). VGCCs have been reported to exist in the central nervous system (CNS),[19] and could thus contribute to excitotoxicity. The ability of known LTCC blockers such as the 1,4-dihydropyridines (DPH) nimodipine and nitrendipine, the phenylalkylamine (PAA) verapamil and the benzothiazepine (BTZ) diltiazem to attenuate excitotoxicity caused by an increase in $[Ca^{2+}]_i$ has been well established.[20-22] Nimodipine has also been shown to be protective in models of acute neurological disorders such as ischemia.[23-25] Nimodipine is highly lipophilic and will cross the blood-brain barrier, which allows this drug to be used in the treatment of neurodegenerative diseases. However, nimodipine can only be used in acute neurological disorders such as ischemia due to its cardiological effects that can lead to hypotension.[20, 26]

There are a few studies in literature that reported a complementary and/or synergistic neuroprotective effect in animal models of cerebral ischemia when VGCC blockers and NMDAR antagonists are used in combination.[27-31] Considering that LTCC

blockers such as nimodipine are of limited value in a clinical setting and that high-affinity NMDAR channel blockers such as MK-801 induce psychotomimetic and neurotoxic effects;[20, 32] it might be of greater value to have a low-affinity multimechanistic drug with the ability to modulate Ca^{2+} influx through both ion channel types. Only in recent years has the concept that a single molecule with multiple mechanisms of action, that could be used to address multiple diseases targets in the same pathology, gained impetus in drug discovery.[33-35] These drugs are called multifunctional or multimechanistic drugs and holds an advantage in cases such as ischemic stroke where a combination of therapies have been shown to be beneficial.[36] Such an approach retains the beneficial therapeutic effect of combining multiple drugs, while simultaneously limiting the side-effect profile to that of only one drug.[37]

Our interest in neuroprotective agents with multiple mechanisms of actions was prompted with the discovery that 8-benzylamino-8,11-oxapentacyclo-[5.4.0.$0^{2,6}$.$0^{3,10}$.$0^{5,9}$]undecane (NGP1-01), a member of the family of pentacycloundecylamines initially characterized as an LTCC blocker,[38-41] also had activity as a potent uncompetitive NMDAR antagonist.[42, 43] The clinical success of memantine, which also has a polycyclic structure, gave impetus to further the search for other polycyclic compounds with the ability to act as multimechanistic neuroprotective drugs.[34] Several studies investigated the ability of the pentacycloundecylamines and triquinylamines (both have polycyclic structures) to modulate Ca^{2+} influx through either the NMDA receptor or the LTCC.[39-43] These studies revealed that most of these polycyclic compounds have the ability to modulate Ca^{2+} entry though both the NMDA receptor and the LTCC and established NGP1-01 (**7a**) as the lead compound. It is this dual-mechanistic action that gives these compounds a unique advantage in the treatment of neurodegenerative disorders over compounds such as nimodipine, which only has the ability to block the LTCC. The benefit of a multimechanistic approach has been demonstrated in cases such as ischemic stroke where a combination of therapies have been shown to be beneficial as shown with the combination of memantine and clenbuterol.[36] NGP1-01 has also been proven to be neuroprotective *in vivo* using the middle cerebral artery occlusion mouse model of stroke,[44] and also offer protection in a transient model of stroke following reperfusion.[45] NGP1-01 (**7a**) was included in the oxa-pentacycloundecane series

evaluated in this study to offer the opportunity for direct correlation with the other polycyclic compounds that would allow us to draw conclusions as to their functional role as LTCC blockers and possible neuroprotective drugs.

Although much is known about pentacycloundecylamines such as **7a**,[42] the IC_{50} values for LTCC blocking activity has not yet been determined for a series of derivatives. This study was designed to evaluate several polycyclic compounds as LTCC blockers by their ability to attenuate rises in $[Ca^{2+}]_i$ and for the first time calculate their IC_{50} values. We will also explore several *in vitro* methods (biochemical assays) to asses the ability of these compounds to offer protection against induced cell death which in the future might serve as valuable tools in screening possible drug candidates before proceeding to more complex *in vivo* studies.

1.2 Hypothesis

Based on our prior knowledge of polycyclic compounds – in particular pentacycloundecylamine compounds – their mechanism(s) of action, and the role of calcium overload in the neurodegenerative process, we will test the following hypothesis in the current research project:

Pentacycloundecylamine and related compounds exhibit a structure-activity relationship that will enable us to synthesize new derivatives that will direct calcium-blocking activity to both intra- and extracellular conduits of calcium transport, thereby mitigating degenerative cascades in appropriate in vitro models.

In order to test our hypothesis, we have set out to explore the following Aims and Objectives:

1.3 Aims and objectives

1. As part of the ongoing investigation into the pharmacological activity of the polycyclic amines we wanted to determine the IC_{50} values for a series of pentacycloundecylamines and triquinylamines as LTCC blockers. For this purpose we developed a high throughput fluorescence Ca^{2+} flux assay in rat undifferentiated PC12 cells utilizing Fura-2/AM as fluorescent probe. The

ability of these compounds to attenuate potassium-induced Ca^{2+} influx will be compared, based on their IC_{50} value, to that of known LTCC blocker such as nimodipine, nitrendipine, verapamil and diltiazem.

2. In this study we also aimed to elucidated the structural conformation of the tricyclo[6.3.0.$0^{2,6}$]undecane-4,9-diene-3,11-dione (**9**), tricyclo[6.3.0.$0^{2,6}$]-undecane-3,11-dione (**10**) and a derivative, *N*-(3-methoxybenzyl)-3,11-azatricyclo[6.3.0.$0^{2,6}$]undecane (**14f**) by means of X-ray crystallography. These were the only compounds that we were able to obtain in a crystalline form with crystals suitable for X-ray crystallography. Structural data obtained from crystallographic analysis would give us valuable insight into the size and geometrical configuration of these compounds and allow us to discuss some key structural features.

3. We evaluated several *in vitro* cell viability assays to develop a preliminary study to assess the potential of these compounds to offer protection against cytotoxin-induced cell death. Cell viability assays is a valuable tool in the screening of possible drug candidates before proceeding to more complex *in vivo* studies. For this purpose we evaluated several quantitative cell viability assays such as the LDH-assay, which measures lactate dehydrogenase (LDH) release by cells undergoing apoptosis; the MTT-assay, which measures the reduction of yellow tetrazolium salt (MTT) in metabolically active cells and the Trypan blue staining assay, which evaluate membrane integrity by measuring trypan blue uptake in non-viable cells. We also performed an Annexin V-FITC staining assay to assess the observed toxicity of compound (**14c**). These cell viability assays will also allow us to determine if the compounds by themselves exhibit any inherent toxicity.

4. To assess the ability of the selected compounds to modulate Ca^{2+} flux through intracellular Ca^{2+} channels. For this purpose we utilized the high throughput fluorescence Ca^{2+} flux assay in rat undifferentiated PC12 cells with Fura-2/AM as fluorescent probe. We examine calcium release from the ER by treatment with 1 μM thapsigargin in the presence of extracellular Ca^{2+}, which

allowed us to asses the interaction of these compounds on sarco-endoplasmic reticulum Ca^{2+}-ATPase (SERCA) pump and the inositol-1,4,5-triphosphate receptors (IP_3Rs). We also examine calcium release from the ER by an underlying mechanism of Ca^{2+}-induced Ca^{2+} release (CICR), designated as voltage-induced Ca^{2+} release (VICaR) in the absence of extracellular Ca^{2+} after depolarization with 50 mM KCl. This allowed us to assess the interaction of these compounds with the ryanodine receptors (RyRs).

CHAPTER 2

LITERATURE REVIEW

2.1 Background

2.1.1 Calcium homeostasis under normal physiological conditions

Ca^{2+} homeostasis under normal physiological conditions is regulated in a precise way to control changes in intracellular free calcium ($[Ca^{2+}]_i$) and allow for the generation of a variety Ca^{2+} signaling processes.[46] In neurons Ca^{2+} regulate multiple neuronal functions including the release of neurotransmitters, synaptic transmission, plasticity and cell survival.[47] In postsynaptic neurons, the release of neurotransmitters will activate excitatory ionotropic receptors such as the NMDAR, AMPA receptor and kainate receptor; as well as metabotropic receptors.[48, 49] These receptors are known as ionotropic ligand-gated or receptor-operated Ca^{2+} channels (ROCCs) and are activated by their physiological agonist glutamate which is a major excitatory neurotransmitter in the central nervous system. Apart from the ROCCs, voltage-gated Ca^{2+} channels have been shown to be another major gateway for Ca^{2+} influx from the extracellular environment and present an attractive opportunity for therapeutic intervention.[8, 50] VGCCs are permeable to Ca^{2+} and found only in excitable cells which can be activated by depolarization of the cell membrane or by activation of the ROCCs such as the NMDAR. VGCCs channels can be classified as L, N, T and P/Q-type and initiate different neuronal functions.[8]

Within the cell Ca^{2+} homeostasis is maintained by Ca^{2+} buffering and clearance mechanisms that regulate changes in $[Ca^{2+}]_i$ as illustrated in Figure 2.1. Cytoplasmic Ca^{2+} concentration is maintained at about 50 – 300 nM at rest and 1 – 500 μM upon activation.[4] Rapid Ca^{2+} sequestration is achieved by Ca^{2+}-binding proteins such as calmodulin, calbindin, calretinin and parvalbumin that buffer increases in cytoplasmic Ca^{2+} concentration.[4, 51] Slower Ca^{2+} clearance is mediated by Ca^{2+} pumps and

exchangers which facilitate Ca^{2+} uptake into intracellular organelles such as the mitochondria, endoplasmic reticulum (ER) and the Golgi apparatus.[4, 46, 52] Mitochondrial Ca^{2+} uptake occurs mainly by active transport through a large conductance channel, the mitochondrial Ca^{2+}-uniporter (MCU) which is an electrogenic pathway dependant on the transmembrane potential.[53, 54] The mitochondria have a large capacity for Ca^{2+} sequestration and offer protection against large rises in $[Ca^{2+}]_i$.[55] Ca^{2+} release from the mitochondria under normal conditions occurs mainly through the Na^+/Ca^{2+} exchanger (mNCX).[54] ER Ca^{2+} uptake occurs mainly through the sarco-endoplasmic reticulum Ca^{2+}-ATPase (SERCA) pumps which is ATP dependent and pump Ca^{2+} into the lumen of the ER. Ca^{2+} release from the ER occurs *via* the ryanodine receptors (RyRs) and inositol-1,4,5-triphosphate receptors (IP_3Rs).[56, 57] Ca^{2+} release through the IP_3Rs requires binding of the second messenger IP_3 generated by phospholipase C (PLC) in response to the activation of various G-protein-coupled receptors (GPCRs) or tyrosine kinase-linked receptors on the cell membrane.[46] Increased cytoplasmic Ca^{2+} concentrations will also sensitize IP_3Rs to IP_3 and activate Ca^{2+}-induced Ca^{2+} release (CICR).[58-60] Ca^{2+} release *via* the RyRs is mainly triggered by CICR. The RyRs are also regulated by other intraneuronal factors, such as cyclic adenosine diphosphate ribose (cADP-ribose). Another mechanism by which Ca^{2+} can be removed from the cytoplasm is by the Na^+/Ca^{2+} exchanger (NCX) located in the cell membrane and the plasma membrane Ca^{2+} ATPase (PMCA) channel that pump Ca^{2+} ions out against the concentration gradient.[4] The Na^+/K^+-ATPase, also located in the cell membrane, maintain the Na^+ gradient to allow for continuous Ca^{2+} cycling.[9] Together, all of these mechanisms work to control Ca^{2+} signaling within the cell and maintain Ca^{2+} homeostasis.

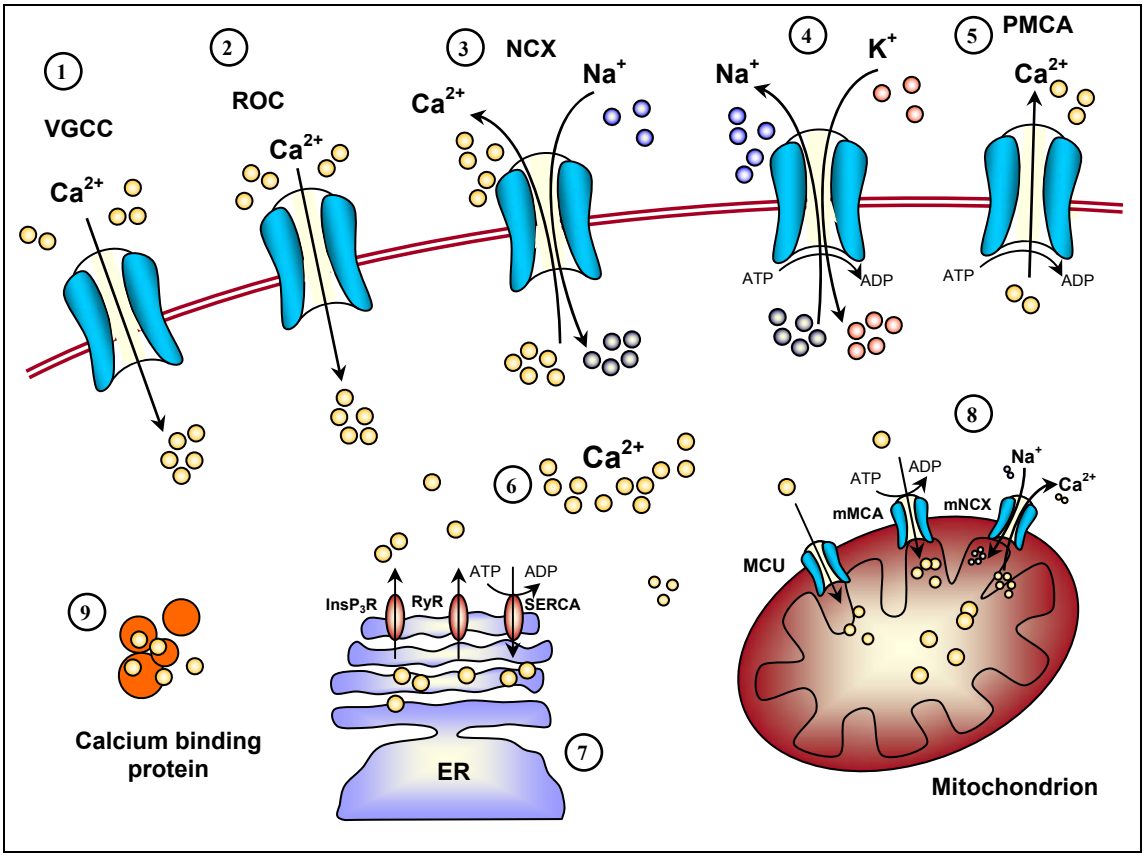

Figure 2.1. A schematic representation of Ca^{2+} homeostasis under normal physiological conditions. (**1**) Ca^{2+} influx *via* VGCC, (**2**) Ca^{2+} influx *via* NMDAR, (**3**) Ca^{2+} extrusion *via* the Na^{+}/Ca^{2+}-exchanger (NCX), (**4**) Na^{+} extrusion *via* the plasma membrane Na^{+}/K^{+}-ATPase, (**5**) Ca^{2+} extrusion *via* the plasma membrane Ca^{2+} ATPase (PMCA) (**6**) accumulation of Ca^{2+} intracellular, (**7**) sequestration and release of Ca^{2+} by the ER, (**8**) sequestration and release of Ca^{2+} by the mitochondria, (**9**) Ca^{2+} buffering by Ca^{2+} binding proteins.

2.1.2 Perturbed Ca^{2+} homeostasis

Persistent cellular stress can overcome the cells ability to regulate Ca^{2+} homeostasis which will lead to increased cytoplasmic Ca^{2+} levels resulting in either a rapid increase or prolonged elevation of $[Ca^{2+}]_i$.[61-64] The perturbation of Ca^{2+} homeostasis and elevated $[Ca^{2+}]_i$ and have been shown to be directly involved in cell death.[65-67] Elevation in $[Ca^{2+}]_i$ will activate several catabolic processes catalyzed by Ca^{2+}-activated proteases (calpains), phospholipases, and endonucleases, eventually

resulting in cell death.[68] Neurodegeneration can occur by two distinct pathways: necrosis (or rapid neurodegeneration) and apoptosis (or slow progressive neurodegeneration); and are dependent on the bioenergetic balance of the cell, the intensity, duration and nature of the insult.[69-71] Each of these are manifested in acute and chronic neurological disorders, however both apoptosis and necrosis can be present simultaniosly.[72, 73] Although the initial events may be the same in both types of cell death, the downstream events and outcomes are distinctly different. For example, for many acute neurological disorders, such as stroke or head trauma also known as traumatic brain injury (TBI), necrosis is the primary cause of cell death. Necrosis is distinguished by a cascade of events that elicits cellular swelling and membrane lyses that results in loss of cellular content which leads to cell death.[56, 74] For chronic neurological disorder such as Parkinson's disease (PD), Alzheimer's disease (AD) and Huntington's disease (HD), apoptosis or programmed cell death (PCD) is the primary cause of cell death.[4, 62] The apoptotic pathway is considerably more complicated and involves oxidative stress (in which free radicals cause damage to cellular lipids, proteins and nucleic acids), excitotoxicity (marked by perturbed Ca^{2+} homeostasis),[75] and metabolic compromise (marked by mitochondrial dysfunction and activation of cysteine proteases called caspases).[56] Apoptotic cell death is characterized by cellular shrinkage, chromatin condensation and DNA degradation.[76]

As mentioned in both pathways Ca^{2+} homeostasis is compromised, and this is an initial event that both necrotic and apoptotic cell death have in common. Increased $[Ca^{2+}]_i$ can be the result of excessive Ca^{2+} influx from the extracellular environment or release from the intracellular Ca^{2+} stores as illustrated in Figure 2.2. Excitotoxicity is mediated by excessive release of the excitatory neurotransmitter, glutamate (reviewed in [77]). This will lead to excessive activation of the NMDARs that result in an increased influx of Ca^{2+} through these receptors. In turn the activation of the NMDARs will also lead to depolarization of the cell membrane and opening of the VGCCs, which also leads to excessive Ca^{2+} influx through these channels.[4, 77] Oxidative stress conditions will lead to a decline in ATP levels that will compromise Ca^{2+} extrusion mechanisms that are ATP-dependent. This will affect the Ca^{2+}-ATPase

pump directly which utilizes ATP to remove Ca^{2+} from the cytoplasm.[78] Secondly it will affect the Na^{+}/Ca^{2+} exchanger indirectly by inhibiting the operation of the Na^{+}/K^{+}-ATPase. The Na^{+}/Ca^{2+} exchanger utilizes the Na^{+} electrochemical gradients to pump Ca^{2+} out and under stress conditions where the $[Na^{+}]_i$ is elevated, may reverse to pump Na^{+} out and Ca^{2+} into neurons.[79, 80]

The principal dysfunction of Ca^{2+} buffering is observed in the mitochondria. The electrical gradient between the mitochondrial matrix and the cytosol favors Ca^{2+} influx through the mitochondrial Ca^{2+} uniporter (MCU) and the transmembrane potential is the driving force for continuous Ca^{2+} pumping. However, during Ca^{2+} uptake the membrane potential decreases and massive Ca^{2+} accumulation in the mitochondria leads to collapse of the membrane potential (Ψ).[81] Ca^{2+} accumulation would also lead to an increase in production of reactive oxygen species (ROS) and the formation of the mitochondrial permeability transition pore (mPTP),[82] a high-conductance, non-selective channel through which Ca^{2+} and cytochrome c is release as a result of mitochondrial dysfunction.[4, 54, 76, 83] The binding of cytochrome c with Apaf-1 initiates the upstream activation of caspases-9 leading to the downstream activation of caspase-3, thereby eliciting apoptosis.[56, 64] The increased production of ROS under oxidative stress conditions result from mitochondrial oxidative metabolism, Ca^{2+}-activated nitric oxide synthase (NOS) and the uncoupling of electron transport chain; which will cause oxidative damage and depolarization of the mitochondrial membrane.[84, 85] Depolarization of the mitochondria membrane impairs the ability of these organelles to sequester excess Ca^{2+}, which as mentioned may cause Ca^{2+} release from the mitochondria that will add to elevated $[Ca^{2+}]_i$. Mitochondrial Ca^{2+} efflux under normal conditions occurs through the mNCX that will pump Ca^{2+} out, however the mNCX will become saturated with excessive increase in the $[Ca^{2+}]_m$.[54]

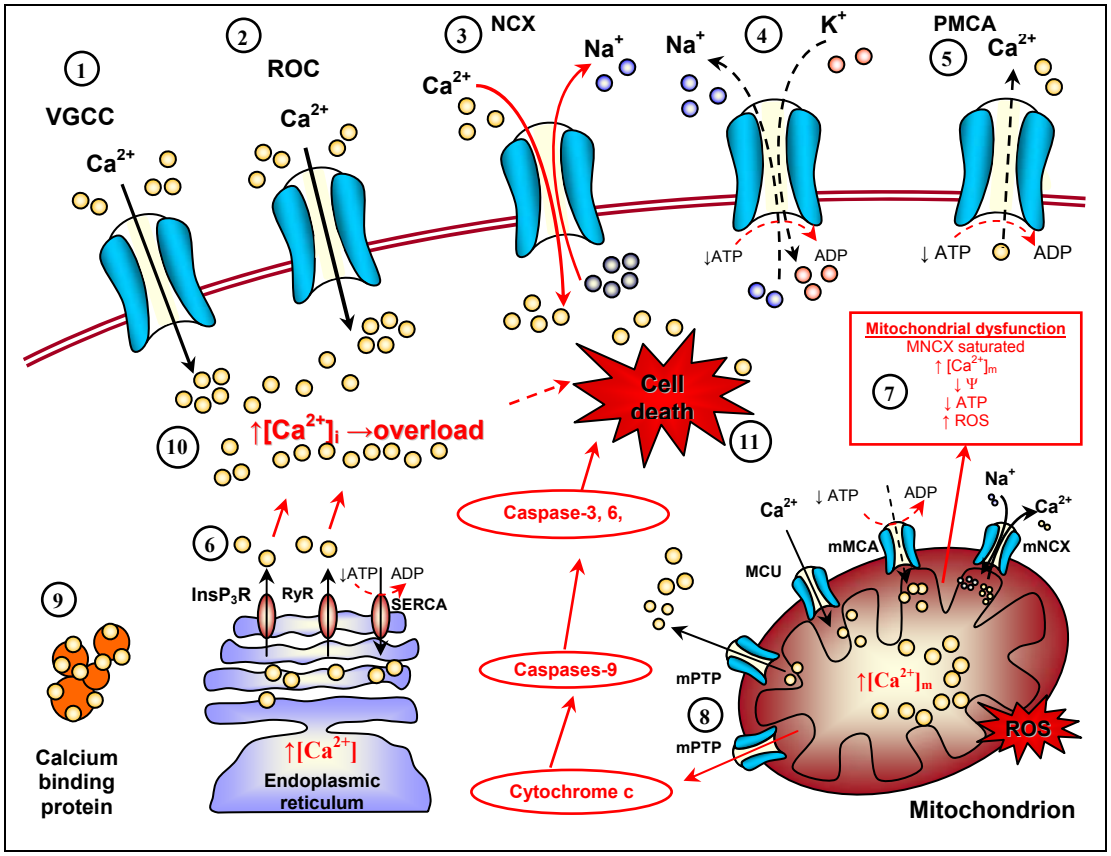

Figure 2.2. A schematic representation of perturbed Ca^{2+} homeostasis and death cascade. (**1**) excessive Ca^{2+} influx *via* VGCC, (**2**) excessive Ca^{2+} influx *via* NMDAR, (**3**) reversal of Na^{+}/Ca^{2+} exchanger (NCX), (**4**) ATP depletion causes decreased Na^{+} extrusion *via* the plasma membrane Na^{+}/K^{+}-ATPase, (**5**) ATP depletion causes decreased Ca^{2+} extrusion *via* the plasma membrane Ca^{2+}-ATPase (PMCA), (**6**) Ca^{2+}-induced Ca^{2+} release by the ER, (**7**) metabolic compromise & mitochondrial dysfunction, (**8**) formation of mPTP and release of pro-apoptotic factors as well as Ca^{2+}, (**9**) saturation of Ca^{2+} binding proteins capacity, (**10**) elevated $[Ca^{2+}]_i$ resulting in excitotoxicity, (**11**) cell death.

Necrosis also leads to a loss of ion homeostasis that results in elevated cytosolic Ca^{2+} concentrations. As a downstream mechanism for necrosis the increased $[Ca^{2+}]_i$ will activate calpain-mediated cathepsin release from lysosomes that will digest target proteins which will lead to plasma membrane rupture resulting in necrotic cell death.[76]

2.1.3 Pharmacological intervention

As explained in the above literature neurodegenerative disorders, whether chronic or acute, share some common key mediator in the process of neuronal cell death; whether apoptotic or necrotic cell death.[74] Multiple pathways are involved in neuronal cell death, as describe in above literature, with multiple targets for pharmacological intervention.[4, 74] This implies that it would be beneficial to employ multiple treatment strategies aimed at multiple target sites to increase the likelihood of success. There are many disadvantages in the use of multiple drugs (polypharmacy) to treat a disease with multiple etiologies. Multiple drug regime can decrease patient compliance and increase drug side effects, drug-drug interaction as well as drug toxicity.[35, 86] It would be more beneficial to employ a single molecule with multiple mechanisms of action, that can address multiple target in the same pathology.[33-35] These drugs are called multifunctional or multimechanistic drugs and holds an advantage in cases such as ischemic stroke where a combination of therapies have been shown to be beneficial.[36] Such an approach retains the beneficial therapeutic effect of combining multiple drugs, while simultaneously limiting the side-effect profile to that of only one drug.[37]

Ca^{2+} overload can be used as a conceptual scaffolding, with a wide variety of targets for pharmacological intervention that might protect neurons against neurodegeneration.[67] Identification of the mechanisms and pathways involved in dysregulation of Ca^{2+} homeostasis reveals several possible drug targets.[74] The most notable of these are Ca^{2+} overload that occur by direct Ca^{2+} entry through the ion-channel complex of the NMDAR, or indirectly by depolarization of the membrane potential and opening of the VGCC.[74] Thus the NMDAR pathway serve as a potential drug target for regulation of Ca^{2+} homeostasis.[87] NMDAR blockers such as MK-801 where unsuccessful clinically due to the associated side effects of a high-affinity NMDAR blocker such as hallucinations, delirium, and psychosis.[32] However, drugs such as memantine have been successfully used clinically in patients with moderately severe to severe Alzheimer's disease.[88] Memantine; a low-affinity, uncompetitive antagonist is well-tolerated due to its fast on-off binding kinetics. This means that it only blocks Ca^{2+} influx when the channel is in the open state. Memantine has a

polycyclic structure and is currently the only drug, under the trade name Namenda®, clinically used to treat Alzheimer's disease.[17, 18] Likewise, the VGCC may serve as a potential drug target in the treatment of neurodegenerative diseases. LTCC blockers such as the 1,4-dihydropyridines (DPH) nimodipine have been shown to be protective in models of acute neurological disorders such as ischemia.[23-25, 24] Also among the LTCC blockers is the 1,4-dihydropyridines (DPH) nitrendipine, the phenylalkylamine (PAA) verapamil and the benzothiazepine (BTZ) diltiazem which demonstrated the ability to attenuate excitotoxicity caused by an increase in $[Ca^{2+}]_i$, resulting in apoptotic and/or necrotic cell death.[20, 21] Nimodipine is highly lipophilic and will cross the blood-brain barrier, which allows this drug to be used in the treatment of neurodegenerative diseases. However, nimodipine can only be used in acute neurological disorders such as ischemia due to its cardiological effects that can lead to hypotension.[20, 26, 89]

Perturbed ER Ca^{2+} homeostasis and excessive Ca^{2+} release through intracellular Ca^{2+} channels will also contribute to neuronal apoptosis and excitotoxicity. Pathways involved in intracellular Ca^{2+} regulation, specifically targeting intracellular Ca^{2+} channels, have been explored to a lesser extent as possible drug targets for the treatment of neurodegenerative disorders. Some of the compounds that have been evaluated for their ability to attenuate ER-mediated Ca^{2+} release and to offer protection against excitotoxicity are: dantrolene, block Ca^{2+} release from RyR;[90] dauricine, inhibit ER Ca^{2+} release and offer protection against hypoxia and hypoglycemia;[91] Xestospongin C, an inhibitor of the IP_3R which partially attenuate Aβ peptide neurotoxicity;[92] 2-aminoethoxydiphenyl borate (2APB) an inhibitor of the IP_3R which partially attenuate Aβ peptide neurotoxicity;[92] and KF 506 an inhibitor of the RyR which partially attenuate Aβ peptide neurotoxicity.[92] The ER play a major role in controlling levels of cytoplasmic free Ca^{2+} and should thus be considered a possible target for pharmacological intervention (reviewed in [93]). However; we should bear in mind that ER Ca^{2+} signaling are integrated with many pathways essential for neuronal functioning,[93] and therefore we would have to employ compounds that function in a use-dependent manner to regulate Ca^{2+} flux through either IP_3R or RyR to maintain homeostasis and not completely block Ca^{2+} flux through these receptors.

Thus, a multimechanistic drug with the ability to modulate Ca^{2+} flux through multiple pathways in a use-dependent manner would be the ideal towards more effective therapy in the treatment of neurodegenerative diseases.

2.2 Compounds selected

Several studies investigated the ability of both the pentacycloundecylamines and triquinylamines to modulate Ca^{2+} influx through either the NMDA receptor or the LTCC.[34, 40-43, 45, 94] These studies revealed that most of these compounds have the ability to modulate Ca^{2+} entry though both the NMDA receptor and the LTCC, however non of them calculated the IC_{50} values for these compounds as LTCC blockers. The dual-mechanistic action of these compounds gives them a unique advantage in the treatment of neurodegenerative disorders over compounds such as nimodipine, which only has the ability to block LTCC's; and memantine, a low-affinity NMDAR blocker. There is still much to be learned about the pharmacological profile of both the pentacycloundecylamines and triquinylamines as potential neuroprotective agents and it is the purpose of this study to further contribute to the elucidation of the mechanism of action for these novel compounds and for the first time calculate their IC_{50} values as LTCC blockers as well as evaluating their ability to modulate Ca^{2+} flux through intracellular Ca^{2+} channels.

NGP1-01 (**7a**), which has been established as a lead structure for the pentacycloundecylamines served as a starting point for the selection of two series; the aza-pentacycloundecylamines and the oxa- pentacycloundecylamines. The choices of **R** substituents guided by structure-activity relationship (SAR) data gathered from previous studies.[40, 41, 95] We also selected a series of *cis-syn-cis* triquinane derivatives which is thermal fragmented derivatives of the pentacycloundecanes. One of the required pharmacophoric features of polyquinane LTCC blockers is a bulky, lipophilic schaffold.[40, 95] The triquinane scaffold (**10**) retains the bulkiness (± 10%) of the pentacycloundecane (**4**) as expressed in molecular volume (**4**: 498 $Å^3$ and **10**: 552 $Å^3$) and solvent accessible surface area (**4**: 325 $Å^2$ and **10**: 351 $Å^2$).[95] The triquinane scaffold has some flexibility, compared to the pentacycloundecane

scaffold, which can be beneficial when designing compounds that act as ion channel blockers, due to the ability to flex and adjust conformation to give a better fit within the ion channel pore. We included a series of aliphatic and aromatic aza-triquinylamine derivatives in this study to compare to series of pentacycloundecylamine derivatives.

The synthesis of these two series of compounds can be described as follow: The pentacyclo[5.4.0.$0^{2,6}$.$0^{3,10}$.$0^{5,9}$]undecane-8-11-dione (**4**), also called Cookson's "cage" compound, can be synthesized by photo chemically initiated intramolecular [2 + 2] cycloaddion of the Diels-Alder adduct (**3**) obtained from the reaction of 1,3-cyclopentadiene (**2**) with *p*-benzoquinone (**1**).[96] The oxa-pentacycloundecylamine derivatives (**7a-e**) illustrated in scheme 4.1, can be obtained by the reductive amination of **4** with the desired primary amine side chains.[40, 97] To obtain the oxa-bridge compound, reduction of the Schiff base imine intermediate (**6**) can be performed with sodium borohydride, to facilitate ring closure through a transannular reaction. In order to obtain the aza-bridged derivatives (**8a-c**), reductive amination can be done with sodium cyanoborohydride. Compound (**19**) was selected to evaluate whether the absence of the aromatic side chain moiety would influence the ability of the polycyclic cage amine compound to bind within the LTCC. This compound was previously synthesized by Geldenhuys *et al*., and the synthesis is described in the original paper.[97]

Scheme 1[a]

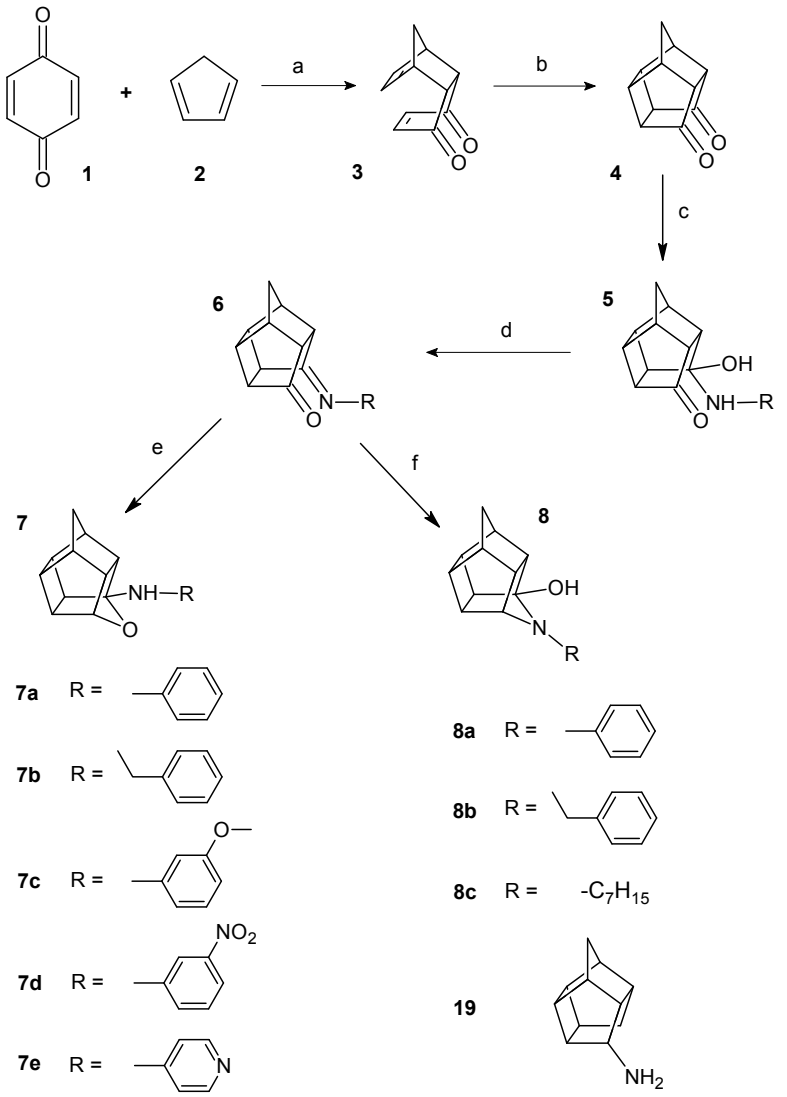

[a] Reagents and conditions: (a) Benzene, 5 °C; (b) Acetone, UV, 6 h; (c) THF, 5 °C, NH_2-R; (d) Benzene, Δ, -H_2O, 1 h; (e) MeOH, THF, $NaBH_4$; (f) HOAc, MeOH, $NaBH_3CN$, 12 h. The synthesis of **19** was achieved by selective decarboxylation of (**4**) by means of Huang-Minlon reaction followed by reductive amination with $NaBH_4$.

The *cis,syn,cis* triquinane system can only be derived through thermal fragmentation of the pentacyclo[5.4.0.$0^{2,6}$.$0^{3,10}$.$0^{5,9}$]undecane-8-11-dione (**4**) as first described by Mehta *et al.*, (1981).[98] The thermal fragmentation (step a, Scheme 2) was performed through flash vacuum pyrolysis (FVP) also known as flash thermolysis.[95, 98, 99] We

successfully attempted this complex synthesis in a previous study in which we also had to design and build the FVP apparatus necessary to perform the synthesis.[99] The synthesis for the aza-triquinylamines (**14a-g**) is shown in Scheme 2. For the design of the apparatus and synthesis we utilized a combination of methods described by several authors.[95, 98, 100] In short, the thermal fragmentation of the saturated four-membered ring (**4**), afforded the *cis,syn,cis* triquinane system: tricyclo[6.3.0.$0^{2,6}$]undecane-4,9-diene-3,11-dione (**9**). FVP was carried out in a quartz vigreux column connected to a substrate tube and a vacuum line provided with a liquid nitrogen cold trap. Sublimation of the substrate **4**, which was contained in a borosilicate glass tube, was achieved at 150 °C under vacuum of 1 torr. The sublimate slowly traveled through the quartz vigreux column, which was heated to a temperature of 650 °C under vacuum of 1 torr. The condensate was deposited in a specially designed freeze fall that was cooled with liquid nitrogen, and afforded the tricyclo[6.3.0.$0^{2,6}$]undecane-4,9-diene-3,11-dione (**9**). Before pyrolysis commenced the entire apparatus was flushed with nitrogen gas and then evacuated to 1 torr by a high-capacity rotary vane oil pump.

The product of thermolysis (**9**) was hydrogenated over 10% Pd-C catalyst to yield tricyclo[6.3.0.$0^{2,6}$]undecane-3,11-dione (**10**). The aza-triquinylamine compounds (**14a-g**) can be obtained by reductive amination (Scheme 2, steps d-f) of **10** with the desired primary amine side chains. To obtain the aza-bridge compound reduction of the imine intermediate (**13**) was done with sodium cyanoborohydride to facilitate ring closure through a transannular reaction. To obtain the oxa-bridge compound (**11**), reduction of the **13** was accomplished with sodium borohydride. The series of aza-pentacycloundecylamines (**8a-c**), oxa-pentacycloundecylamines (**7a-e**) and aza-triquinylamines (**14 a-g**) included compounds that are devoid of aromatic alkyl substitution (**8c**, **11**, **14d**, **14e** and **19**) to explore the functional role of the polycyclic moiety in isolation, as well as several compounds that contain electron withdrawing or donating moieties (**7c**, **7d** and **14f**). We also included several compounds were the chain length was altered to asses binding within the channel pore (**7b**, **8b**, **14b** and **14c**).

Scheme 2[a]

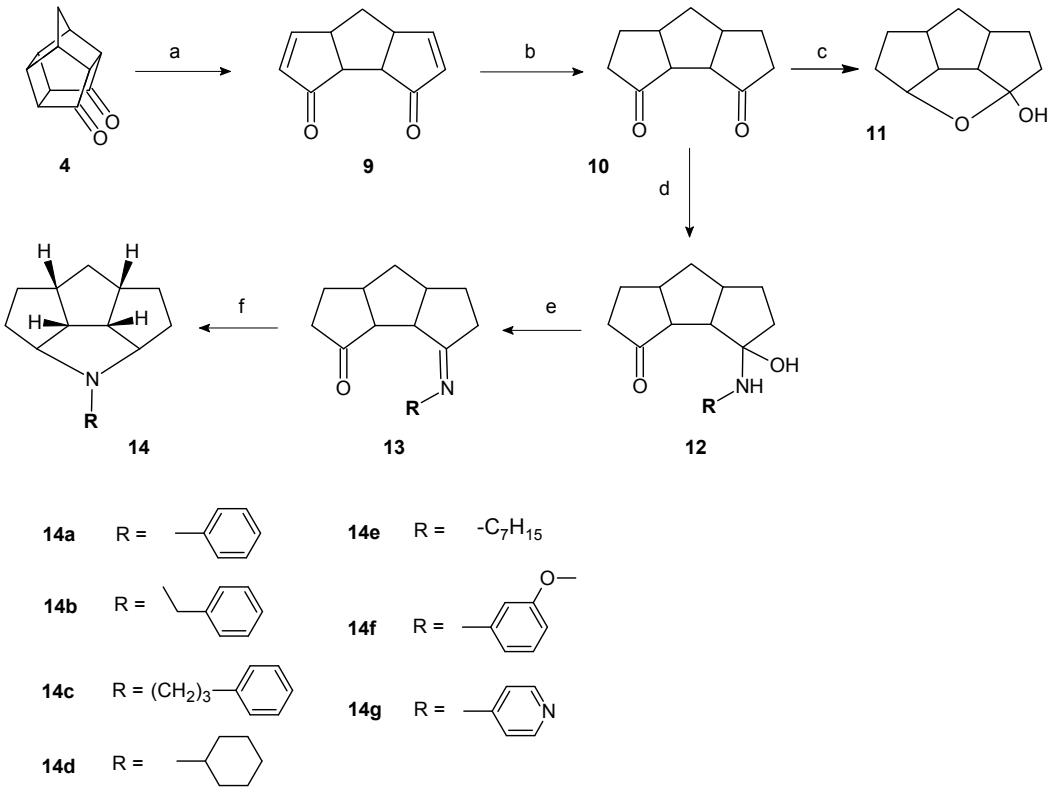

[a] Reagents and conditions: (a) Δ, 650 °C, 1 torr, 45 min; (b) EtOAc, 2 atm H_2, 10 % Pd/C, 40 min; (c) MeOH, THF, $NaBH_4$; (d) THF, 5 °C, NH_2-R, 6 h; (e) Benzene, Δ, -H_2O, 1 h; (f) MeOH, THF, $NaBH_3CN$, 18 h.

2.3 Biological evaluation

In this study we developed a high-throughput fluorescence Ca^{2+} flux assay to evaluate the ability of our novel series of compounds to attenuate KCl-induce Ca^{2+} influx in PC12 cells. We also evaluated several cell viability assays to find the most effective *in vitro* models that would allow us to screen and identify the most active compounds before proceeding to more complex *in vivo* studies. Undifferentiated rat pheochromocytoma (PC12) cells obtained from the American Type Culture Collection (ATCC, Manassas, VA, USA) were used in this study. PC12 cells are derived from rat adrenal medulla chromaffin cells and are commonly used as an *in vitro* model to study neurodegenerative diseases and Ca^{2+} homeostasis.[101-103] Undifferentiated PC12 have been successfully used in studies investigating the

stimulation and inhibition of VGCC.[101, 104, 105] Undifferentiated PC12 cells express voltage-dependent Ca^{2+} channels, having similar biophysical and pharmacological properties to those expressed by neurons and these include the L - type Ca^{2+} channels.[106-108]

2.3.1 Evaluation of calcium influx

The most commonly used approach to measure changes in $[Ca^{2+}]_i$ in cell culture is to monitor the fluorescence of a Ca^{2+} indicator. Several instruments and techniques can be utilized to measure the changes in fluorescence such as fluorescence microscopy or a fluorescence microplate reader. For this study we decided to utilize the BioTech Synergy 4 microplate reader, which will allow us to develop high-throughput, cell based, fluorescence experiments with the ability to measure Ca^{2+} influx after depolarization in a 96 well plate.[109] There are several different types of fluorescent Ca^{2+} indicators that can be used in the measurement of $[Ca^{2+}]_i$ flux,[110] and for this experiment we decided to utilize the most commonly use indicator Fura-2/AM.[111-113] Fura-2/AM is a ratiometric Ca^{2+} indicator that undergoes a shift in absorption rather than the emission peak. For the Ca^{2+}-bound form excitation is at 340 nm and for the Ca^{2+}-unbound form excitation is at 380 nm. The emission peak for both the Ca^{2+}-bound and Ca^{2+}-unbound forms is at 500 nm.[113] The use of a ratiometric indicator allows for the correction of differences in path length and accessible volume in three-dimensional specimens. The ratio signal from a ratiometric indicator is also not dependent on dye concentration. Therefore, since dye leakage and photo bleaching leads to loss of indicator during an experiment, the ratiometric indicator will give a more accurate measurement of $[Ca^{2+}]_i$. The ratiometric measurements also produce an additional increase in sensitivity because it is not dependent on dye concentration, illumination intensity, or optical path length and therefore not affected by variations in these parameters.[113] We also decided to use the acetoxymethyl ester (AM) form of Fura-2 which is cell permeable and will allow for direct cell loading. The AM form of the indicator can passively diffuse across the cell membranes and, once inside the cell, the AM group will be cleaved by esterase's rendering the indicator cell impermeable.

Rendering the indicator cell impermeable after it entered the cell will minimize dye leakage.[111, 113]

To evaluate Ca^{2+} influx through VGCCs such as the LTCC, membrane depolarization can be induced by the addition of a high concentration potassium chloride (50 mM KCl) to modulate the membrane potential of the cells and thereby the conformational state of ion channel proteins.[109] This will result in an influx of Ca^{2+} and a rise in the cytosolic $[Ca^{2+}]_i$. As mentioned these changes in $[Ca^{2+}]_i$ can be measured by utilizing a fluorescent Ca^{2+} indicator such as Fura-2/AM and the fluorescence can be read in high-throughput format (96-well) on a fluorescence microplate reader.[109] In the present study we utilized this technique to evaluate the ability of our novel series of compounds to modulate the influx of Ca^{2+} through the LTCCs after depolarization with 50 mM KCl and calculated their IC_{50} values. We also evaluated several known LTCC blockers such as nimodipine, nitrendipine, verapamil and diltiazem to serve as control.

2.3.2 Cell viability

The measurement of cell viability is a valuable screening tool in the development of drugs in the treatment of neurodegenerative disorders. It allows for basic screening of a large selection of compounds before proceeding to more complex and more expensive *in vivo* studies. There are several approaches in the assessment of the ability of compounds to offer protections against cytotoxic insults. Trypan blue staining assay is a simple yet effective way to evaluate cell membrane integrity, but the method is not sensitive and cannot be adapted for high-throughput screening. This method however, is routinely used in correlation with the LDH or MTT assay to affirm results. The MTT assay involves the reduction of the yellow tetrazolium salt (MTT) in metabolically active cells and is a quantitative, more sensitive assay that can be adapted for high-throughput screening in a 96 well plate. The growth or death rate of cells can be quantitatively measured because there is a linear relationship between cell activity and absorbance, whereas a qualitative assay such as the trypan blue staining assay only indicates if a cell is alive. The measurement of lactate

dehydrogenase release (LDH) is another quantitative method to measure cell viability. LDH is an enzymatic assay based on the principal that cytosolic LDH leaks out of cells of which the membrane integrity has been compromised. Both the LDH and MTT assay are rapid and reliable methods, however good correlation is not always found between these two assays.[114] The advantage of the LDH assay is that it is a more sensitive method and the MTT assay has been found not to be compatible with all types of cell lines.[115] In this study we will explored all three methods to determine the most effective assays under our experimental condition.

2.3.2.1 Estimation of LDH release

Cytotoxicity can be assayed by measuring the loss of membrane integrity and subsequent release of the cytosolic enzyme, LDH.[116] This assay was originally used to measure neuronal cell death occurring *via* necrosis,[115] but more recently has been shown to accurately measure neuronal apoptosis in cortical cultures.[117] Most cells contain the LDH enzyme which catalyze the interconversion of pyruvate, the final product of glycolysis, and lactate with parallel interconversion of NADH and NAD^+ during the anaerobic cycle (Figure 2.3). LDH is released from the cell when the cell membrane is compromised during cytotoxicity. The released LDH can be quantitatively measured with the coupled enzymatic reaction in which LDH catalyze the reduction of NAD^+ to NADH and H^+ by the oxidation of lactate to pyruvate. From this conversion diaphorase utilizes the formed NADH and H^+ to catalyze the reduction of a tetrazolium salt, iodonitrotetrazolium (INT), into a red color formazan which absorbs at 490 nm. The amount of formazan production is proportional to the amount of LDH released into the culture medium as a result of cytotoxicity. Thus we utilized the LDH assay as a colorimetric method to evaluate the ability of selected compounds to offer protection against 200 μM H_2O_2 induced cell death. This method was developed according to literature descriptions and Cayman® manufacturer's protocols.[115, 116, 118]

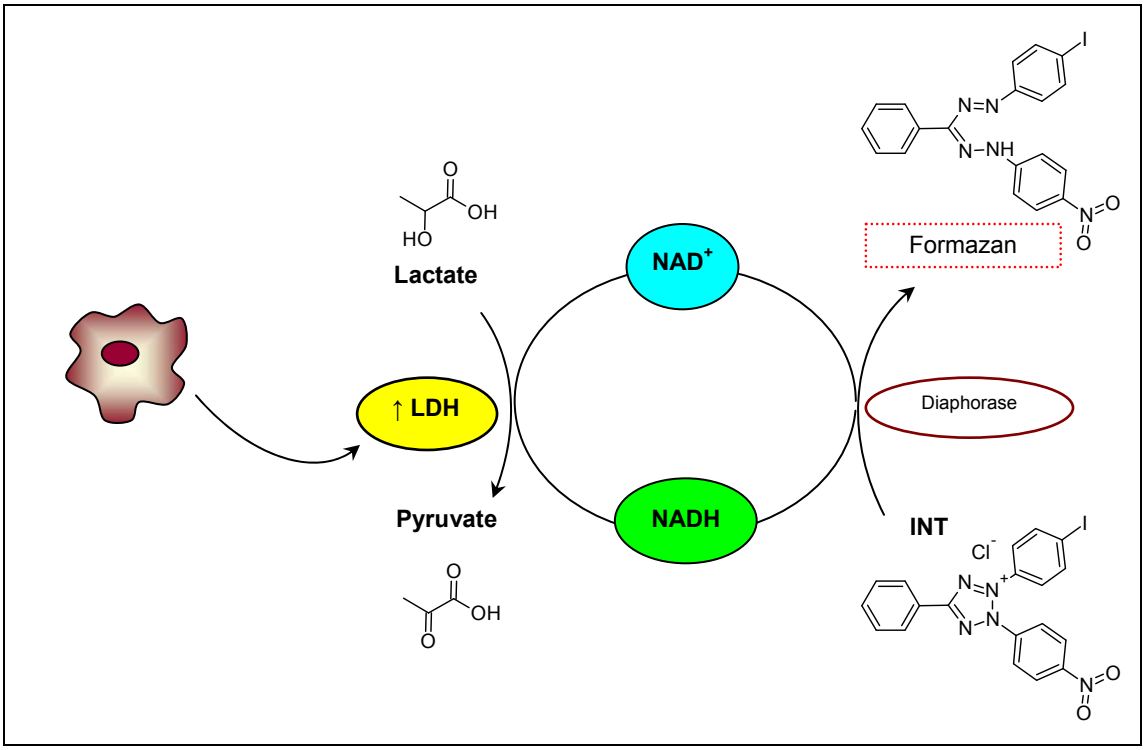

Figure 2.3. Measurement of LDH release (Schematic adapted from the GBioscience® website http://www.gbiosciences.com/).

2.3.2.2 Determination of MTT reduction

Cytotoxicity can also be quantified by measuring the reduction of 3-(4,5-dimethylthiazol-2-yl)-2,5-diphenyltetrazolium bromide (MTT), a yellow water-soluble tetrazolium dye that is reduced by metabolically active cells to dark purple water-insoluble formazan crystals.[119] The resulting dark purple formazan crystals can be solubilized in DMSO and quantified by spectrophotometrically measuring the absorbance at 570 nm. The reduction of MTT is thought to mainly occur in the mitochondria through the action of succinate dehydrogenase enzymes, therefore providing a measure of mitochondrial function.[120] The MTT assay measures cell proliferation by assessing biochemical perturbation of the mitochondria,[121] and conversely, when metabolic events lead to apoptosis or necrosis, the reduction in cell viability. Thus we also utilized the MTT assay as a colorimetric method to evaluate the ability of selected compounds to offer protection against 200 μM H_2O_2 induced cell death. Compromised cell viability will lead to decreased MTT reduction and a

decrease in absorbance at 570 nm. This method was developed according to literature descriptions.[121, 122]

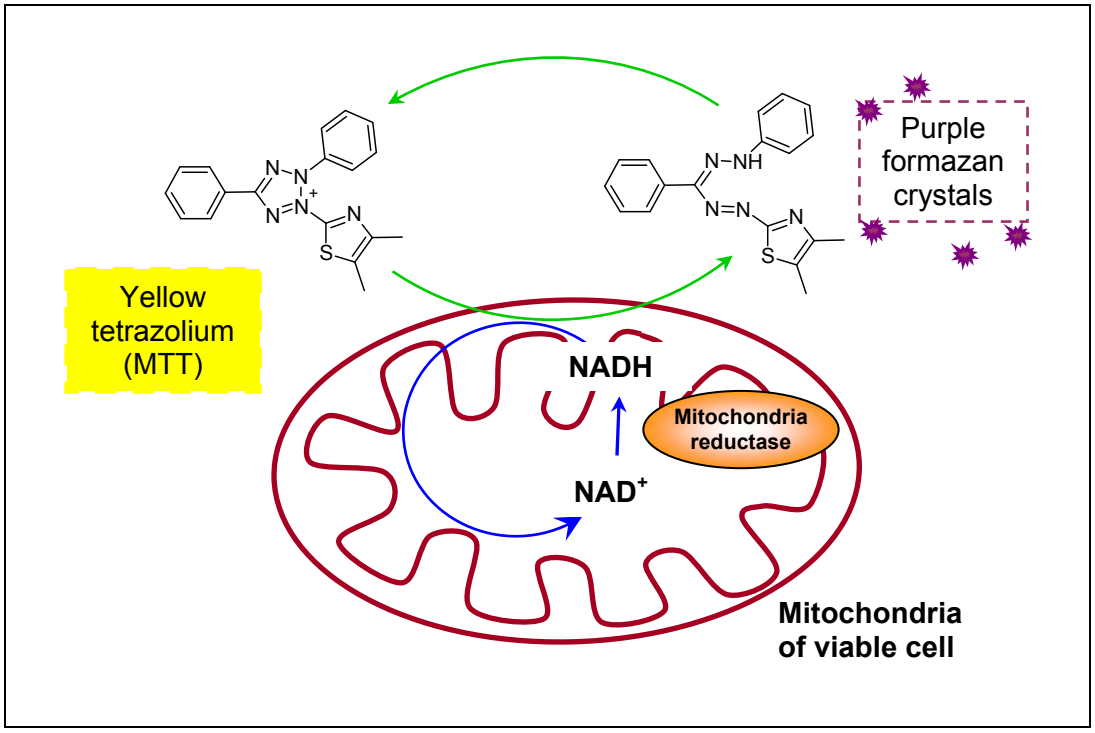

Figure 2.4. Schematic representation of MTT reduction.

2.3.2.3 Trypan Blue staining

The trypan blue staining assay is commonly used to determine the number of viable cells. Trypan blue is a large (MW = 960.81 g/mol) hydrophilic molecule that can only cross the cell membrane of cells that has lost their membrane integrity. The trypan blue staining assay is based on the principle that viable cells possess intact cell membranes that exclude certain dyes, such as trypan blue, whereas dead cell with compromised membrane integrity do not have the ability to exclude the dye. Cells are visually examined under a phase contrast microscope to determine the number of cells that excluded the dye or not.[123] A viable cell will have a clear cytoplasm whereas the cytoplasm of a non viable cell will be stained blue. These cells can then be counted to determine the percentage viable cells. This assay is commonly used in correlation

with the LDH or MTT assay, however cannot distinguish between necrotic or apoptotic cell death and is only an indication of late stage cell injury.[73, 114, 124]

2.3.2.4 Fluorescence microscopy analysis of Annexin V-FITC staining

Apoptosis is associated with characteristic morphological and biochemical changes, including cell shrinkage, membrane blebbing, chromatin condensation, DNA fragmentation, and cell surface changes.[56] In addition to these changes in cell morphology, a loss in membrane phospholipid asymmetry will also occur. Early in apoptosis phosphatidylserine (PS), an aminophospholipid normally present in the inner leaflet of the plasma membrane to the cytoplasmic face, will translocate from the inner to the outer surface of the plasma membrane.[125, 126] Externalization of PS to the cell surface of apoptotic cells serves as a "signal" for recognition by macrophages, facilitating the removal of dying cells by phagocytosis before the loss of plasma membrane integrity. Exposure of PS on the cell surface provides a sensitive and easy method for detecting apoptosis in the early stages. Annexin V is a Ca^{2+}-dependent, phospholipid binding protein with a high affinity for PS. When PS is exposed on the extracellular face of the cell membrane, the fluorescein isothiocyanate (FITC) conjugates of Annexin V can be used to monitor PS translocation and thus indirectly detect apoptosis.[127] The Annexin V-FITC positive cells can be detected by fluorescence microscopy. In this study we utilized the Annexin V-FITC assay to evaluate inherent toxicity displayed by selected compounds and to identify whether these compounds induce apoptotic cell death. As a positive control for apoptosis, one chamber was treated with Staurosporine. Staurosporine is a broad spectrum protein kinase inhibitor and has been used to induce cell death in a wide range of cell types.[128-130]

CHAPTER 3

BIOLOGICAL EVALUATION OF PENTACYCLOUNDECYLAMINES AND TRIQUINYLAMINES AS BLOCKERS OF VOLTAGE GATED CALCIUM CHANNELS, AND ANTI-APOPTOTIC AGENTS

3.1 Introduction

As mentioned perturbation of Ca^{2+} homeostasis and subsequent Ca^{2+} overload have been implicated in both acute and chronic neurological disorders, as well as physiological ageing.[1-5] For these conditions one common key mediator in the neuronal death is Ca^{2+}. Excessive influx of Ca^{2+} together with Ca^{2+} release from intracellular compartments can overwhelm Ca^{2+}-regulatory mechanisms and lead to cell death.[6] Apart from the *N*-methyl-D-aspartate receptor (NMDAR), voltage-gated Ca^{2+} channels (VGCCs) such as the L-type Ca^{2+} channels (LTCCs) have also been implicated as a major gateway for Ca^{2+} entry from the extracellular environment.[8] Thus LTCC blockers such as nimodipine, which has been shown to be protective in models of acute neurological disorders such as ischemia,[23-25] could be used in the treatment of neurodegenerative diseases. Other LTCC blockers such nitrendipine, verapamil and diltiazem has also demonstrated the ability to attenuate excitotoxicity caused by an increase in $[Ca^{2+}]_i$.[20, 21] However, LTCC blockers can only be used in acute neurological disorders such as ischemia due to its cardiological side effects that can lead to hypotension.[20, 26]

The complementary and/or synergistic neuroprotective effect of using VGCC antagonists and NMDAR channel blockers in combination has also been demonstrated in animal models of cerebral ischemia.[27-31] However, LTCC blockers such as nimodipine and NMDAR channel blockers such as MK-801 have a side effect profile the renders them of limited value in a clinical setting.[20, 32, 131] It might be of greater value to have a low-affinity, use-dependent dual mechanistic drug with the

ability to modulate Ca^{2+} influx through both ion channel types. Only in recent years has the concept of a single molecule with multiple mechanisms, that could be used to address multiple diseases targets in the same pathology, gained impetus in drug discovery.[33-35] These drugs are called multifunctional or multimechanistic drugs and holds an advantage in cases such as ischemic stroke where a combination of therapies have been shown to be beneficial.[36]

Our interest in neuroprotective agents with multiple mechanisms of actions was prompted with the discovery that NGP1-01 (**7a**), a member of the pentacycloundecylamines initially characterized as an LTCC blocker,[38, 132] also had activity as a potent uncompetitive NMDAR channel blocker.[42, 43] Further studies investigated the ability of both the pentacycloundecylamines and triquinylamines to modulate Ca^{2+} influx through either the NMDA receptor or the LTCC.[39-43] These studies revealed that most of these polycyclic compounds have the ability to modulate Ca^{2+} entry through both the NMDA receptor and the LTCC and established NGP1-01 (**7a**) as the lead compound. NGP1-01 has also been proven to be neuroprotective *in vivo* using the middle cerebral artery occlusion mouse model of stroke,[44] and also offer protection in a transient model of stroke following reperfusion.[45] Numerous studies have been done to elucidate the NMDAR channel blocking activity and determine the IC_{50} values of NGP1-01 and several other pentacycloundecane derivatives,[42] however the IC_{50} values for LTCC blocking activity has not yet been determined for a full series of derivatives. This study was designed to observe the effects of a series polycyclic compounds on LTCCs by their ability to attenuate rises in $[Ca^{2+}]_i$ and to report their IC_{50} values. Ca^{2+} influx was determined by a high-throughput fluorescence microplate assay utilizing Fura-2/AM in rat undifferentiated PC12 cells. Additionally, we evaluate several methods to assess the ability of these compounds to offer protection against induced cell death by means of the LDH, MTT and trypan blue staining assays.

3.2 Experimental

3.2.1 Chemistry

In order to perform the complex thermal fragmentation reaction (Scheme 2, step a) from pentacyclo[5.4.0.0^{2,6}.0^{3,10}.0^{5,9}]undecane-8-11-dione (**4**) to tricyclo[6.3.0.0^{2,6}]undecane-4,9-diene-3,11-dione (**9**), we designed and build the flash vacuum pyrolysis (FVP) apparatus (Figure 3.1 a-b) from descriptions given in literature;[100, 133] as part of a previous study. Much was learned from performing the synthesis and as part of the present study we redesigned the FVP apparatus (Figure 3.1 c-f) and made several improvements to simplify and optimize the synthesis of the triquinane. The improvements made to the apparatus also added to the safety of performing this complicated synthesis, which is subjected to extreme conditions. The first adjustment we made was to the cold finger of the liquid nitrogen cold trap. We noticed that with the rapid cooling after sublimation the formation of the resulting crystals quickly clogged up the neck of the collecting tube. This would result in the remainder of the pyrolysate being unable to pass through and being turned into tar by prolonged exposure to the extreme heat from the pyrolysis furnace. To resolve this problem we widened the neck of the collection tube just below the joint, which allowed more pyrolysate to pass through the neck and crystallize at the bottom of the tube.

Instead of using heating tape to initiate sublimation as described in our previous study,[101] we built a second furnace to heat the sublimation tube (compare Figure 3.1 b to d). We encountered numerous problems using the heating tape in the first design. Since only 1g can be sublimated at a time, it meant that we had to wait for the heating tape to cool down in order to be removed before the next sublimation tube could be placed. This was a very time consuming process and had a through-put time of about 75 minutes to an hour. The sublimation through-put rate was approximately 45 minutes and thereafter it took about 30 minutes to allow for sufficient cooling and changing of the sublimation tube. The heating tape was also not insulated very well which resulted in heat loss during the heating process. The heating tape would also crack after repeated use and expose the wires, which posed the risk of electrical shock

and short circuiting. To resolve this problem we designed a second furnace that could slide over the sublimation tube (Figure 3.1 e). The second furnace was well insulated and did not have to cool down between sublimations. The sublimation furnace gave more rapid and even heating, resulting in more starting material being sublimated successfully and less tar formation. We still had to use heating tape just after the pyrolysis furnace to prevent the pyrolysate from crystallizing in the neck before the freeze fall. Instead of using silicone heating tape as in the previous study, we used a heavy insulated fiberglass mess type of heating tape. We also added extra Shinko Ramp/Soak Auto tune PID controllers (Wika Instruments, Johannesburg, South Africa), to control the sublimation furnace and heating tape in addition to the pyrolysis furnace. These gave us the ability to slowly ramp up the temperature for even safe heating and more control at keeping the temperature constant. The temperature was measured with K-type thermocouples which were connected to the PID controllers. The last addition we made was an electronic vacuum gauge for more accuracy, since the performing the synthesis under a vacuum of 1 torr is the critical determining factor for the success of this synthesis.

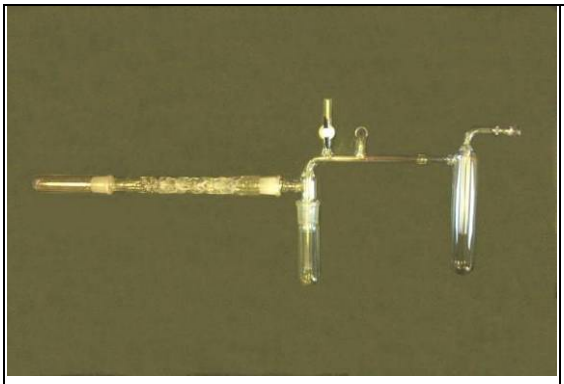

a

b

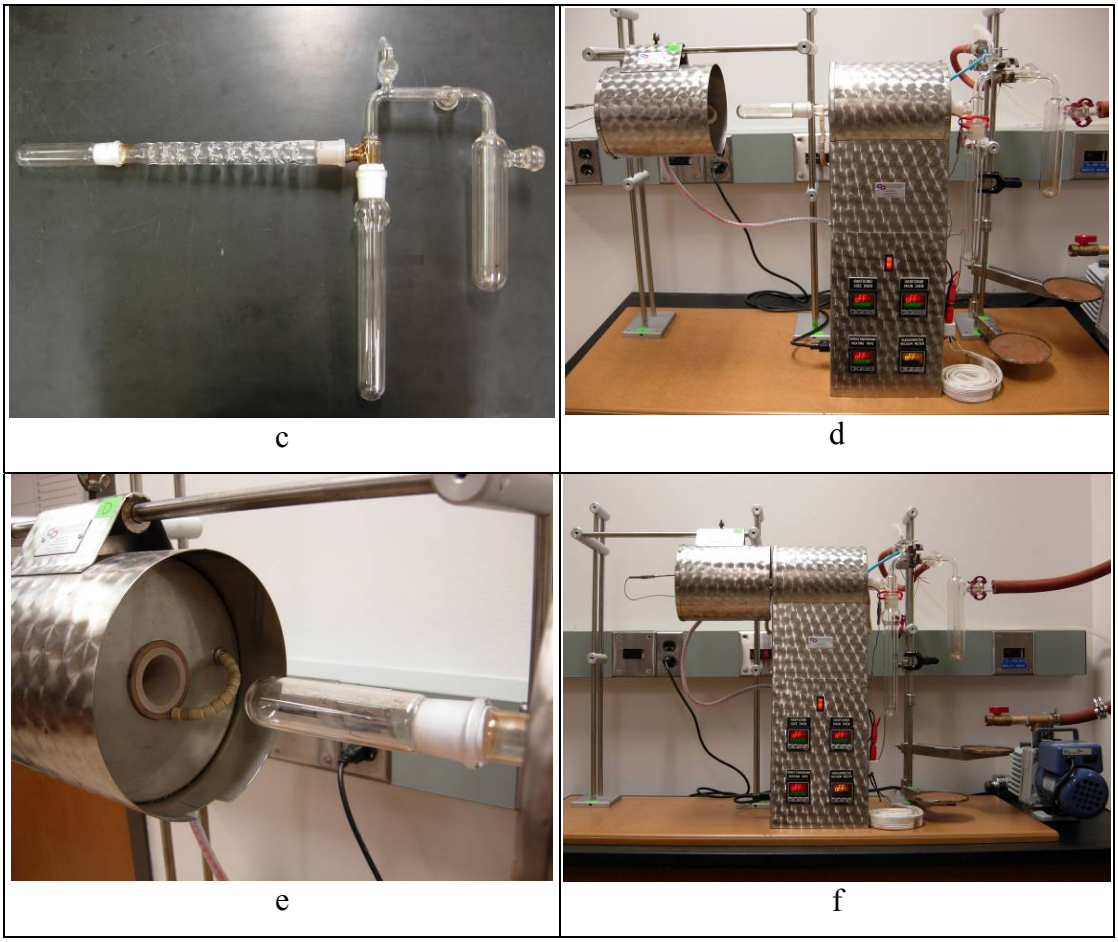

Figure 3.1. Comparison between previous versions (a and b) of the apparatus for flash vacuum pyrolysis (FVP) and the updated version (c-f).

3.2.2 Cell culture

Undifferentiated rat pheochromocytoma (PC12) cells obtained from the American Type Culture Collection (ATCC, Manassas, VA, USA) were used in this study. PC12 cells were cultured in 75 cm^2 tissue culture treated flasks containing RPMI-1640 media (Hyclone, Fisher Scientific, USA) supplemented with 5% fetal bovine serum, 10% horse serum, 0.5% penicillin/streptomycin/amphotericin B, and 1% (2.05 mM) L-glutamine. The medium was formulated for use with 5% CO_2 at 37 ºC. Culture media were changed every 3 days and cells were sub cultivated twice a week.

3.2.3 Evaluation of calcium influx

Procedures similar to those in published studies were used to prepare cell cultures, loading of cells with the fluorescence dye, and to establish the techniques for experimental measurement of Ca^{2+}-related fluorescence.[99, 111, 113, 134-137] These procedures are described in more detail below.

3.2.3.1 Solutions

The acetoxymethyl ester (AM) derivative of Fura-2, and Pluronic F-127 (as a 20% solution in anhydrous dimethyl sulfoxide [DMSO]), were obtained from Invitrogen (Carlsbad, CA, USA). Hanks balanced salt solution (HBSS), used for cell loading and washing, was purchased from Fisher Scientific (Pittsburgh, PA, USA). Buffer constituents were obtained from a selection of commercial sources.

3.2.3.1.1 Fluorescent indicator stock solution (1 mM): 50 µl anhydrous DMSO/Pluronic F-127 were added to 50 µg of the Ca^{2+} indicator (Fura-2/AM). Pluronic F-127 is often used to facilitate cell loading, and is a non-ionic dispersing agent that assists solubilizing of large dye molecules in physiological media. The solution was then vortexed to properly disperse fluorescent dye and covered with aluminum foil to protect from light.

3.2.3.1.2 Loading solution: 50 µl of the fluorescent indicator stock solution (1 mM) was dispersed in 10 ml HBSS to which 50 mg bovine serum albumin (BSA) was added. The solution was vortexed to assist dispersion of the indicator. The final concentration of the fluorescent indicator was 5 µM, which yielded a sufficient amount to load one 96 well plate with 100 µl per well or two 96 well plates with 50 µl per well. The solution was protected from light, and only freshly made solution was used to load cells.

3.2.3.1.3 Test compound solution: 0.1 M, 10^{-2} M, 10^{-3} M, 10^{-4} M, 10^{-5} M, 10^{-6} M and 10^{-7} M stock solutions were prepared by dissolving the compound to be tested in anhydrous DMSO. Loading solutions were prepared by diluting 1 µl of each

stock solution in 1 ml HBSS to give 100 μM, 10 μM, 1 μM, 0.1 μM, 10^{-2} μM, 10^{-3} μM and 10^{-4} μM concentrations of the test compound (highest final concentration DMSO in incubations = 0.1%). The loading solution (200 μM) was prepared by adding 2 μl of the 0.1 M stock solutions in 1 ml HBSS. These serial dilutions allowed us to obtain a dose-response profile and calculate the IC_{50} values of the compounds evaluated.

3.2.3.1.4 Depolarizing solution: consisted of 43 mM NaCl, 100 mM KCl, 10 mM $NaHCO_3$, 1.4 mM $CaCl_2$, 0.9 mM $MgSO_4$, 5.5 mM Glucose, and 20 mM HEPES. The pH was adjusted to 7.4 with NaOH.

3.2.3.1.5 HEPES buffered salt solution or Hanks balanced salt solution (HBSS): HBSS, for loading and washing consisted of 137 mM NaCl, 5 mM KCl, 10 mM $NaHCO_3$, 0.6 mM KH_2PO_4, 0.6 mM Na_2HPO_4, 1.4 mM $CaCl_2$, 0.9 mM $MgSO_4$, 5.5 mM Glucose, and 20 mM HEPES. The pH was adjusted to 7.4 with NaOH.

3.2.3.2 Experimental design

In order to determine if compounds under investigation have the ability to block the LTCC, Ca^{2+} influx was measured by means of a 96-well based high through-put fluorescence assay, utilizing Fura-2/AM as fluorescent probe (Invitrogen™, Molecular Probes™, Eugene, OR, USA). This protocol was based on similar protocols reported in the literature.[109, 113, 138] PC12 cells were plated at a density of 1×10^5 cells per well (100 μl) 24 h prior to conducting the experiments. Seeding was done in black, clear-bottomed 96-well tissue culture treated plates (Costar, Corning, NY, USA) and cultured overnight. Cultures were washed and then loaded with Fura-2/AM (5 μM) in HBSS containing Ca^{2+}, Mg^{2+} and 10% BSA. Pre-incubation with compounds to be evaluated (concentrations ranging from 0.0001 μM to 200 μM, to obtain a dose-response profile) was conducted in HBSS over a 10 min period. The fluorescence was read on a BioTech Synergy 4 microplate reader (Winooski, VT, USA), with the excitation wavelengths set at 340 and 380 nm and the emission wavelength set at 510 nm. After recording for 10 sec cells were depolarized with a

high concentration KCl (50 mM). Ca^{2+} influx through the LTCC was measured (n = 3) and the IC_{50} values were calculated from the dose-response curves.

3.2.3.3 Loading cells with calcium Fura-2/AM and test compounds

The dye loading solution was prepared immediately before use, as described previously in the text, to prevent hydrolysis due to the unstable nature of Fura-2/AM. Dye loading was conducted in a dark room to prevent photodecomposition of the photo labile dye solution. Before loading, the media was aspirated and cells were washed twice with HBSS preheated to 37 °C. Culture medium containing serum should not be used during staining, as serum may contain esterase activity. From this point on, cell were maintained in HBSS containing Ca^{2+}, Mg^{2+} and 10% BSA. The 96-well plates were loaded with 95 µl of dye solution in each well and incubated for 30 min at 37 °C. These variables were adjusted to optimize the dynamic response to stimulation, and to limit sequestration of the indicator into intracellular compartments. After the loading period, the loading solution was aspirated and cells were gently washed twice with PBS (37 °C) to remove the excess amount of extracellular Ca^{2+} indicator. Cells were then incubated in 100 µl of HBSS for 20–30 min after loading to facilitate the de-esterification of the acetoxymethyl (AM) ester moiety of the dye. The Ca^{2+} flux assay should be conducted within an hour after loading to prevent compartmentalization and dye leakage. The dye loaded cells should be protected from light at all times to avoid photo bleaching.

Table 3.1. Experimental layout of 96-well plates for fluorescence experiments.

	1	2	3	4	5	6	7	8	9	10	11	12
A	KCl + DMSO (0.1 %)	Control [Nim] n = 2 100 µM	[Comp 1] n = 3 200 µM			[Comp 2] n = 3 200 µM			[Comp 3] n = 3 200 µM			KCl + DMSO (0.1 %)
B		100 µM	100 µM			100 µM			100 µM			
C		10 µM	10 µM			10 µM			10 µM			
D		10 µM	1 µM			1 µM			1 µM			
E	KCl + DMSO (0.1 %)	1 µM	0.1 µM			0.1 µM			0.1 µM			KCl + DMSO (0.1 %)
F		1 µM	0.01 µM			0.01 µM			0.01 µM			
G		0.1 µM	0.001 µM			0.001 µM			0.001 µM			
H		0.1 µM	0.000 1 µM			0.000 1 µM			0.000 1 µM			

For cells that were loaded with test compounds, the loading procedure commenced 20 minutes into the de-esterification incubation time. Such a protocol still allowed sufficient additional time for de-esterification to reach completion. Stock and loading solutions were prepared as described previously in text. The experimental plate layout (Table 3.1) was designed in such a manner that the plate contained a row of control experiments (in the absence of test compounds), comprising 10 minute incubation times in normal recording solution that contained 0.1% DMSO. Nimodipine (100 µM, 10 µM, 1 µM, 0.1 µM) was included as control test compound (n = 2) on every plate. The test compounds were loaded by aspirating the HBSS in which cells were incubated and adding 100 µl of the test compound solution for each concentration with a replicate of n = 3. Compounds were then incubated for 10 min and experimental recording was performed immediately after incubation.

3.2.3.4 Experimental recording

Experimental recording was done with Fura-2/AM at 37 °C and the fluorescence was read on a BioTech Synergy 4 microplate reader with injectors. The experimental parameters were set up in the kinetic run mode according to Table 3.2. Previously prepared high concentration KCl (100 mM) depolarization solution was used to purge and prime the injector. After 10 sec of recording, to initiate depolarization, 100 µl of the high concentration KCl (100 mM) was injected into 100 µl test compound solution already contained in the wells. This yielded a final concentration of 50 mM KCl. Recording was continued for another 20 sec.

Table 3.2. Recording parameters.

Fura-2/AM	
Excitation λ (nm)	340/380 nm
Emission λ (nm)	510 nm
Excitation filter sets	Set 1 - 340/11 Set 2 - 380/20
Emission filter set	508/20
Optics position	bottom
Sensitivity	100
Runtime	30 sec/well
Interval (msec)	60 msec

3.2.4 *In Silico* calculations utilizing molecular modeling

Structures of the polycyclic compounds were drawn in ACDLabs vs 11, and imported into MOE 2008.10 (Chemical Computing Group) where they were energy minimized using the MMFF94s force field, to an RMS gradient of 0.1. To develop the quantitative structure-activity relationship (QSAR) model, descriptors were generated for each compound in the MOE database. Since several descriptors can be chosen in MOE, we focused on those descriptors which correlate with work published recently by Gleeson,[139] where the molecular properties are those which are intuitive to

medicinal chemists. These included logP, hydrogen bond acceptors and donors, molar refractivity, molecular weight, polar surface area and heavy atom count. The QuaSar-module in MOE was used to generate the multiple linear regression models, to correlate the structural properties of this set of compounds with their Ca^{2+} channel blocking activities. The equation used in calculations was: $p\mathrm{IC}_{50} = -12.26 + 1.69b$, heavy – 0.17 weight + 0.14TPSA + 6.02log*P* + 3.49log*S*.

3.2.5 Measurement of LDH release

3.2.5.1 Experimental design

We developed the LDH assay according to procedures similar to those in publications and as described in manufacturer's protocols.[122, 140] Apoptosis can be assayed by evaluating the plasma membrane damage of PC12 cells and measuring the amount of LDH released in the media. Forty eight hours before the experiment, cells were seeded in clear, flat-bottomed 96-well tissue culture treated plates (Costar®, Corning, NY, USA) at a density of 1×10^5 cells per well (100 µl), and incubated for 24 hours. Media was then switched to serum-deprived media containing (1%) serum and incubated for a further 24 hour. A 10 min pre-incubation with compounds to be evaluated (1, 10 and 100 µM) was done 30 min prior to treatment with 200 µM H_2O_2. We also evaluated the compounds in the absence of H_2O_2 at 10 and 100 µM to assess if the compounds had any inherent toxicity. LDH leakage was measured after the 24 h exposure to H_2O_2, obtained from Sigma-Aldrich (St. Louis, MO, USA). The culture supernatant (100 µl) was collected from each well and the LDH activity was determined according to the manufacturer's protocols using a colorimetric LDH cytotoxicity assay kit that was obtained from Cayman® (Ann Arbor, MI, USA). The absorbance was measured at 490 nm using a microplate reader (Molecular Devices SpectraMax® 340PC^{384} microplate reader, Sunnyvale, CA, USA).

3.2.5.2 Treatments and assay

A 1 M stock solution of H_2O_2 was prepared with Millipore®-filtered H_2O from 30 % H_2O_2 (9.79 M) and diluted to the final applied concentrations, in media. For compounds to be evaluated, 0.1 M stock solutions were prepared in DMSO and diluted to their final applied concentrations with media (highest concentration of DMSO ≤ 0.1 %). In some of the wells the PC12 cells were treated with 10 and 100 µM concentrations of the individual compound without other additions, to assess the effect of compound only on cell viability. Where the ability of test compounds to afford protection against cell death were evaluated, cells were pre-incubated for 10 min with 1, 10 and 100 µM of compound and then treated with 200 µM H_2O_2 to induce apoptosis.

Table 3.3. Experimental layout of 96-well plates for LDH experiments.

	1	2	3	4	5	6	7	8	9	10	11	12
A	Standard 1	Standard 2	Standard 3	Standard 4	Standard 5	Standard 6 Blank	Comp 2, 1µM (n = 3) + H_2O_2			Comp 4, 100µM (n = 3) + H_2O_2		
B	Standard 1	Standard 2	Standard 3	Standard 4	Standard 5	Standard 6 Blank	Comp 3, 100 µM (n = 3)			Comp 4, 10µM (n = 3) + H_2O_2		
C	Control Cells only	Control Cells only	Control Cells only	Comp 1, 10µM (n = 3) + H_2O_2			Comp 3, 10 µM (n = 3)			Comp 4, 1µM (n = 3) + H_2O_2		
D	Control Triton	Control Triton	Control Triton	Comp 1, 1µM (n = 3) + H_2O_2			Comp 3, 100µM (n = 3) + H_2O_2			Comp 5, 100 µM (n = 3)		
E	Control H_2O_2	Control H_2O_2	Control H_2O_2	Comp 2, 100 µM (n = 3)			Comp 3, 10µM (n = 3) + H_2O_2			Comp 5, 10 µM (n = 3)		
F	Comp 1, 100 µM (n = 3)			Comp 2, 10 µM (n = 3)			Comp 3, 1µM (n = 3) + H_2O_2			Comp 5, 100µM (n = 3) + H_2O_2		
G	Comp 1, 10 µM (n = 3)			Comp 2, 100µM (n = 3) + H_2O_2			Comp 4, 100 µM (n = 3)			Comp 5, 10µM (n = 3) + H_2O_2		
H	Comp1, 100µM (n = 3) + H_2O_2			Comp 2, 10µM (n = 3) + H_2O_2			Comp 4, 10 µM (n = 3)			Comp 5, 1µM (n = 3) + H_2O_2		

To obtain a standard curve; rows A and B, cells 1-6 were kept empty (without cells) and a serial dilution of the standard (provided with the assay kit) was placed in these wells as described in the provided protocol. To obtain the maximum amount of LDH, cells in rows D 1-3 were treated with Triton X-100 to lyse the cells and release all the LDH within the cells. Wells that were to be treated with compounds were pre-

incubated for 10 min by adding 100 µl of compound solution (2, 20 and 200 µM) in replicates of three, to the 100 µl volume of media already present in the individual wells. This procedure resulted in final dilutions corresponding to 1, 10 and 100 µM. After 10 min, wells that were destined to receive treatment to induce apoptosis were aspirated and 100 µl of the compound solution (2, 20 and 200 µM) was added back. Thereafter, 100 µl of H_2O_2 (400 µM) was added to render final dilutions of 1, 10 and 100 µM of the test compound and 200 µM of H_2O_2. The cytotoxins remained in the wells and the cells were incubated for another 24 hours. After the 24 hour exposure period the 96-well plate was centrifuged at 400 × G and 100 µl of the media was collected. The amount of LDH released by the cells was determined by using an assay kit (Cayman®, Ann Arbor, MI, USA) according to the manufacturer's protocol. The absorbance of the samples was read at 490 nm with a microplate reader (Molecular Devices SpectraMax® 340PC^{384}, microplate reader Sunnyvale, CA, USA).

3.2.6 Measurement of MTT reduction

3.2.6.1 Experimental design

Procedures similar to those in published studies and described in manufacturer's protocols were used to prepare cell cultures and to establish the techniques for experimental measurement of apoptosis by measuring the reduction of the yellow MTT, obtained from Sigma-Aldrich (St. Louis, MO, USA), to dark purple formazan crystals in metabolically active cells.[121, 122] Twenty four hours before the experiment, cells were seeded in clear, flat-bottomed 96-well tissue culture treated plate (Costar®, Corning, NY, USA) at a density of 1×10^5 cells per well (100 µl), and incubated for 24 hours. MTT reduction was determined in the absence and presence of test compound. A 10 min pre-incubation was done 30 min prior to treatment with 200 µM H_2O_2 with compounds to be evaluated at 0.1, 1, 10 and 100 µM. We also evaluated the compounds in the absence of H_2O_2 at 0.1, 1, 10 and 100 µM to assess if these compounds had any inherent toxicity. MTT reduction was measured after 24h exposure of PC12 cells to 200 µM H_2O_2 by adding 5 mg/ml MTT, to each well and incubating for 2 hours. After the 2 hour incubation, the media was carefully removed and 100 the µl DMSO was added to dissolve the purple formazan crystals and cells.

The absorbance was read at 570 nm with a microplate reader (Molecular Devices SpectraMax® 340PC^{384} microplate reader, Sunnyvale, CA, USA). Cell viability was expressed as a percentage of control (untreated cells).

3.2.6.2 Treatments and assay

The following stock solution was prepared immediately before use: a 1 M stock solution of H_2O_2 was prepared with Millipore®-filtered H_2O from 30 % H_2O_2 (9.79 M) and diluted to the final applied concentrations, in media. For compounds to be evaluated, 0.1 M stock solutions were prepared in DMSO and diluted to their final applied concentrations with media (highest concentration of DMSO ≤ 0.1 %). In some of the wells the PC12 cells were treated (n = 3) with 0.1, 1, 10 and 100 μM concentrations of the individual compound without other additions, to assess the effect of compound only on cell viability. Cells were also pre-incubated for 10 min with 0.1, 1, 10 and 100 μM of compound and then treated with 200 μM H_2O_2 to induce apoptosis and evaluate the ability of test compounds to afford protection against cell death.

For comparison we had two controls where cells were left untreated and where cells were treated with H_2O_2 only. Wells that were to be treated with compounds were pre-incubated for 10 min by adding 100 μl of compound solution (0.2, 2, 20 and 200 μM) in replicates of three, to the 100 μl volume of media already present in the individual wells. This procedure resulted in final dilutions corresponding to 0.1, 1, 10 and 100 μM. After 10 min, wells that were destined to receive H_2O_2 treatment to induce apoptosis were aspirated and 100 μl of the compound solution (0.2, 2, 20 and 200 μM) was added back. Thereafter, 100 μl of the cytotoxin (400 μM H_2O_2) was added to render final dilutions of 0.1, 1, 10 and 100 μM for the compounds evaluated and 200 μM H_2O_2. The cytotoxin remained in the wells and the cells were incubated for another 24 hours. After the exposure period, 50 mg MTT was dissolved in 10 ml PBS and 100 μl was added to each well. The plate was incubated while mixing at 37 °C for 2 hours. Thereafter the media was removed by carefully aspirating; taking care not to disrupt the cell monolayer, 100 μl DMSO was added to each well to

dissolve the formazan crystals. This produced a purple solution of which the absorbance was read at 570 nm with a microplate reader.

Table 3.4. Experimental layout of 96-well plates for MTT experiments.

	1	2	3	4	5	6	7	8	9	10	11	12
A	Control Cells only	Comp 1, 100µM (n = 3) + H_2O_2			Comp 2, 100µM (n = 3) + H_2O_2			Comp 3, 100µM (n = 3) + H_2O_2			Blank	Blank
B	Control Cells only	Comp 1, 10µM (n = 3) + H_2O_2			Comp 2, 10µM (n = 3) + H_2O_2			Comp 3, 10µM (n = 3) + H_2O_2			Blank	Blank
C	Control Cells only	Comp 1, 1µM (n = 3) + H_2O_2			Comp 2, 1µM (n = 3) + H_2O_2			Comp 3, 1µM (n = 3) + H_2O_2			Blank	Blank
D	Control Cells only	Comp 1, 0.1µM (n = 3) + H_2O_2			Comp 2, 0.1µM (n = 3) + H_2O_2			Comp 3, 0.1µM (n = 3) + H_2O_2			Blank	Blank
E	Control H_2O_2 only	Comp 1, 100µM (n = 3)			Comp 2, 100µM (n = 3)			Comp 3, 100µM (n = 3)			Blank	Blank
F	Control H_2O_2 only	Comp 1, 10µM (n = 3)			Comp 2, 10µM (n = 3)			Comp 3, 10µM (n = 3)			Blank	Blank
G	Control H_2O_2 only	Comp 1, 1µM (n = 3)			Comp 2, 1µM (n = 3)			Comp 3, 1µM (n = 3)			Blank	Blank
H	Control H_2O_2 only	Comp 1, 0.1µM (n = 3)			Comp 2, 0.1µM (n = 3)			Comp 3, 0.1µM (n = 3)			Blank	Blank

3.2.7 Measurement of Trypan blue exclusion

3.2.7.1 Experimental design

Conditions, plate layout and treatments under which this assay was performed were the same as for the LDH assay. Cell death was induced by 200 µM H_2O_2 and concentrations and treatment conditions for the pre-incubation with test compounds were also the same as for the LDH assay. After 100 µl of media was removed to perform the LDH assay the cultures were treated with trypan blue 0.4% (Mediatech®, obtain from Fisher Scientific, Pittsburgh, PA, USA). Thus after the 24 h exposure to 200 µM H_2O_2, the cultures were exposed to trypan blue for 30 min by adding 5 µl of Trypan blue to 100 µl of media in the well. Cell injury was estimated by examining the cultures with a phase-contrast microscope (Vista Vision™, VWR, Bridgeport, NJ,

USA). Based on the principle that viable cells with intact cell membranes will exclude the dye, under the microscope these cell will have a clear cytoplasm whereas the cytoplasm of a nonviable cell will be stained blue. These cells can then be counted to determine the percentage viable and nonviable cells. Triton X-100 (11 % v/v) was used to induce 100 % cell death as a control.

3.2.7.2 Microscopy analysis

Since cell are adherent and not in suspension we could not use a hemacytometer to perform the cell counting. The 96-well plate was place on the stage of the microscope and an image was captured of each well for each specific treatment condition using the CCD camera mounted on the phase contras microscope. The images were then imported into Excel (Microsoft® Office 2003, USA) and a specially designed grid (similar to that of a hemacytometer) was overlaid onto the image to assist counting. These cells can then be counted to determine the percentage viable and nonviable cells. Values represent means ± SEM (n = 3, counted 2 fields per repeat), and was presented as percentage of cells stained. Each well contained approximately 1×10^5 cells and the microscopic field was assessed at magnification ×20.

3.2.8 Fluorescence microscopy analysis of Annexin V-FITC staining

3.2.8.1 Experimental design

Immunohistochemistry techniques were utilized to facilitate visual confirmation aimed at determining whether selected compounds have the ability to protect against cellular toxicity, including apoptotic processes. Procedures similar to those reported in publications and described in manufacturer's protocols were used to prepare the cell cultures and establish the techniques for measurement of Annexin V-FITC fluorescence.[125, 141] Cells were seeded 24 hours before experiments into 8-well, collagen type 1 coated culture slide (BD Bioscience, Bedford, MA, USA) at a density of 1×10^5 cells per well (500 µl). The Annexin V-FITC Fluorescence Microscopy Apoptosis Detection Kit, obtained from BD Biosciences Pharmingen™ (San Jose, CA, USA) was used to perform the staining according to the manufacturer's protocol.

Slides were fixed with Vectashield® Hardset™ (Vector Laboratories, Burlingame, CA, USA) mounting medium which contained DAPI to stain nuclei. Fluorescence was observed with an Olympus Provis AX-70 fluorescence microscope (objective: 20×, NA 0.7), and images were capture with a SPOT Digital Camera (Diagnostics Instruments, Sterling Heights, MI). Excitation and emission of each fluorophore were obtained using the respective filters: for DAPI, excitation occurred at 360 nm and emission at 460 nm; and for FITC excitation occurred at 494 nm and emission at 519 nm.

3.2.8.2 H_2O_2 treatment

Table 3.5. Experimental layout of 8-well plate for Annexin V-FITC experiments.

(1) Control untreated	**(2) Control H_2O_2 200 µM**	**(3) Comp 1, 100 µM + H_2O_2 200 µM**	**(4) Comp2, 100 µM + H_2O_2 200 µM**
(5) Control Staurosporine (1 µM)	**(6) Control H_2O_2 100 µM**	**(7) Comp 1, 100 µM**	**(8) Comp 2, 100 µM**

The following stock solutions were prepared immediately before use: a 1 M stock solution of H_2O_2 was prepared with Millipore®-filtered H_2O from 30 % H_2O_2 (9.79 M) and diluted to a final concentration with media. A 0.1 M stock solution of each individual compound to be tested was prepared with DMSO, and diluted to a final concentration with media (highest concentration of DMSO ≤ 0.1 %). Cells in well 1 were left untreated to serve as controls; while cells in wells 2, 5 and 6 were treated for 24 h to undergo apoptosis with either H_2O_2 (100 and 200 µM) or staurosporine (1 µM), both obtained from Sigma-Aldrich (St. Louis, MO, USA). These cells served as controls for apoptosis. Cells in wells 3 and 4 were treated with the individual compounds, and with 200 µM H_2O_2 to induce cell death. These experiments evaluated the ability of individual test compounds to offer protection against cell death. The cells in the latter set of wells were pre-incubated for 10 min with 250 µl media and 250 µl compound solution (200 µM, to render a final dilution of 100 µM). After the 10 min pre-incubation, wells 3 and 4 were aspirated and 250 µl

compound solution (200 µM, to render a final dilution of 100 µM) was added back into the wells together with 250 µl H_2O_2 (400 µM, to render a final dilution of 200 µM) and incubated for 30 min. Thereafter, the treatment was switched to 250 µl media as well as 250 µl compound solution (200 µM, to render a final dilution of 100 µM), which remained in the wells until staining. Cells in well 2 and 6 were also treated with H_2O_2 for 30 min, after which the solution was substituted with 500 µl media. Cells in wells 7 and 8 were treated with compound only by adding 250 µl media as well as 250 µl compound (200 µM, to render a final dilution of 100 µM), to asses if the compounds have any inherent toxicity. After completion of the treatment protocols, the 8-well culture slides were incubated in normal media for 24 hours and then stained with Annexin V-FITC described in the manufacturer's protocol.

3.2.8.3 Staining protocol

The staining protocol was performed according to the manufacturer's protocol. In summary, the 10× binding buffer was diluted 1 part to 9 parts of distilled H_2O. PBS (containing Ca^{2+}) 10× was diluted 1 part to 9 parts of distilled H_2O. Annexin V-FITC fluorescent dye was diluted 1:10 in the 1× binding buffer; thus for 8-wells (2.5 ml total), 250 µl Annexin V-FITC was added to 2.25 ml binding buffer. Before staining cells were washed twice with 1× PBS and then once again with 1× binding buffer. The cells were then stained with 250 µl diluted Annexin V-FITC for 15 min at room temperature, after which work proceeded in the dark under a red light to prevent photodecomposition. After staining, the cells were washed once with 1× binding buffer. All liquids were aspirated and the 8-well chamber was removed from the slide with a special tool provided with the kit. Following removal of the chamber, the slide was fixed by placing two drops of Vectashield® Hardset™ mounting medium containing DAPI on each chamber on the slide. The slides were coverslipped with a 22 × 50 mm, 1.5 mm microscope cover glass (Fisherbrand, Fisher Scientific, Pittsburgh, PA, USA), taking care to remove all air bubbles.

3.2.8.4 Microscopy protocol

Fluorescence was observed with an Olympus Provis AX-70 fluorescence microscope (objective: 20×, NA 0.7) and images were captured with a SPOT Digital Camera (Diagnostics Instruments, Sterling Heights, MI). Excitation and emission wavelengths for each fluorophore were obtained using the respective filters: For DAPI, excitation occurred at 360 nm and emission at 460 nm; and for FITC, excitation occurred at 494 nm and emission at 519 nm.

3.2.9 Statistical analysis

For the Ca^{2+} influx assay all experimental results are presented as the mean ± SDEV. Analyses were performed and graphs drawn in Excel (Microsoft® Office 2003, USA). For the calculation of IC_{50} values the analyses were performed and graphs were drawn in Prism 3.0 (Graph Pad, San Diego, CA), and results presented as the mean ± SDEV. For the LDH, MTT and Trypan blue staining assays all experimental results are presented as the mean ± SEM and statistical significance of differences between the means was determined by one-way ANOVA analysis followed by Dunnett's *post hoc* test to compare relevant groups with controls. Where the compounds were evaluated by themselves, comparisons were done with control of untreated cells. Where compounds were evaluated in the presence of H_2O_2, the comparisons were done with the control of H_2O_2 treatment alone. The level of statistical significance was taken at $^{+}P < 0.05$ and $^{++}P < 0.01$. Prism 3.0 (Graph Pad, San Diego, CA) statistical software was used to perform analyses.

3.3 Results and Discussion

3.3.1 Chemistry

The synthesis of the three series of compounds evaluated in this study has been previously accomplished by our group.[40, 97, 99, 142] For further evaluation in this study we selected a series of aza-pentacycloundecylamines (**8a-c**), oxa-pentacycloundecylamines (**7a-e**) and aza-triquinylamines (**14 a-g**). For the

pentacycloundecylamines, **7a** served as a lead compound and our choice in **R** substituents was guided by structure-activity relationship (SAR) data from previous studies.[40, 41, 95] We redesigned and built the flash vacuum pyrolysis (FVP) apparatus (Figure 3.2), making changes to components such as the tube furnaces to heat the sublimation tube and glass components. The glass components and quartz column were all custom made. Our improvements on the design attributed to a more safe and effective synthesis, increasing in yield from the 79.8% previously reported,[99] to 81.75 %. We were also able to increase the through-put time from 1 g every 75 minutes to 1 g ever 30 minutes. Although the yield did not show a substantial increase, the reduction in through-put time was substantial and included no waiting time between sublimations.

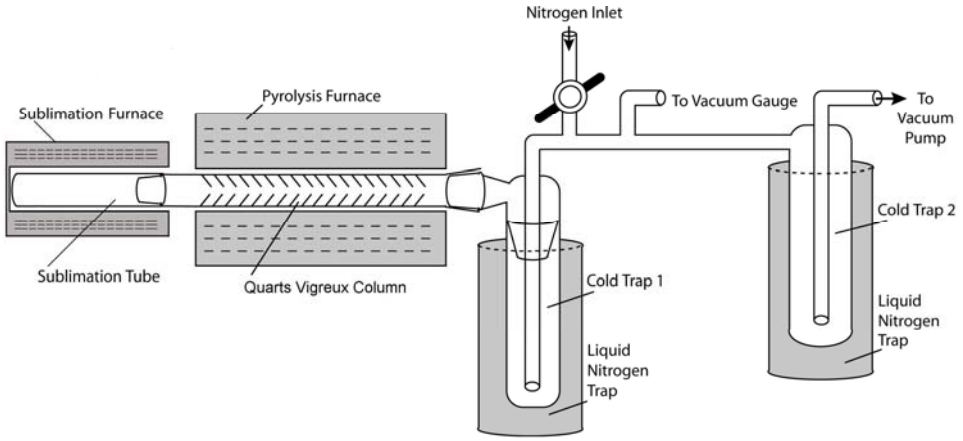

Figure 3.2. Schematic representation of apparatus for flash vacuum pyrolysis (FVP).

3.3.2 Fluorescence Measurement of Calcium Influx

To examine the ability of these compounds to modulate Ca^{2+} influx through the VGCC, and to determine their IC_{50} values, we developed a high throughput fluorescence Ca^{2+} flux assay in PC12 cells loaded with Fura-2/AM. Depolarizing the cell membrane by increasing the extracellular $[K^+]_0$ is known to increase the influx of Ca^{2+} through the VGCC.[143] PC12 cells responded to the addition of 50 mM KCl, with a rapid increase in $[Ca^{2+}]_i$. This increase was observed as a rapid rise in the F340/F380 signal, which reached a peak level within ~20 sec and then declined to an elevated

plateau that was sustained for the remainder of the recording time (Figure 3.3 a-d and Figure 3.4 a-q). Depolarization with 50 mM KCl in the absence of any test compound served as the control for normal physiological function and experiments was done in triplicate. To further characterize the Ca^{2+} influx, several known LTCC blockers were evaluated to serve as references for the amplitude of Ca^{2+} influx suppression and to confirm that LTCC were involved. We also calculated the IC_{50} values of the reference compounds for this assay. To this purpose we evaluated nimodipine, nitrendipine, verapamil and diltiazem. The behavior of all the reference compounds resembled that of nimodipine (Figure 3.3 a-d), which gave a concentration-dependent suppression of Ca^{2+} influx. We then proceeded to evaluate the ability of several polycyclic amine compounds, which included the oxa-pentacycloundecylamines (**7a-e**), aza-pentacycloundecylamines (**8a-c**) and aza-triquinylamines (**14a-g**), to suppress Ca^{2+} influx after depolarization with 50 mM KCl and calculated their IC_{50} values (Figure 3.4 a-q). The test compounds were pre-incubated for 10 min with increasing concentrations (0.0001 µM to 200 µM) before the application of 50 mM KCl. Fluorescence intensity (ratio of 340/380 nm) was normalized for each graph to start at 1 and plotted as a function of time (sec). The graphs in Figure 3.4 a-q illustrate the inhibitory potency of the compounds in a dose dependent manner.

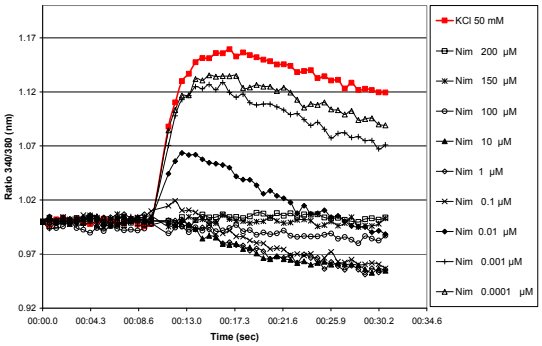

(a) Nimodipine

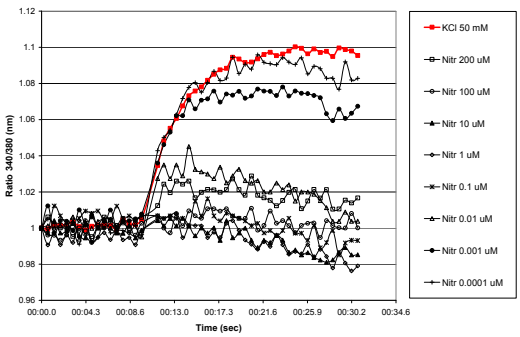

(b) Nitrendipine

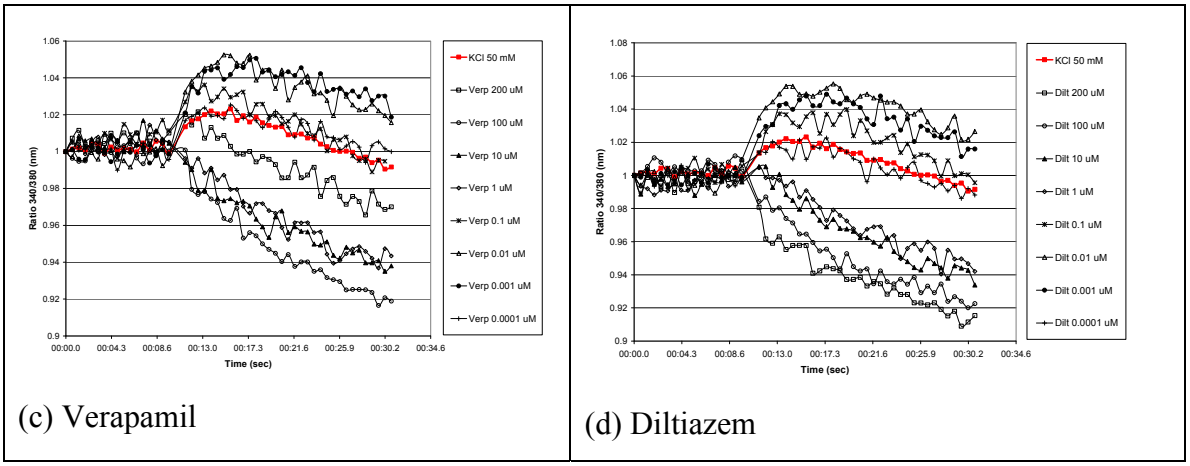

(c) Verapamil (d) Diltiazem

Figure 3.3. Antagonist inhibition of Ca^{2+} influx induced by (50 mM) KCl in the absence and presence of various concentrations of reference compounds. Fluorescence was read at 60 msec intervals for 30.8 sec using Fura-2/AM. The ratiometric (340/380 nm) measurement of the fluorescence intensity was normalized for each graph to start at 1 and plotted as a function of time (sec). Results are presented as the mean (n = 3-6) for each concentration evaluated.

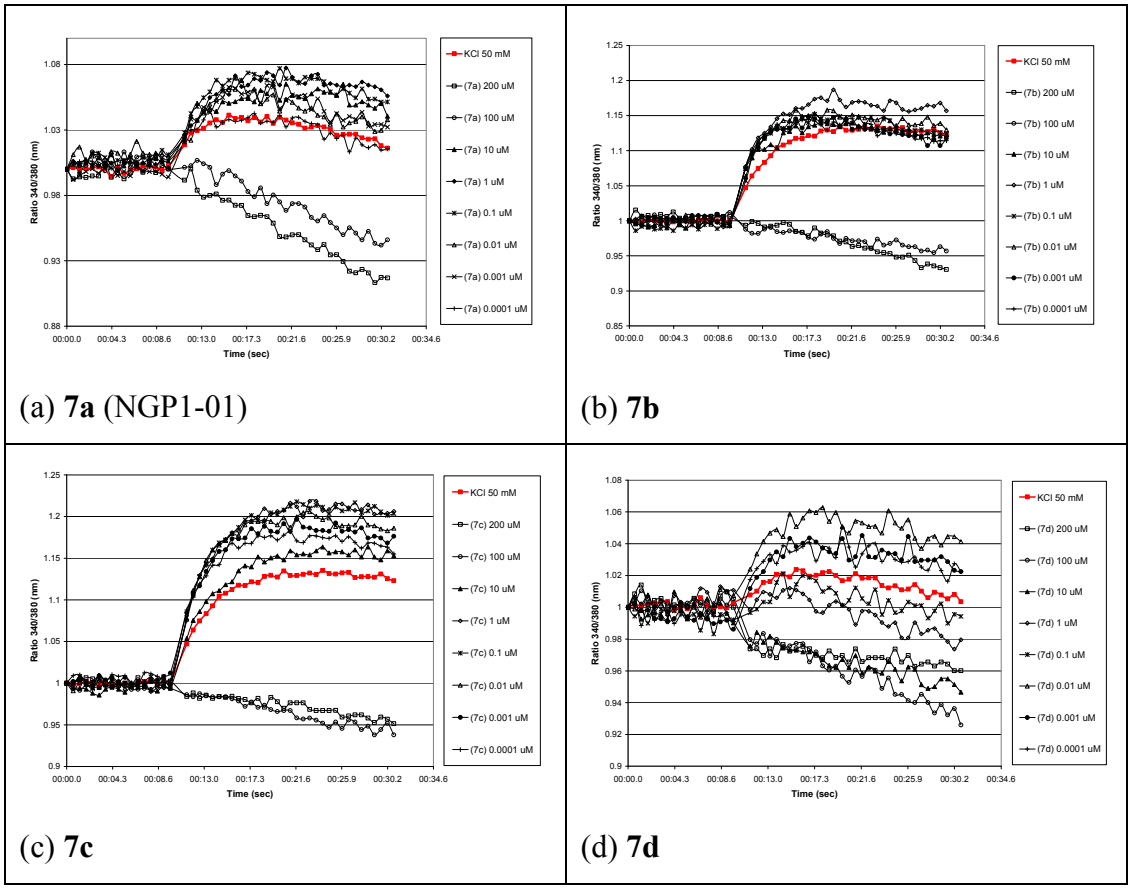

(a) **7a** (NGP1-01) (b) **7b**

(c) **7c** (d) **7d**

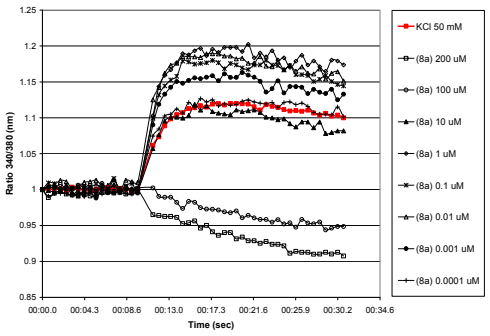

(e) **8a**

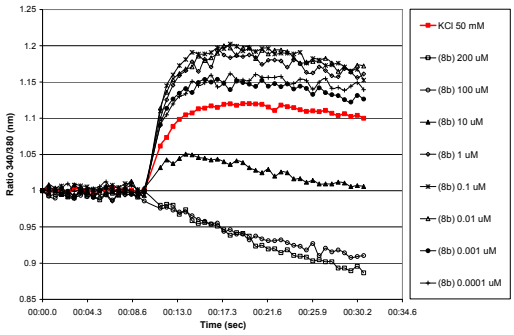

(f) **8b**

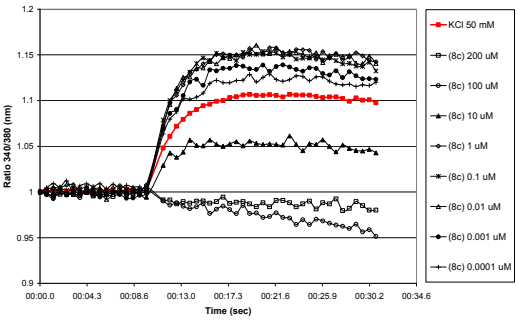

(g) **8c**

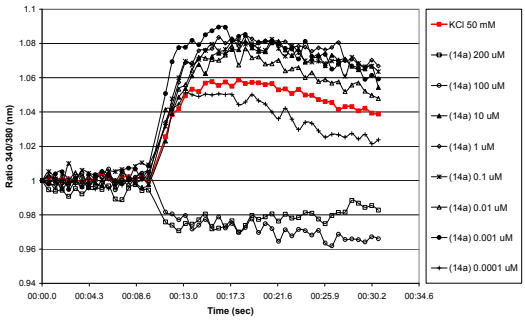

(h) **14a**

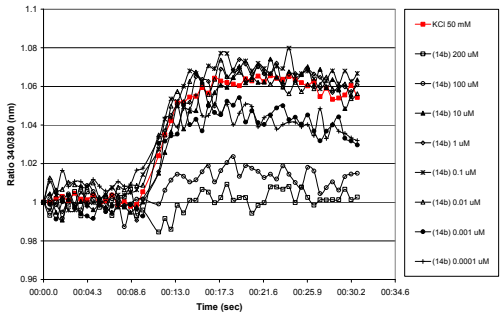

(i) **14b**

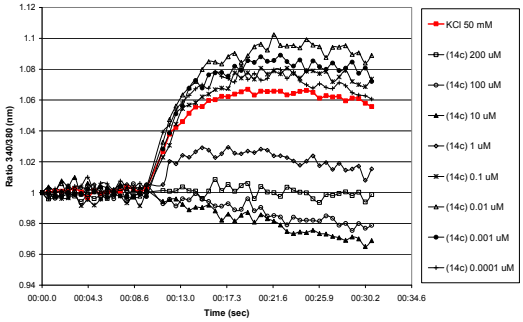

(j) **14c**

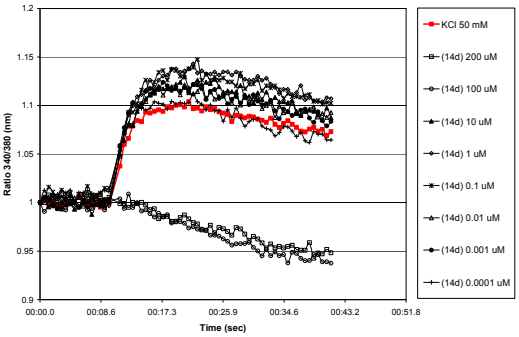

(k) **14d**

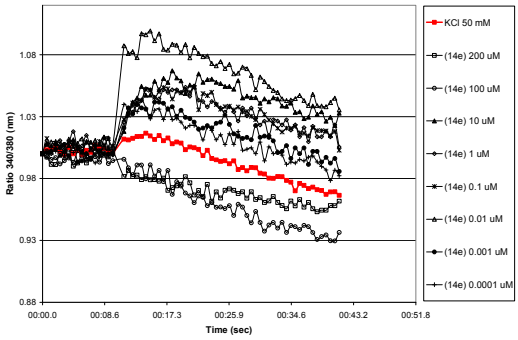

(l) **14 e**

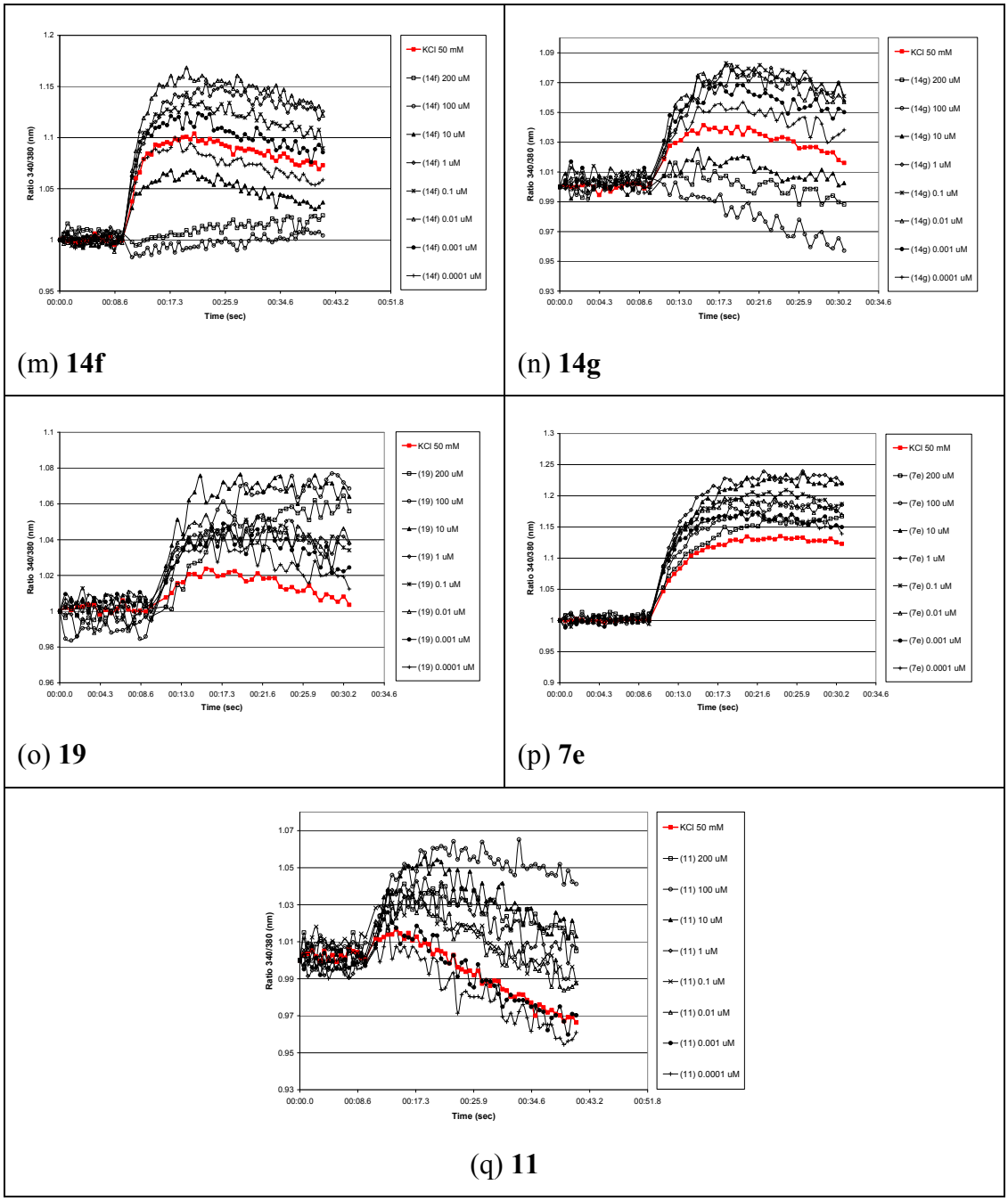

Figure 3.4. Antagonist inhibition of Ca^{2+} influx induced by (50 mM) KCl in the absence and presence of various concentrations of test compounds. Fluorescence was read at 60 msec intervals for 30.8 sec using Fura-2/AM. The ratiometric (340/380 nm) measurement of the fluorescence intensity was normalized for each graph to start at 1 and plotted as a function of time (sec). Results are presented as the mean (n = 3-6) for each concentration evaluated.

From the fluorescence results we were able to determine the functional activity for the compounds by calculating the increase from the base line to the maximum amplitude for each concentration, which were then plotted as a dose-response curve, from which the IC_{50} values could be calculated. The IC_{50} values are summarized in Table 3.7 and the log concentration-response graphs are presented in Figure 3.5 a-w.

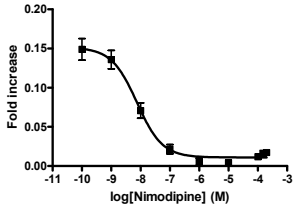

(a)

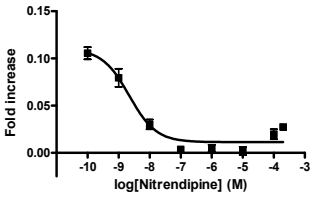

(b)

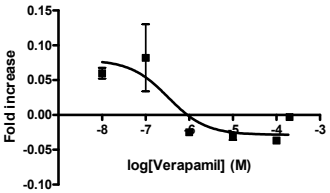

(c)

(d)

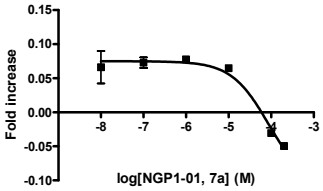

(e) 7a (NGP1-01)

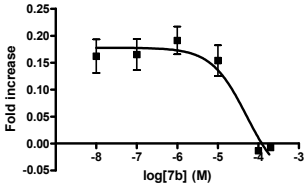

(f) 7b

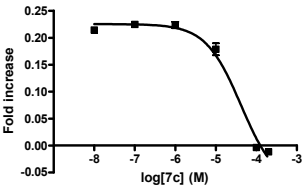

(g) 7c

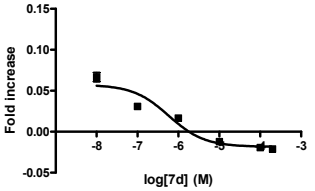

(h) 7d

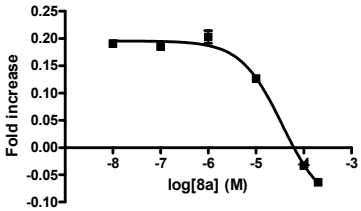

(i) 8a

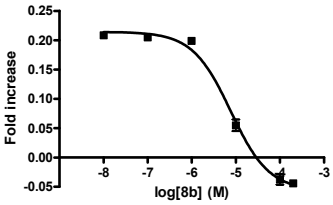

(j) 8b

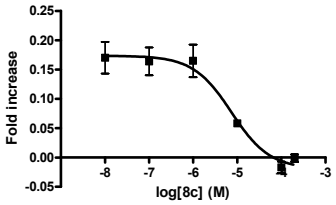

(k) 8c

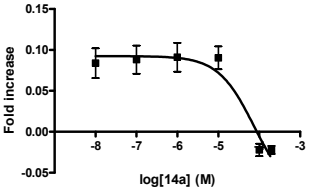

(l) 14a

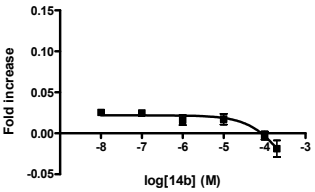

(m) 14b

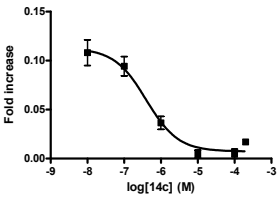

(n) 14c

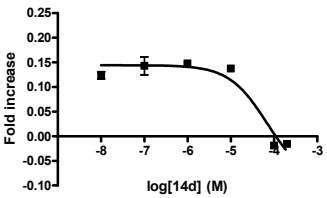

(o) 14d

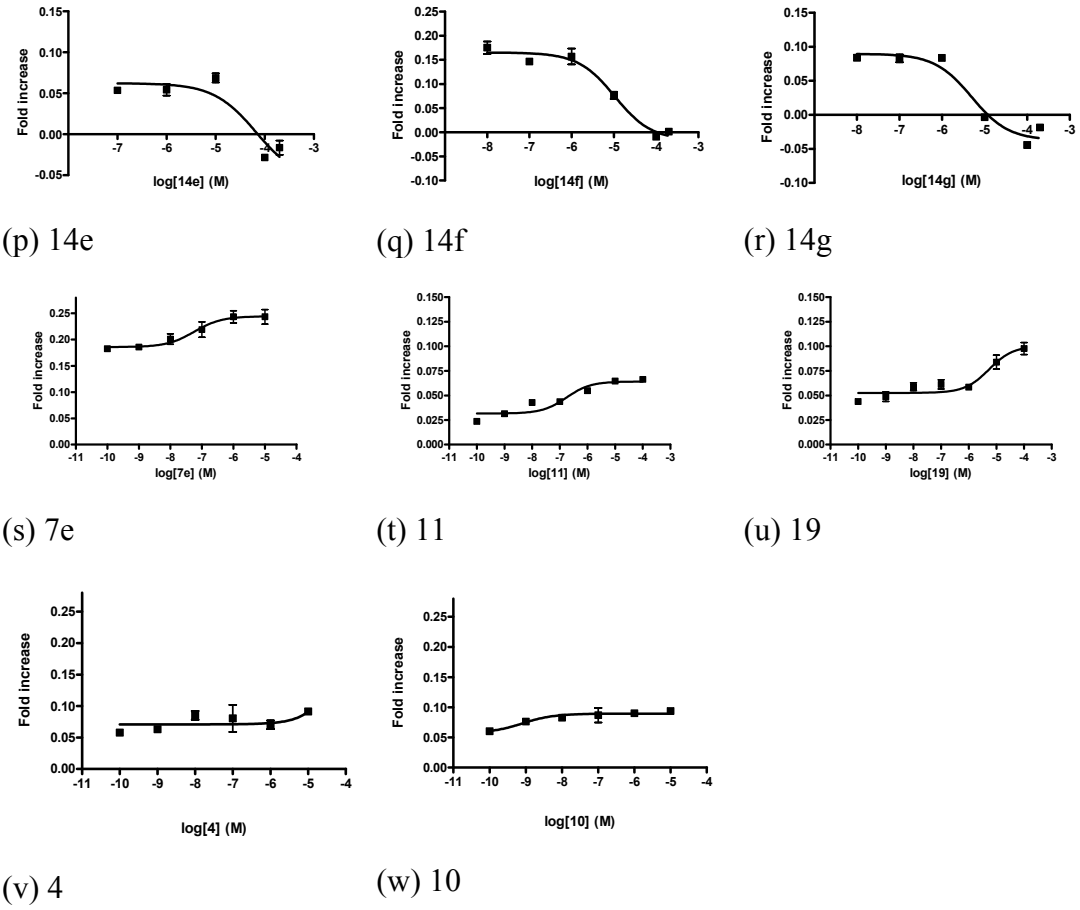

Figure 3.5. The dose-response relationship of (a – r) indicate antagonist inhibition of K^+-induced Ca^{2+} influx. The dose-response relationship of (s – w) indicate a potentiating effect after K^+-induced depolarization. Results are presented as the mean ± STDEV (n = 3-6). Where error bars are not shown, these are covered by the point itself.

For this assay, the IC_{50} values for the series of the reference compounds were determined to be 0.008 μM for nimodipine, 0.002 μM for nitrendipine, 0.328 μM for verapamil and 0.449 μM for diltiazem. All the values correlated well with that reported in literature.[144] According to their inhibitory potency the test compounds fell into three categories, with **14c** and **7d** (IC_{50} value of 0.398 μM and 0.580 μM, respectively) being the most potent and matching the IC_{50} values of the reference compounds. Compounds **8b**, **8c**, **14f** and **14g** fell into the second category with IC_{50} values ranging from 5 – 11 μM; and the remainder fell into the third category with

IC_{50} values ranging from 35 – 86 μM. All of the compounds tested had higher potency as LTCC antagonists than the lead compound **7a** (NGP1-01, IC_{50} = 86 μM).

When comparing the dose-response profiles of the reference compounds to the test compounds (Figure 3.5 a-w), several observations can be made from the graphs. All of the compounds were able to block K^+-induced Ca^{2+} influx in a dose-dependent manner. Compound **14c** (IC_{50} = 0.398 μM) an aza-triquinylamine with a phenylpropyl substituent had a similar inhibition profile than nimodipine and nitrendipine, which as previously mentioned are both compounds in the dihydropyridine classification of high-affinity voltage dependent LTCC blockers. From this observation we can conclude that this compound would also interact with the LTCC in a similar manner. Compounds **7d** and **14g**, with the second and third lowest IC_{50} values (0.580 μM and 5 μM, respectively) had similar inhibition profiles to verapamil and diltiazem. The inhibition profiles of all the other compounds evaluated were comparable to that of **7a.** For compounds **7e**, **11**, and **19** we observed agonist-like sigmoidal dose-response profile. These were compounds that demonstrated a potentiating effect. A possible explanation could be that neither compound **11** nor **19** had substituents that could extend to interact with binding site within the channel pore; therefore these compounds might act in a similar manner as (S)-Bay and FPL (LTCC agonist or activators),[145] by locking the channel in the open state. This observation was also made when we evaluated the lipophilic scaffolds **4** and **10**, (Figure 3.5 v-w). The pentacycloundecane (**4**) had no activity, where the triquinane-dione (**10**) had a slight potentiating effect but no antagonistic activity. For compound **7e,** the pentacycloundecane with the oxa-bridged pyridine substituent, the only explanation that could be offered for the lack of activity is that the orientation within the channel is unfavorable for binding especially since its counterpart the triquinane **14g** with the aza-bridged pyridine substituent showed favorable activity (IC_{50} = 5 μM). We also observed that for most compounds the graphs illustrate the inhibitory potency which increased in a dose dependent manner between 10 μM to 200 μM. However, between 0.0001 μM and 1 μM we observed a potentiating effect which could be due to Ca^{2+}-induced Ca^{2+} release (CICR). These compounds may not have the ability at lower concentrations to block KCl-induced increases in $[Ca^{2+}]_i$, which has been shown to induce Ca^{2+} release from intracellular stores.[146, 147] We will attempt to further

elaborate on this observation. This biphasic profile was also described by another group that evaluated the 1,2,4-oxadiazol-5-one derivatives, and also attributed their observations to CICR from the sarcoplasmic reticulum.[148]

Although this was a preliminary study some structure-activity relationships can be drawn for the series evaluated. For all three series of compounds the unsubstituted benzylamine derivatives (**7a**, **8a** and **14a**) were found to be the least active. Increases in chain length (**7b**, **8b** and **14c**) increased the inhibition of Ca^{2+} influx and the aza-triquinylamine derivative (**14c**), with a phenylpropyl substituent, had the highest potency. This might indicate better access to the binding sites within the channel. Overall the aliphatic derivatives were more active than their aromatic counterparts. The aliphatic heptylamine (**8c**) derivative had the highest potency of the aza-pentacycloundecylamines and for the aza-triquinylamines the two aliphatic derivatives (**14e** and **14d**) were equal in activity and slightly more active than the unsubstituted benzylamine (**14a**). In general it was observed that substitution in the *meta* position with an electron-donating moiety such as methoxy (**7c** and **14f**) and an electron-withdrawing moiety such as nitro (**7d**), increased the activity when compared to the unsubstituted derivatives (**7a** and **14a**). The electron rich 4-substituted pyridine (**14g**) was observed to be more active for the aza-triquinanes when compared with (**14a**) and also more active than the *meta*-methoxy substituent. Substitution in the *meta* position with an electron-withdrawing moiety such as nitro (**7d**) led to an increase in activity and compounds with such substitution patterns were more active than those containing a methoxy moiety.

Table 3.7. The IC_{50} (μM) values for the inhibition of K^+-induced Ca^{2+} influx as determined experimentally and predicted values from the MLR QSAR model for the series of 8,11-oxapentacycloundecylamines (**7a-d**); 8,11-azapentacycloundecylamines (**8a-c**) and 3,11-azatricycloundecylamines (**14a-g**).

Compound	Experimental		Predicted		
	IC_{50} (μM)	pIC50 (M)	pPRED	Residual	logP
7a	86	4.07	3.78	0.29	2.11
7b	51	4.29	4.20	0.09	2.4
7c	42	4.38	4.49	-0.12	1.95
7d	0.580	-	-	-	-
8a	35	4.46	4.79	-0.33	1.85
8b	8	5.10	5.21	-0.11	2.14
8c	7	5.15	5.12	0.04	2.78
14a	74	4.13	3.85	0.28	3.67
14b	310.9	3.51	4.27	-0.76	3.96
14c	0.398	6.40	6.22	0.18	3
14d	68	4.17	4.17	0.00	4.06
14e	68	4.17	4.18	-0.01	4.6
14f	11	4.96	4.57	0.39	3.51
14g	5	5.30	5.22	0.08	2.45

[a] Experimental values are means of at least three experiments (n = 3). IC_{50} values of reference compounds were calculated to be: nimodipine 0.008 μM (n = 6), nitrendipine 0.002 μM (n = 3), verapamil 0.328 μM (n = 3) and diltiazem 0.449 μM (n = 3).

To support future efforts of structure design and optimization we developed a quantitative structure-activity relationship (QSAR) model to describe physiochemical properties of compounds evaluated and to assess whether this model would be able to give us an accurate prediction of the functional activity. The QSAR model we developed was based on descriptors which include molecular properties such as logP, hydrogen bond acceptor and donors, molar refractivity, molecular weight, polar

surface are and heavy atom count. The linear regression model that was generated (n=13) to correlate the structural properties for the series of compounds evaluated with their Ca^{2+} channel blocking properties (IC_{50} values) and is presented in Figure 3.6 and summarized in Table 3.7. The linear regression model delivered $r^2 = 0.83$, which indicated a favorable correlation between the predicted and experimental IC_{50} values. The predicted values were very close to experimental IC_{50} values and this model could thus serve as valuable predictor for future structural design and optimization.

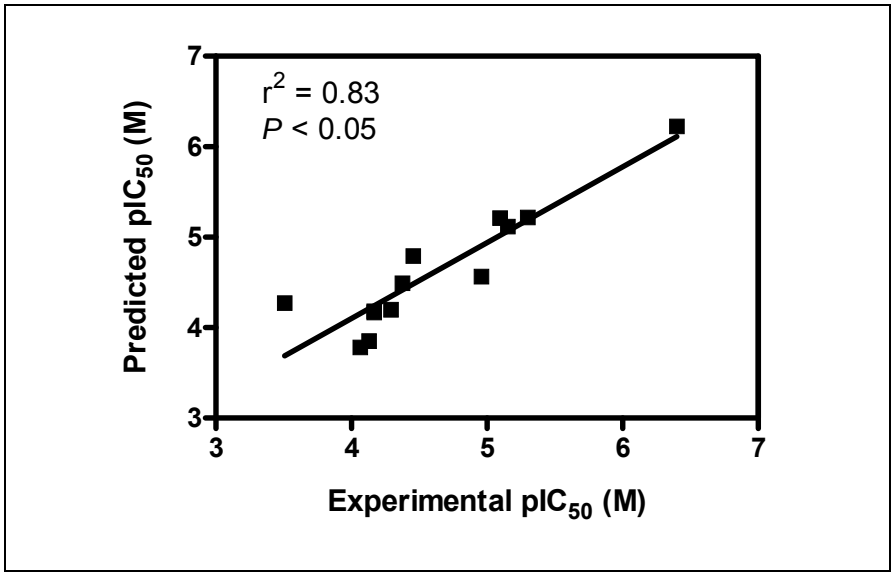

Figure 3.6. The correlation between the predicted activity and experimental activity as LTCC blockers of the compounds discussed in the text.

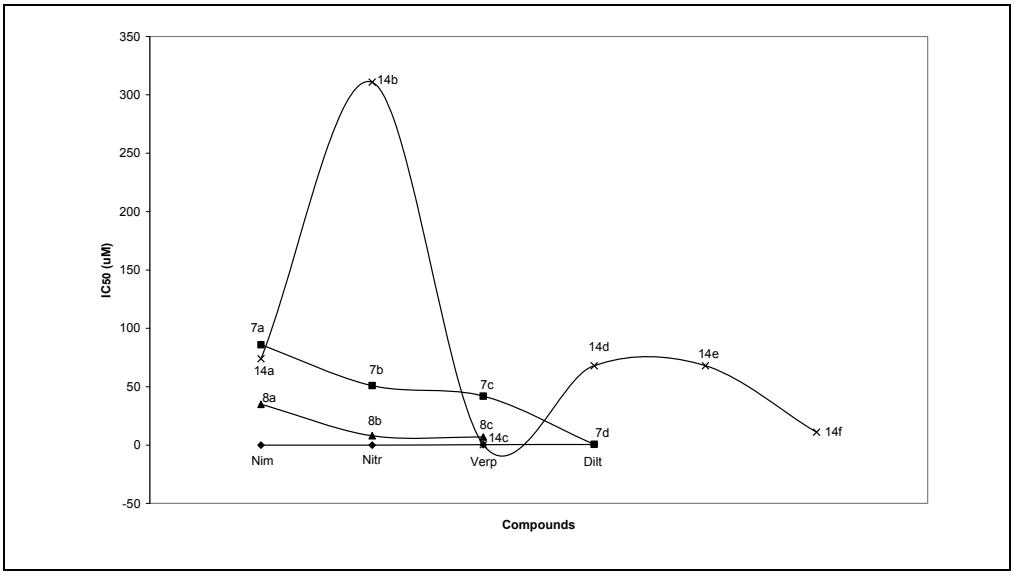

Figure 3.7. Structure-activity relationships (SAR) correlation for reference compounds as well as (**7a-d**) oxa-pentacycloundecylamines, (**8a-c**) aza-pentacycloundecylamines and (**14a-f**) aza-triquinylamines.

3.3.3 Measurement of cell viability

It is well known that an increase in $[Ca^{2+}]_i$ plays an important role in the mechanism of apoptosis and necrosis, which can be induced by oxidative stress.[73,75] We performed cell viability studies utilizing the LDH, MTT and Trypan blue staining assays to investigate whether our compounds, which have the ability to regulate Ca^{2+} influx through the LTCC, would offer protection against H_2O_2-induced cell death.

3.3.3.1 Estimation of LDH release

We evaluated the plasma membrane damage in PC12 cells by measuring the amount of intracellular LDH released in the media (Figure 3.8). When evaluated in the absence of H_2O_2, compounds **14c** and **14g** caused significant LDH release ($^{++}P < 0.01$), but only at the highest concentration tested (100 μM). The aberrant cytotoxicity observed for compound **14c**, which also had the lowest IC_{50} value (IC_{50} = 0.398 μM) as an LTCC blocker, was more than what was observed for the control of H_2O_2 treatment alone. We speculate that the observed toxicity might be due to this compound being the most potent Ca^{2+} channel blocker evaluated, which may have

caused $[Ca^{2+}]_i$ depletion and thus the observed toxicity. Compounds **7a** and **8b** caused some LDH release at 100 μM, although this was found not to be significant ($^{+}P > 0.05$). Pretreatment with the selected test compounds attenuated subsequent H_2O_2-induced LDH release in general. Compound **8b** showed significant attenuation of LDH release at concentrations (1 and 10 μM) as did compound **14g** at higher concentrations (10 and 100 μM). Overall, compound **7a** were the most active in this assay with no significant toxicity displayed and the ability to significantly (**P < 0.01) reduce H_2O_2-induced LDH release at all three concentrations (1, 10 and 100 μM) evaluated.

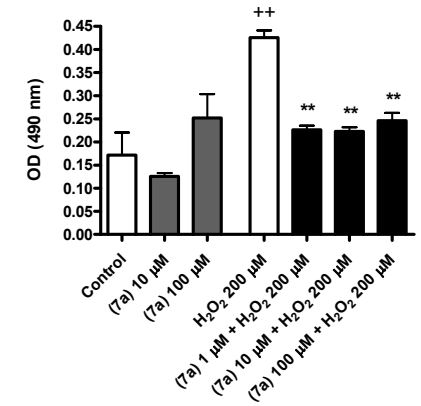

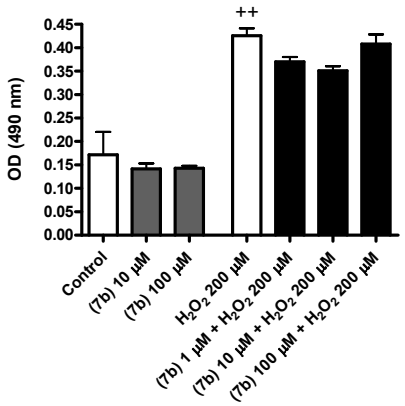

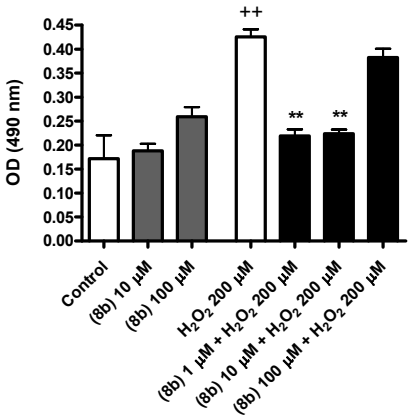

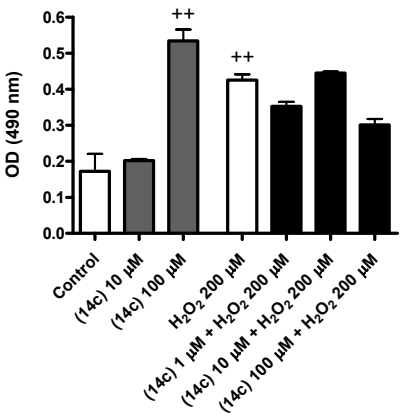

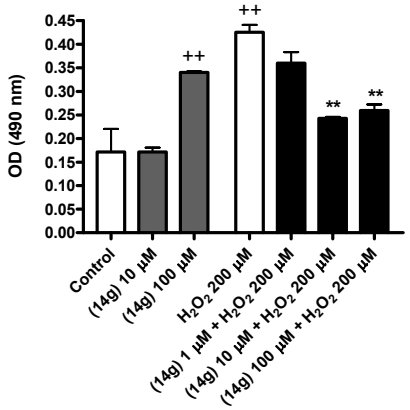

Figure 3.8. The effect of selected compounds on LDH release after cell injury induced by 200 µM H_2O_2. Data are mean ± SEM (n = 3). Data were subjected to an ANOVA analysis, followed by Dunn's post test and significance was defined as $^{++}P < 0.01$ compared to control untreated cells and **P < 0.01 compared to 200 µM H_2O_2.

3.3.3.2 Measurement of MTT reduction

In addition to LDH release we also assayed the effect of selected test compounds on cell viability by means of the MTT assay, which measures the inhibition of 3-(4,5-dimethylthiazol-2-yl)2,5-diphenyl-tetrazolium bromide (MTT) reduction. Results are presented in Figure 3.9. The control represents untreated cells. Without H_2O_2 treatment, the evaluation of compounds **7a**, **7b** and **14c** by themselves, did not decrease cell viability and thus showed no toxicity. Treatment with 200 µM H_2O_2 significantly decreased cell viability to 57% ($^{++}P < 0.01$). In general the pretreatment with selected compounds did not significantly attenuate H_2O_2-induced cell death, which is contrary to observations made by both the LDH and trypan blue assays. Where there were responses, we saw no dose dependent attenuation for selected compounds. Compound **7a** at a concentration of 0.1 µM and compound **7b** at concentrations of 0.1 and 100 µM were able to significantly reduce H_2O_2-induced cell death (*P < 0.05 and **P < 0.01, Figure 3.9); however this was not in a concentration dependant manner.

We found that the MTT assay was not effective or consistent in quantifying the protective effect of compounds evaluated and that it did not correlate well with results obtained from both the LDH assay and trypan blue staining assay. This observation was also reported by another group that compared the LDH and MTT assays for quantifying cell death.[114]

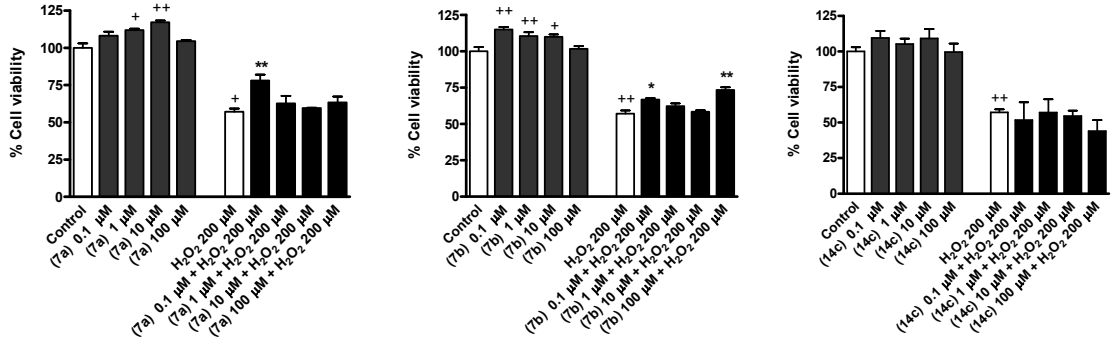

Figure 3.9. The effect of selected compounds on cell viability, determined by the MTT assay after cell injury induced by 200 µM H_2O_2. Data are mean ± SEM (n = 3). Data were subjected to analysis of Unpaired Student's t-test and significance was defined as $^{+}P < 0.05$ or $^{++}P < 0.01$ compared to control (viable untreated cells) and $^{*}P < 0.05$ or $^{**}P < 0.01$ compared to H_2O_2 (200 µM).

3.3.3.3 Trypan blue exclusion

Trypan blue staining assays were performed to verify results from the LDH assays. Cell viability was assessed by criterion of trypan blue exclusion (Figure 3.10). The failure to exclude trypan blue dye reflects a loss of plasma membrane integrity associated with necrosis. The results corresponded well to the results obtained with the LDH assay (compare Figure 3.8 to Figure 3.10). When compounds were evaluated in the absence of H_2O_2, compounds **7a**, **7b, 8b** and **14g** caused some decrease in cell viability at 10 µM and 100 µM, compared to the control of viable untreated cells ($^{+}P < 0.05$). Compound **14c** showed considerable reductions (97.91 %) in cell viability at 100 µM, compared to the control of viable untreated cells (**P < 0.01), which indicates cytotoxicity for this compound at higher concentrations. This observation also correlates with results from the LDH assay for this compound at the same

concentration and we conclude, as for the LDH assay, that this could be due to $[Ca^{2+}]_i$ depletion. Treatment with 200 μM H_2O_2 caused significant (73.6 %) reduction in cell viability ($^{++}P < 0.01$). Pretreatment with selected test compounds generally attenuated H_2O_2-induced cell injury when compared to H_2O_2 treatment alone. Of the compounds tested, **7a** demonstrated the most favorable pharmacological profile, with significant reduction ($^{+}P < 0.01$) of H_2O_2-induced toxicity at all concentrations evaluated (1, 10 and 100 μM). The same observation was made for this compound as with the LDH assay.

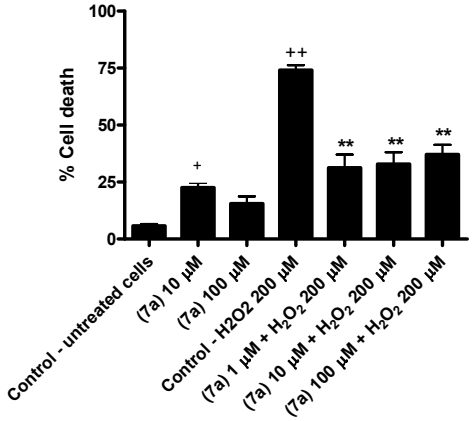

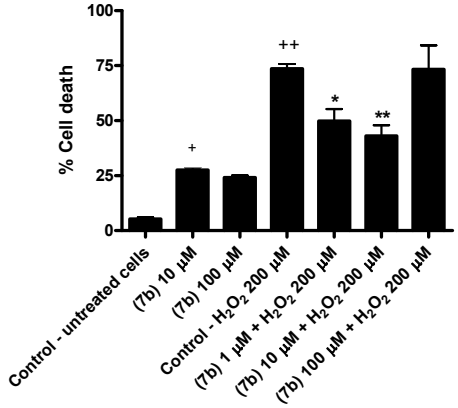

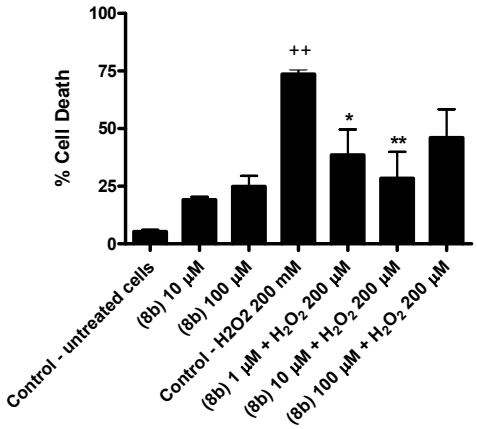

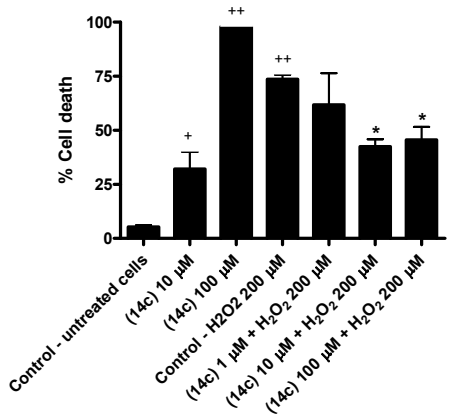

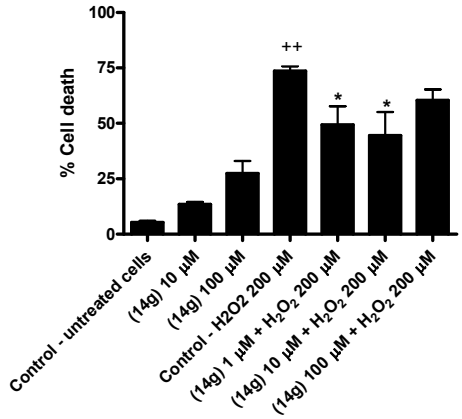

Figure 3.10. Assessment of percentage cell viability by means of trypan blue uptake and exclusion. The effect of compounds alone was assessed by counting viable cells and comparing to control of untreated viable cells. The ability of selected compounds to offer protection against cell injury induced by 200 µM H_2O_2 was assessed by counting stained non-viable cells and comparing to the control of cells treated with 200 µM H_2O_2. Data are mean ± SEM (n = 3, counted 2 fields per repeat). Data were subjected to an ANOVA analysis, followed by Dunn's post test and significance was defined as $^{+}P < 0.05$ or $^{++}P < 0.01$ compared to control (viable untreated cells) and *P < 0.05 or **P < 0.01 compared to 200 µM H_2O_2.

3.3.3.4 Fluorescence microscopy analysis of Annexin V-FITC staining

Immunohistochemistry was utilized as a visual confirmation of the toxicity displayed by compound **14d** at 100 µM and whether this aberrant toxicity is the result of apoptosis (Figure 3.11). As controls, PC12 cells were left untreated or apoptosis was induced with Staurosporine (1 µM, 24 h). Cells were also treated with 200 µM H_2O_2, which are the same conditions used in the LDH, MTT and trypan blue staining assays to induce cell death. Compound **14d** was evaluated by itself and with subsequent addition of 200 µM H_2O_2. As observed by both the LDH assay and trypan blue staining assay, compound **14d** induced cell death when evaluated by itself, which indicate inherent toxicity for this compound at higher concentrations. This is possibly due to intracellular Ca^{2+} depletion as mentioned before, which will also result in cell death.

Although excessive Ca^{2+} influx result in cell death, the depletion of $[Ca^{2+}]_i$ in turn will also facilitate cell death.[149-151] The polycyclic compounds in general are effective in offering protection against excessive Ca^{2+} influx due to their use-dependent uncompetitive block of both the NMDA receptor and LTCC,[43] which regulate Ca^{2+} influx and will not result in $[Ca^{2+}]_i$ depletion. This gives these compounds an advantage over LTCC blocker such as nimodipine. From the observed toxicity for compound **14c** we can conclude that this compound might not have the same binding kinetics as the other polycyclic compounds evaluated in this study and is not a low-affinity, use-dependent LTCC blocker. This could also be the reason why **14c** had the lowest IC_{50} value (0.398 μM), due to the fact that it does not have the same on-off binding kinetics that the other polycyclic compounds have.

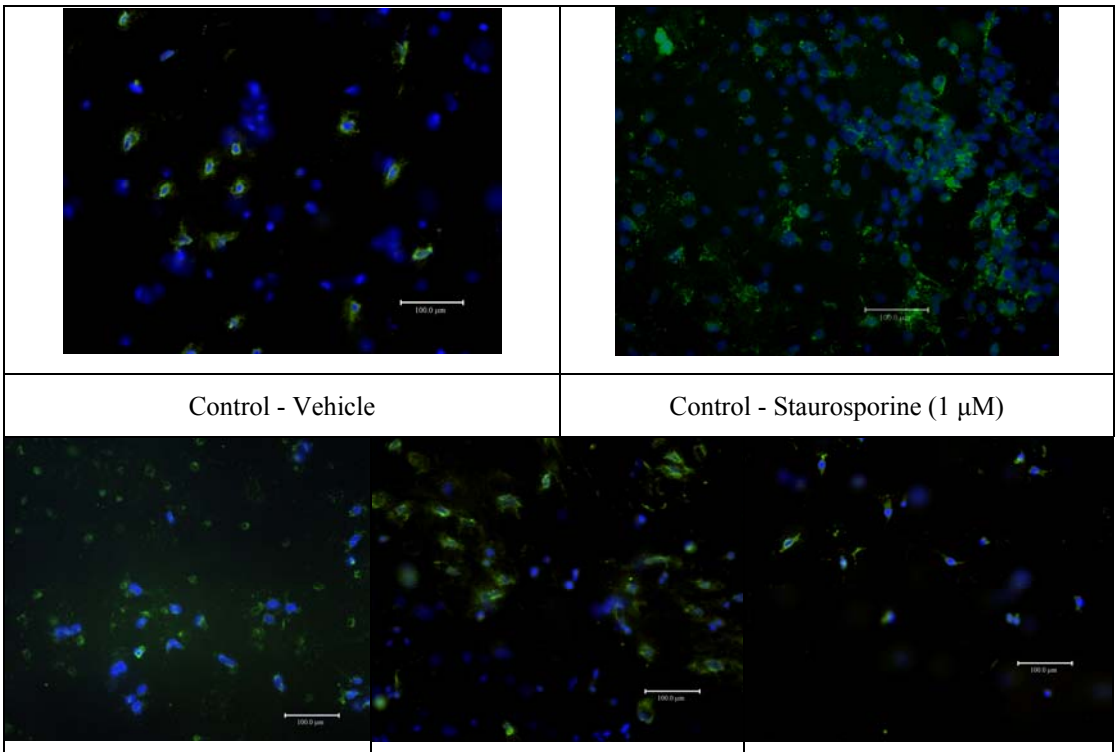

Figure 3.11. Fluorescence microscopy evaluation of Annexin V-FITC staining. The effect of compound **14c** on cell viability was evaluated through immunohistochemistry for the compound by itself or after cell death was induced with 200 μM H_2O_2. Fluorescent stain was done with DAPI (blue) to indicate nuclei and

Annexin V-FITC (green) as an indicator for apoptosis. For the controls, cells were left untreated or apoptosis was induced with Staurosporine (1 μM) and H_2O_2 (200 μM).

3.4 Conclusion

In this study we evaluated the ability of several polycyclic compounds to inhibit Ca^{2+} influx through the LTCC by means of a fluorescence Ca^{2+} flux assay utilizing Fura-2/AM. We determined that the inhibition potency (IC_{50} values) of several compounds was comparable to that of the known LTCC blockers such as nimodipine, nitrendipine, verapamil and diltiazem. For compounds (**14c** and **7d**) the IC_{50} values (0.398 μM and 0.580 μM, respectively) and dose-response profiles were comparable to that of verapamil (IC_{50} = 0.328 μM) and diltiazem (IC_{50} = 0.449 μM). This suggests that these compounds are also potent inhibitors of the LTCC. However, **14c** showed significant toxicity at 100 μM when evaluated in the absence of H_2O_2 in both the LDH and trypan blue staining cell viability assays. This compound had the lowest IC_{50} value (0.398 μM) and we attributed this toxicity to this compound possibly being a high-affinity LTCC blocker which might cause $[Ca^{2+}]_i$ depletion. Interestingly, this compound was still able to offer some protection against H_2O_2 induced toxicity in both assays. Annexin V-FITC staining also visually confirmed apoptotic cell death induced by **14c** which was comparable to apoptosis induced by Staurosporine (1 μM). The IC_{50} value for **7a** was determined to be 86 μM. Even though this compound was not the most potent LTCC blocker, the IC_{50} value still fell within an expectable range, and **7a** had the most favorable pharmacological profile overall with the ability to attenuate cell death in the cell viability assays. This compound also displayed no toxicity when evaluated in the absence of H_2O_2. Taken together the results for **7a** from this study and previous studies where this compound has been characterized as an LTCC blocker,[38, 40, 41, 43] an NMDA receptor channel blocker,[34, 42, 43, 152, 153] and has been shown to be neuroprotective,[44, 45] we can draw the conclusion that this compound remains a promising lead as a multimechanistic drug in the treatment of neurodegenerative disease.[34] Compounds **7b** and **8b**, oxa- and aza-pentacycloundecylamines which both have phenethyl substituents, had favorable activity as LTCC blockers (IC_{50} = 51 μM and 8 μM, respectively). These compounds were also able to offer some protection in the cell viability assays, although not as

significant as seen with **7a**. Compound **14g** a triquinane with the electron rich pyridine ring, were a potent LTCC blocker (IC_{50} = 5 μM) and were also able to offer protection against H_2O_2-induced toxicity at higher concentrations. In general it would appear that the aza-pentacycloundecylamines (**8a-c**) were the most potent LTCC blockers. In the cell viability assays compound **8b** offered protection at lower concentrations but showed some toxicity at 100 μM.

Concerning the SAR, it is interesting to note that the compounds evaluated in this study are structurally unrelated to established LTCC blockers. Therefore, studies such as this are of importance to provide information regarding which molecular features are important or detrimental for biological activity. Based on the IC_{50} values obtained from the fluorescence Ca^{2+} flux assay we were able to draw some conclusions regarding the SAR. For this series of compounds SAR are dominated by electronic effect as illustrated by the increase in activity for the methoxy, nitro and pyridine substituents. Modifying the "cage" moiety of the pentacycloundecane skeleton (**4**) by thermal fragmentation to obtain the *cis-syn-cis* triquinane system (**9**) did not diminish activity and in general the triquinane compounds were more active as LTCC blockers. However, they were not more active than the aza-pentacycloundecylamines. As observed in the crystallographic study,[154] the introduction of the aza-bridge in derivatives of compound **10** result in some loss of the flexibility and strain relieve and therefore the advantage of improved conformation and better fit within the ion channel pore. Activity was diminished for compounds such as **11** and **19** that did not have the amino side chain moiety. From this observation we can conclude that the amino side chain moiety is necessary for binding and that the biological activity resides primarily in the combination of the amino side chain and the bulky hydrocarbon polycycle.[40, 95] We observed that an increase in chain length lead to an increase in activity, which might suggest that the compound conformation is more suitable to interact with the DHP binding site located within the LTCC pore. We also found that compounds with aliphatic side chains (**8c**, **14e** and **14d**) were more active than their aromatic counterparts (**7a**, **8a** and **14a**). Since these compounds lack the lipophilic group necessary for interaction with the DHP binding site, we could speculate that these compounds are pore-blocking drugs like verapamil.[155] PAA's

inhibit Ca^{2+} influx by binding to a different binding site and occluding the transmembrane pore,[155] thus acting as pore-blocking drugs.

SAR data reported in literature for the LTCC blockers suggest that compounds such as the DHP's bind to the DHP binding site in a use dependent manner and block the pore indirectly by stabilizing the channel in the open/inactive state. A study done by the group of Van der Schyf *et al*.,[38] characterized NGP1-01 as a frequency and voltage-dependent Ca^{2+} channel blocker with a mechanism favoring open channel block, which resembles the mechanism of action for the DHP's. This could also be a possible mechanism for the compounds with longer aromatic side chains such as (**7b**, **8b**, **14b** and **14c**). SAR studies for nimodipine suggest that lipophilic substituents could establish π-π charge-transfer interaction within the centre of the pore, thus the aromatic benzyl moiety would be able to do the same if it were able to reach the lipophilic binding site within the pore. This could also offer and explanation for the increase in activity observed with an increase in chain length.

In this study we also set out to evaluate several *in vitro* cell viability assays which allowed us to screening possible drug candidates before proceeding to more complex *in vivo* studies. These assays also allowed us to determine if the compounds by themselves exhibit any inherent toxicity. From our assessment, both the LDH and trypan blue staining assays gave consistent results. However, we found the MTT assay of limited value with no consistency compared to the other assays and no real indication of cell death among the compounds evaluated at different concentrations. We also utilized the Annexin V-FITC staining assay to assess the observed toxicity of compound (**14c**). Although we were able to obtain results, this assay provided numerous problems with cells detaching after treatment with the cytotoxin to induce cell death. The assay contains multiple wash steps during the staining process that would then wash these cells away. Only after performing this assay numerous times, taking great care during the staining protocol to limit the amount of cells lost, were we able to obtain results. We thus conclude that the Annexin V-FITC staining assay is not an effective method for screening compounds and should only be used on a small scale to assess whether cell death occur via apoptosis or necrosis.

CHAPTER 4

SYNTHESIS AND CRYSTAL STRUCTURE OF THE TRIQUINANE SCAFFOLD AND ITS DERIVATIVE, *N*-(3-METHOXYBENZYL)-3,11-AZATRICYCLO[6.3.0.0^{2,6}]UNDECANE

4.1 Introduction

Pentacyclo[5.4.0.0^{2,6}.0^{3,10}.0^{5,9}]undecane-8,11-dione (PCU, **4**) is of interest in drug discovery because of its unique cage-like structure that serves as a lipophilic scaffold for synthesizing drugs with neuroprotective properties and the ability to cross the blood brain barrier.[156] The polycyclic scaffold also has the ability to modify and improve pharmacokinetic and pharmacodynamic properties of drugs.[157] A well known example of such a derivative is 8-benzylamino-8,11-oxopentacyclo[5.4.0.0^{2,6}.0^{3,10}.0^{5,9}]undecane (NGP1-01), widely reported for its activity as a multifunctional neuroprotective drug.[42, 43] NGP1-01 has been shown to be an L-type Ca^{2+} channel (LTCC) blocker[158,159] in both neuronal and heart cells, and also acts – in a dual mechanistic way – as an *N*-methyl-D-aspartate (NMDA) receptor antagonist.[160] PCU (**4**) is also utilized as an intermediate in the synthesis of polyquinane natural products,[98] of which tricyclo[6.3.0.0^{2,6}]undecane-4,9-dien-3,11-dione (**9**) and tricyclo[6.3.0.0^{2,6}]undecane-3,11-dione (**10**) and their derivatives are of particular interest to our group. The triquinane scaffold was first synthesized by our group to test the validity of the hypothesis that the pentacycloundecane skeleton serves as a bulk contributor to the biological activity of the polycyclic cage and its derivatives.[95]

The triquinane scaffold and triquinylamine derivatives can be obtained *via* thermal fragmentation of PCU and subsequent catalytic reduction.[95] These derivatives showed suppression of the Ca^{2+} action potential (AP) in guinea-pig papillary muscle.[95] These compounds were also able to significantly slow heart rate. It was concluded that ring opening of the cage moiety did not diminish the Ca^{2+} channel blocking activity, or the negative chronotropic effects of these types of compounds. These findings reiterated

that the triquinane system may afford a useful and novel synthon, and together with appropriate side chain derivatization, it can be utilized to develop pharmacologically interesting compounds that may also be of use in the treatment of neurodegenerative diseases. The concept of utilizing LTCC blockers in the treatment of neurodegenerative diseases has also been explored by other authors.[20] This study forms part of a more extensive investigation in which we utilized several pentacycloundecane and triquinane derivatives to determine their IC_{50} values as LTCC blockers (Chapter 3). Here we report the X-ray crystal structure investigations of the two scaffolds; tricyclo[6.3.0.0^{2,6}]undecane-4,9-diene-3,11-dione (**9**) and tricyclo[6.3.0.0^{2,6}]undecane-3,11-dione (**10**) as well as a substituted derivative, *N*-(3-methoxybenzyl)-3,11-azatricyclo[6.3.0.0^{2,6}]undecane (**14f**). This derivative (**14f**) showed promising potential as an LTCC blocker as described in Chapter 3. Additionally, we elaborate on the reaction mechanism of the cycloreversion of (**4**) and the retro cycloaddition of (**9**) utilizing molecular modeling.

4.2 Experimental

4.2.1 Synthesis

Pentacyclo[5.4.0.0^{2,6}.0^{3,10}.0^{5,9}]undecane-8,11-dione (**4**) was synthesized as previously described (Scheme 4.3),[96] and the crystal structure for this compound has also been reported.[96, 161] Tricyclo[6.3.0.0^{2,6}]undecane-4,9-diene-3,11-dione (**9**) can be obtained through thermal fragmentation (Scheme 4.1), by means of flash vacuum pyrolysis of the saturated four-membered ring (**4**).[98] The melting point of (**9**) was determined by DSC to be 97.23 ºC. Catalytic hydrogenation of the thermolysis product (**9**) yielded tricyclo[6.3.0.0^{2,6}]undecane-3,11-dione (**10**).[95] The melting point of this compound was determined by DSC to be 95.82 ºC. We have also encountered the reversible nature of the cycloreversion[162] that yielded the *cis-syn-cis* linearly fused triquinane system (Scheme 4.3), in our attempts to polymerize (**9**) *via* a radical mechanism utilizing ultra violet (UV) irradiation through a 450 W UV lamp (quartz, EtOAc).

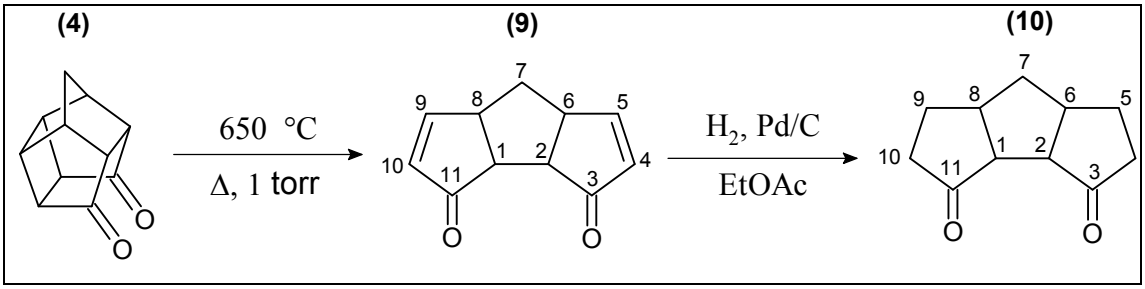

Scheme 4.1. The synthesis route to obtain tricyclo[6.3.0.0^{2,6}]undecane-4,9-diene-3,11-dione (**9**) and tricyclo[6.3.0.0^{2,6}]undecane-3,11-dione (**10**).

To obtain *N*-(3-methoxybenzyl)-3,11-azatricyclo[6.3.0.0^{2,6}]undecane (**14f**) (Scheme 4.2), tricyclo[6.3.0.0^{2,6}]undecane-3,11-dione (**10**) (3.01 g, 0.0169 mol) was dissolved in anhydrous THF (30 ml), stirred and cooled to 5 °C on an external ice bath. An equimolar quantity of 3-methoxybenzylamine (2.32 g, 0.0169 mol) was slowly added, while the mixture was stirred for approximately 6 h at reduced temperature. Upon completion the solvent was removed *in vacuo* to yield the carbonyl amine (**12**) as an oil. This product was dehydrated under Dean Stark conditions for approximately 1 h using 40 ml anhydrous benzene. The benzene was removed *in vacuo* to afford Schiff base **13**. The resulting oil was dissolved in anhydrous MeOH (20 ml) and anhydrous THF (75 ml). Reduction was carried out by the addition of $NaBH_3CN$ in one molar excess and stirring overnight (18 h) at room temperature. The solvent was removed *in vacuo* to yield the final product (**14f**) as a dark colored oil. This oil was suspended in approximately 50 ml of distilled water in a separation funnel. The product was extracted with DCM (4 × 20 ml) and the combined DCM fractions were washed with distilled water (2 × 50 ml). The organic phase was dried over anhydrous $CaSO_4$ and filtered. The solvent was removed *in vacuo*. The compound was purified using a two step silica column chromatography approach. The first purification step utilized PE:$CHCl_3$:EtOAc, 10:6:1 as the eluent mixture, and the second PE:THF, 5:1 at a lower temperature (5 °C). Purification afforded a light yellow oil (yield: 0.4523 g, 0.002 mol, 9.46 %). From this oil the compound was crystallized in EtOAc to obtain colorless crystals suitable for X-ray crystallographic analysis.

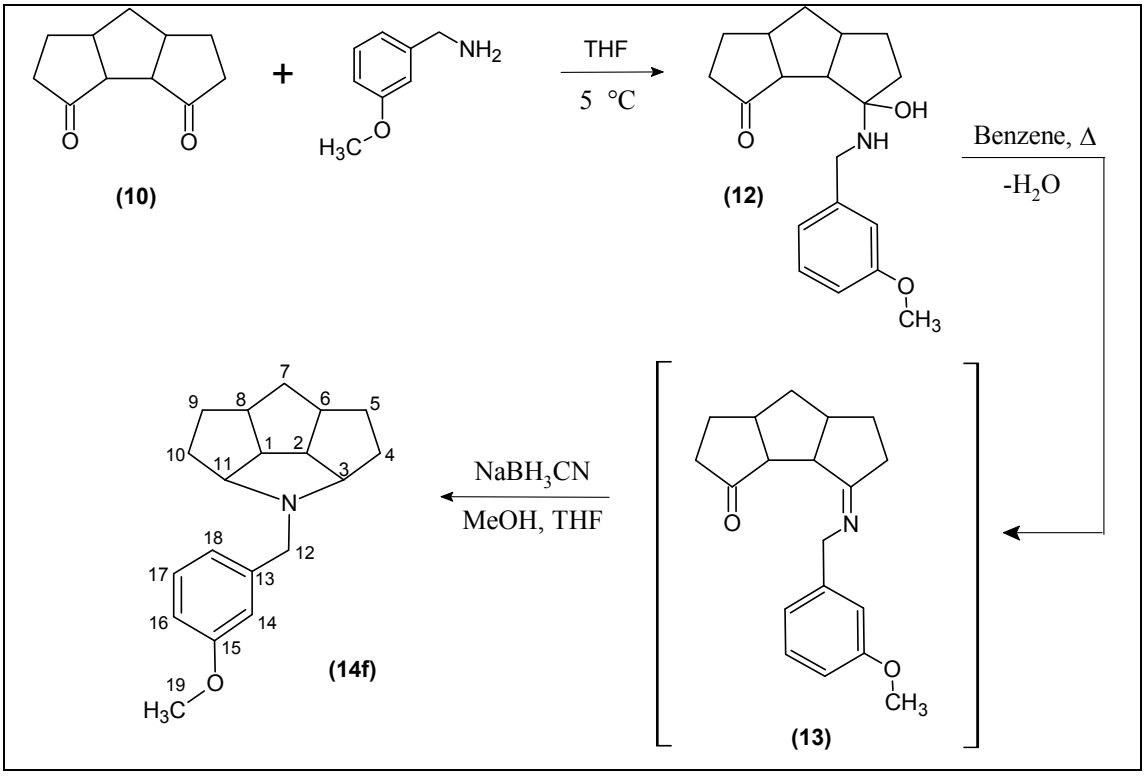

Scheme 4.2. The synthesis route to obtain *N*-(3-methoxybenzyl)-3,11-azatricyclo[6.3.0.0^{2,6}]undecane (**14f**).

4.2.2 NMR spectroscopy

^{1}H-NMR and ^{13}C-NMR spectra were obtained using a Varian Gemini 300 spectrometer at a frequency of 300.075 MHz and 75.462 MHz, respectively. This was done in a 7 Tesla magnetic field and tetramethylsilane (TMS) was used as internal standard. A bandwidth of 1,000 MHz at 24 kG was applied for ^{1}H-^{13}C-decoupling. All chemical shifts are reported in parts per million (ppm) relative to the signal of TMS ($\delta = 0$) added to the deuterated solvent, $CDCl_3$. Distorsionless Enhancement by Polarisation Transfer (DEPT) experiments were also conducted for these compounds.

4.2.3 X-ray crystallography analysis

Diffraction data for (**9**), (**10**) and (**14f**) were collected on a Bruker AXS SMART APEX CCD diffractometer at 100(2) K using monochromatic Mo Kα radiation with omega scan technique. The unit cells were determined using SMART and SAINT+,[163-165] and the data were corrected for absorption using SADABS.[163-165] The structures were solved by direct methods and refined by full matrix least squares against F^2 with all reflections using SHELXTL.[166, 167] Refinement of an extinction coefficient was found to be insignificant. All non-hydrogen atoms were refined anisotropically. Hydrogen atoms were placed in calculated positions and were refined with an isotropic displacement parameter 1.2 (C-H and CH_2) or 1.5 (CH_3) times that of the adjacent carbon atom. Crystal data and refinement details are listed in Tables 4.2 – 4.6 (Annexure B).

4.2.4 Molecular calculations

Ab initio and semi-empirical calculations were performed using the SPARTAN `04 program (Wavefunction Inc. 18401 Von Karman Avenue, Suite 370 Irvine, CA 92612). Semi-empirical calculations were carried out *in vacuo* with AM1, while *ab initio* Hartree-Fock calculations were performed using the 6-31G* basis set, and density functional theory (DFT) theory calculations were conducted using the B3LYP functional and a 6-31G* basis sets.

4.3 Results and Discussion

4.3.1 Spectroscopic analysis

^{1}H-NMR signals observed were used to identify compound **14f** and suggest the structure that was later confirmed by X-ray crystallography. Compounds **4**, **9** and **10** have been previously synthesized and characterized by means of NMR spectroscopy.[95, 96, 168] However, the crystal structure for **9** and **10** had never been reported. For the novel compound (**14f**), signals for both the 'bridge' hydrogens (H-7a, 7b) were observed at δ_H 1.34 and δ_H 1.16 ppm. The multiplet observed at 1.47 –

2.00 ppm that integrated for eight protons was assigned to H-4a, 4b, 5a, 5b, 9a, 9b, 10a, 10b. The multiplet observed at 2.35 – 2.62 ppm that integrated for two protons was assigned to H-6 and H-8. The multiplet observed at 2.66 – 2.88 ppm that integrated for two protons was assigned to H-1 and H-2. The quartet at 3.05 – 3.30 ppm that integrated for two protons was assigned to H-3 and H-11. The singlet at 3.57 – 3.69 ppm that integrated for two protons was assigned to H-12a and H-12b and the three protons of the methoxy OCH_3-19 correspond to the singlet at 3.74 – 3.93 ppm. We observed a doublet of doublets at 6.58 – 6.80 ppm that integrated for one proton and we assigned this to H-16. At 6.82 – 6.95 ppm we observed a multiplet that integrated for two protons and we assigned this to H-14 and H-18. The triplet at 7.06 – 7.23 ppm that integrated for one proton was assigned to H-17. The ^{13}C-NMR data are presented in Table 4.1 (Annexure B) and show 14 resonances. The data obtained from the spectroscopic analysis are in full agreement with the X-ray structure.

4.3.2 X-ray analyses

One important aspect in molecular recognition is shape. Overall size (i.e. volume) and general geometry (e.g. the x-y-z aspect ratio of a molecule) play crucial roles as to whether a molecule is recognized by a receptor, an active site of a protein, or other shape driven interactions of a small compound with biological macromolecules. For interactions of molecules with membrane ion channels, size, surface area, and geometrical conformation are of particular importance and it is these properties that determine the blocking ability of a molecule. For polycyclic compounds, for example, the LTCC blocking activity depends at least partially on the size and geometry of the polycyclic scaffold. To be able to better evaluate the relationship between molecular shape of molecules **9**, **10** and **14f**, and their Ca^{2+} channel blocking activity in comparison to the pentacycloundecanes, we determined the single crystal structures of the two triquinane scaffolds (**9** and **10**) and of the substituted derivative (**14f**). The ORTEP plots in Figures 4.1 a and 4.2 a (Annexure B) give perspective views of tricyclo[6.3.0.0^{2,6}]undecane-4,9-diene-3,11-dione (**9**) and tricyclo[6.3.0.0^{2,6}]undecane-3,11-dione (**10**). The crystal packing for the two compounds is represented in Figure 4.1 (b & c, Annexure B) and 4.2 (b, c & d, Annexure B). The *cis-syn-cis* linear

configuration for both **9** and **10** are clearly visible in the ORTEP plots. This is a unique feature for these compounds as this configuration can only be obtained through thermal fragmentation of the cage structure **4**. Any other approach towards linearly fused triquinanes would result in the *cis-trans-cis* tricyclopentanoid framework.[169] For compound **9** the double bonds between C2 and C3 as well as C7 and C8 provide rigidity to the structure and its framework does not have much flexibility as can also be seen in the crystal packing. Compound **10** lacks the double bonds between C2 and C3 as well as C7 and C8, and this allows for a somewhat enhanced flexibility. When compared to their related pentacycloundecane counterparts,[170] the two triquinane scaffolds **9** and **10** are both more flexible and are also more asymmetric and less globular than the equivalent tetra- or pentacycloundecanes (Figure 4.3), with much larger x-y aspect ratios than the pentacyclo(5.4.0.0^{2,6}.0^{3,10}.0^{5,9})undecane-8,11-dione (**4,** CCDC entry code: FOBPAO), or related compounds tetracyclo(6.3.0.0^{4,11}.0^{5,9})undecane-2,7-dione (**15**, CCDC entry code: TOHZUL) or pentacyclo(6.2.1.0^{2,7}.0^{4,10}.0^{5,9})undecane-endo-endo-3,6-diol (**16**, CCDC entry code: XIJPEL). An overlay of these compounds which all feature a $C_{11}O_2$ skeleton is shown in Figure 4.3 b. The triquinanes, **9** (red) and especially **10** (blue) are the by far the most asymmetric molecules and are much wider than the tetra- or pentacycloundecanes **4**, **15** and **16**. The largest C···C distances within one molecule, indicative of the length of the molecule, are between 3.620 and 3.682 Å for the tetra- and pentacycloundecanes respectively. Compounds (**9** and **10**), on the other hand, feature maximum C···C distances of 4.025 and 5.304 Å, respectively. The width of the molecules (measured as the distance between the center of the two oxygen atoms and the methylene carbon atoms at the opposing end of the molecules), on the other hand, are much more uniform and vary only between 4.661 Å and 4.158 Å. The smallest value of 4.148 Å is associated with compound (**10**), again emphasizing its distorted elongated shape of this molecule. Contributing factors for this observation are of course the absence of the bridging bonds between the carbon atoms in **9** and **10**, and the associated release of strain. In **9** the presence of the sp_2 hybridized carbon atoms somewhat limits the conformational freedom of the carbon skeleton and this molecule has an appearance not too different from that of the tetra- or pentacycloundecanes, but with the molecule expanded along the direction of the now missing C-C bond. As a consequence, triquinane **9**, as well as the tetra- or

pentacycloundecanes, adhere predominantly to pseudo-mirror symmetry. The sp_2 hybridization of the carbon atoms leads to a highly strained *cis-syn-cis* linear configuration not too different from those seen for the tetra- or pentacycloundecanes. In **10**, on the other hand, the substitution of the bridgehead or sp_2 hybridized C atoms by sp_3 hybridized CH_2 groups releases most of this strain despite its *cis-syn-cis* linear configuration. Molecule **10** assumes a conformation distinctively different from and much more asymmetric than that of the other four molecules. It has no approximate local mirror symmetry, and the five membered rings are substantially tilted away from each other. This asymmetry and greater flexibility also affects the crystal packing of **10**. The molecules are capable of folding into each other as can be seen in Figure 4.2 d (Annexure B).

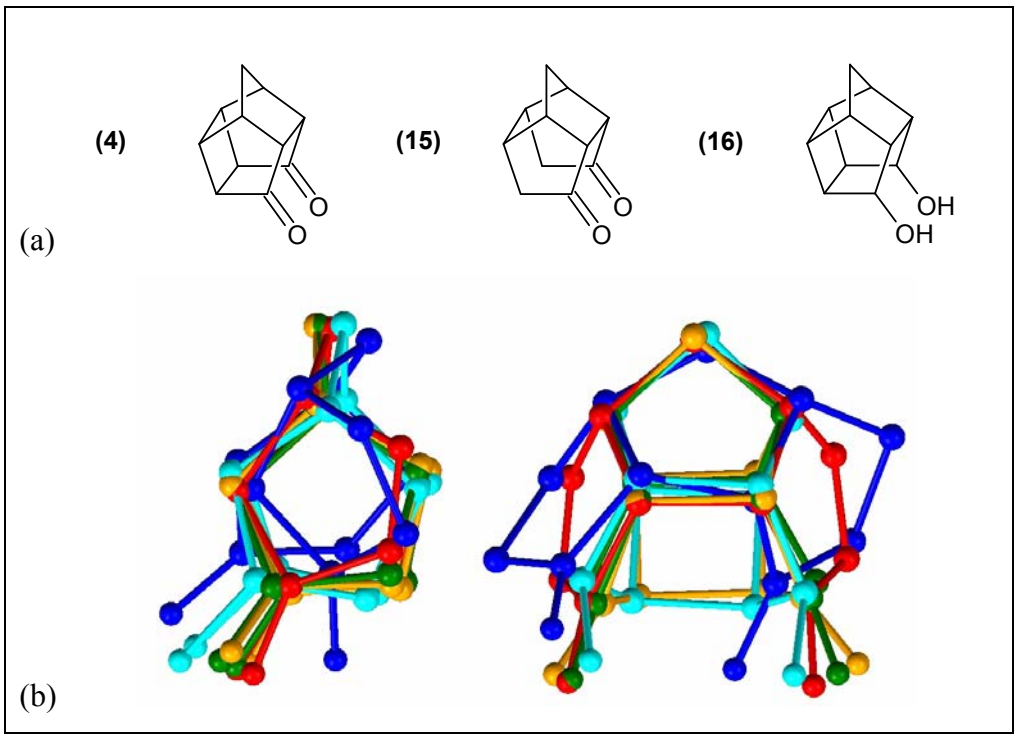

Figure 4.3. Overlay of the tetracycloundecane **15** and pentacycloundecanes **4** and **16,** as well as the two triquinanes **9** and **10**. Colour coding: (**4**) yellow, (**15**) green, (**16**) turquoise, (**9**) red and (**10**) blue.

The increased flexibility of **10** and of its derivative **14f** might be beneficial when designing compounds that act as ion channel blockers due to their ability to flex and adjust their conformation to give a better fit within the ion-channel. The ORTEP plot

in Figure 4.4, gives a perspective view of *N*-(3-methoxybenzyl)-3,11-azatricyclo[6.3.0.0^{2,6}]undecane (**14f**), which is a biologically active derivative of **10**. This crystal structure confirms the results obtained by NMR spectroscopy for this novel compound. From the crystal structure it is evident that the methoxybenzyl side chain does not substantially fold back onto the triquinane scaffold. This is an important observation that has an influence on the activity as an LTCC blocker as it was described for the pentacycloundecylamines that compounds where the side chain was able to fold back onto the scaffold had the lowest activity as LTCC blockers.[40] Another aspect that can be seen from the structure of **14f** is that the introduction of the aza bridge between the two halves of the molecule resulted in some loss of the strain relieve experienced by compound **10**, despite having ethylene groups rather than double bonded sp_2 carbon atoms in the structure. Molecule **14f**, when compared to compound **9**, is again much more rigid and the polycyclic part of the molecule now exhibits again a pseudo-mirror plane (Figure 4.4).

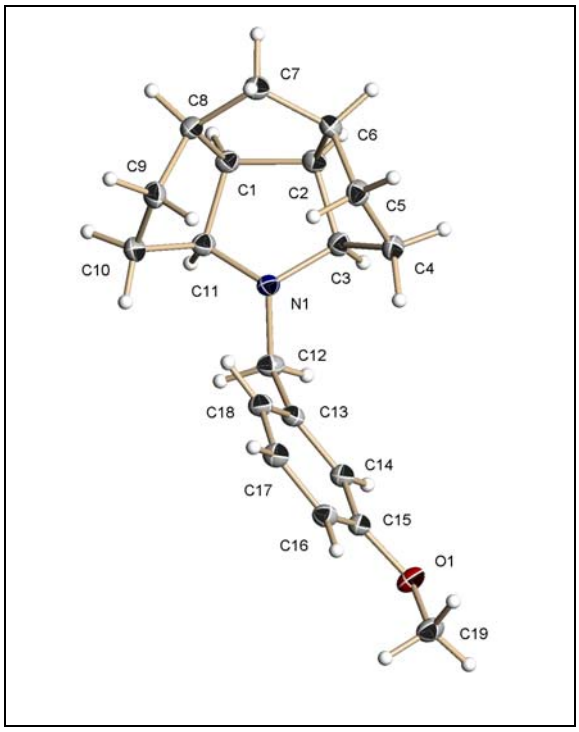

Figure 4.4. The molecular conformation of *N*-(3-methoxybenzyl)-3,11-azatricyclo[6.3.0.0^{2,6}]undecane (**14f**), showing the atomic numbering scheme and displacement ellipsoids at the 50% probability level

A previous study [95] investigated the reactivity of **10** with reducing agents such as $NaBH_3CN$ and $NaBH_4$. The authors were however unable to obtain crystals of either **10** or any of the products obtained that were amendable for X-ray analysis, which left some doubts with respect to the exact nature of the reaction products. In their study they thus calculated (MM2 calculations, ALCHEMY II®, Tripos Associates, St. Louise, Mo) the inter-carbonyl distance to evaluate whether the intramolecular carbonyl-carbonyl proximity was within range to allow for a transannular reaction to occur upon reduction to yield aza- or oxa-bridged compounds (when using $NaBH_3CN$ and $NaBH_4$ as the reactants, respectively), or if other not ring-closed compounds were obtained. The intramolecular carbonyl-carbonyl distance (O1─O2 ≈ 3.326 Å) obtained here via X-ray diffraction for **10** compares well to the value (O1─O2 ≈ 2.94 Å) obtained in the previous study, thus conforming their conclusions that a transannular reaction to yield aza- or oxa-bridged compounds did indeed occur as also seen with the X-ray crystal structure of (**14f**).[95] The single crystal structure of **14f** now provides final unambiguous proof for the formation of an aza-bridged derivative with $NaBH_3CN$ reduction, and confirms the authors' conclusions as well as the NMR-data based structure assignment for **14f**.

4.3.3 Cyclization reaction mechanism

Although the retro cyclization of (**9**) has been reported,[162] we wish to elaborate on the mechanism that has been proposed for the somewhat unusual $[\pi 2_s + \pi 2_s]$ photochemical cycloaddition of this highly strained polycyclic system. In the synthesis of **4**, the *endo* Diels-Alder adduct (**3**) was easily converted into the saturated cage isomer (**4**) by photochemical cycloaddition.[96] The proposed mechanism (Scheme 4.3) for the conversion can be described as excitation of electrons from the highest filled molecular orbital of the bicycloheptene double bond to the lowest vacant molecular orbitals of the enedione chromophore,[96] thus allowing for $[\pi 2_s + \pi 2_s]$ photochemical cyclization to occur according to the Möbius-Hückel theory.[171]

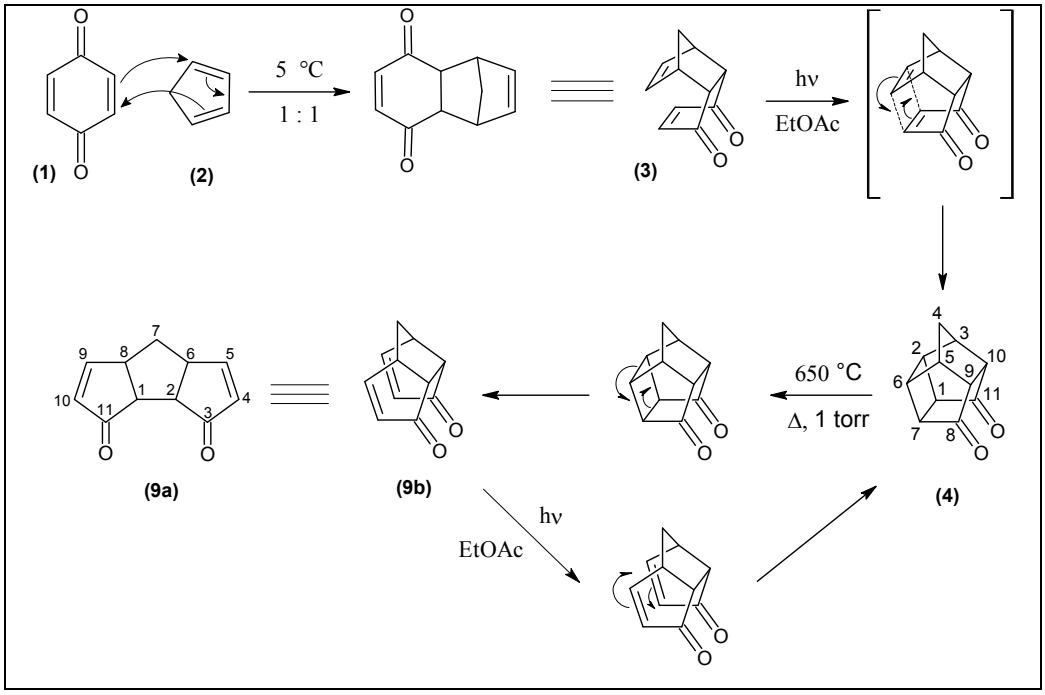

Scheme 4.3. Diels-Alder reaction yielding the Diels-Adler adduct (**3**) followed by UV-initiated photochemical cyclization to yield Cookson's cage compound (**4**). Thermal fragmentation of the pentacyclo[5.4.0.0^{2,6}.0^{3,10}.0^{5,9}]undecane-8,11-dione (**4**) to yield the tricyclo[6.3.0.0^{2,6}]undecane-4,9-diene-3,11-dione (**9**) and the reversion back to **4**.

Thermal cleavage or cycloreversion (Scheme 4.3) of **4** operates by the diradical mechanism, the reverse of a [$_{\pi}2_s$ + $_{\pi}2_s$] photochemical cycloaddition.[171] However it should be noted that the product formed (**9b**) does not resemble the precursor (**3**) to the cycloaddition. This is due to the fact that during the cycloreversion bonds 1, 7 and 2, 6 are cleaved instead of 1, 2 and 6, 7 that formed during the cycloaddition step. The isomer that formed is also stereospecific with a *cis-syn-cis* conformation which is unachievable by any other mechanism.[98] The reversion of (**9**) back to (**4**) reaffirms the *cis-syn-cis* stereo structure which allows the intramolecular [$_{\pi}2_s$ + $_{\pi}2_s$] cycloaddition.[98, 172, 173]

Explaining the mechanism for the [2+2] cycloaddition and cycloreversion can also be aided by Frontier molecular orbital theory (FMO) which has been shown to be a helpful tool in understanding chemical reactions.[174] The DFT level of theory has been

found to give satisfactory results for pericyclic reactions, as well as Diels-Alder reactions[174] and was therefore chosen for the FMO evaluations as shown in this study. Single point energies were calculated using the semi-empirical AM1 module. The LUMO (Lowest Unoccupied Molecular Orbital) and HUMO (Highest Occupied Molecular Orbital) were also calculated (Figure 4.5). As can be seen from Figure 4.5, for the photochemically initiated cycloaddition of **3** to give the cage structure **4**, the [2+2] system can easily form under photochemical conditions, to ensure phase alignment of the HOMO-LUMO orbitals. Similarly, DFT calculations also show how the retro-cycloaddition of **9b** back to **4** is possible, as the energy in the form of UV light is able to phase align the orbitals for sufficient overlap to form a bond. From the calculations, it can be seen that **3** is more likely to undergo cyclization with UV light, as opposed to **9b**, since less phase alignment is needed with **3** than **9b**.

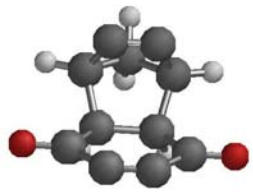		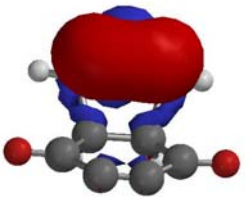
3	**LUMO**	**HOMO**
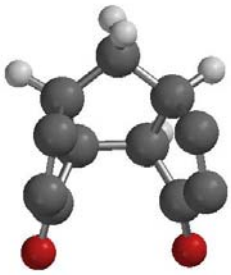	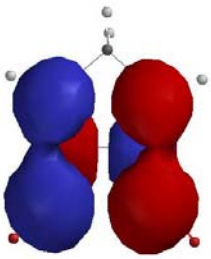	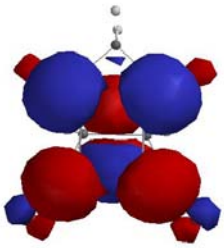
9b	**LUMO**	**HOMO**

Figure 4.5. Calculated HOMO & LUMO surfaces for compounds **3** and **9b**.

4.4 Conclusion

Here we presented crystal structure data and explored some of the structural features for two triquinane scaffolds (**9** and **10**) that are structurally related to the pentacycloundecane scaffold (**4**) and potentially useful in the design of multifunctional neuroprotective drugs with activity on both the NMDA receptor channel and the LTCC. An example of such a compound would be *N*-(3-methoxybenzyl)-3,11-azatricyclo[6.3.0.$0^{2,6}$]undecane (**14f**), a derivative of **10** for which we were able to obtain a single crystal structure. This compound had significant activity as an LTCC blocker (IC_{50} = 11 μM) as determined in the previous study (Chapter 3). The data obtained from the crystallographic analysis confirmed the NMR-data based structural assignments done for these compounds in previous studies.[95, 175] By obtaining single crystal structure of **14f** we were also able to confirm the formation of an aza-bridged derivative with $NaBH_3CN$ reduction. Least squares overlays illustrated the strain release experienced with substitution of the sp_2 hybridized C atoms by sp_3 hybridized CH_2 groups, which result in increased flexibility for the triquinane scaffold (**10**). From the structural overlays we were also able to compare the size and geometry. We also explored the probability of the photocyclization and cycloreversion reaction mechanisms by means of computational calculations to predicting the alignment of the HOMO-LUMO orbitals.

Supplementary crystallographic data for this study have been deposited at the Cambridge Crystallographic Data Centre (CCDC). These data can be obtained free of charge from CCDC via www.ccdc.cam.ac.uk/data_request/cif.

Acknowledgments: The X-ray diffractometer was funded by NSF Grant 0087210, Ohio Board of Regents Grant CAP-491, and by Youngstown State University.

CHAPTER 5

ABILITY OF POLYCYCLIC COMPOUNDS TO MODULATE CALCIUM FLUX THROUGH INTRACELLULAR CALCIUM CHANNELS

5.1 Introduction

In this study we investigated the possibility that the polycyclic compounds, both the pentacycloundecylamines and triquinylamines, might have the ability to modulate Ca^{2+} flux through intracellular Ca^{2+} channels in addition to their ability to modulate Ca^{2+} influx from the extracellular environment through receptor operated Ca^{2+} channels (ROC) such as the *N*-methyl-D-aspartate receptor (NMDAR) and voltage-gated Ca^{2+} channels (VGCCs) such as the L-type Ca^{2+} channels (LTCCs). This assumption is base on observations made in a previous study (Chapter 3) where we noticed a potentiating effect for all of the compounds evaluated at lower concentrations (0.0001 μM to 1 μM). This effect was also observed for verapamil and diltiazem, known LTCC blockers evaluated as reference compounds,[22] but not for nimodipine and nitrendipine. We speculated that this could be due to Ca^{2+}-induced Ca^{2+} release (CICR), where these compounds may not have the ability at lower concentrations to block KCl-induced increases in intracellular calcium concentration ($[Ca^{2+}]_i$), which has been shown to induce Ca^{2+} release from intracellular stores.[146, 147] This biphasic profile was also described by another groups that evaluated 1,2,4-oxadiazol-5-one derivatives and 2-aminoethoxydiphenyl borate (2APB), and also attributed their observations to CICR from the endoplasmic reticulum (ER) and the interaction of their compounds with intracellular Ca^{2+} channels.[148, 176] For compounds **7e**, **11**, and **19** we observed an agonist-like sigmoidal dose-response profile including all the concentrations at which these compounds were evaluated. In other words these compounds demonstrated a potentiating effect and had no activity as LTCC antagonist. It is interesting to note that that neither compound **11** nor **19** had substituents that could extend to interact with binding site within the LTCC pore. This

was also the case with triquinane scaffold (**10**), which had a slight potentiating effect but no antagonistic activity.

To review; literature reports that Ca^{2+} homeostasis regulate the $[Ca^{2+}]_i$ by a number of mechanisms, for example Ca^{2+} entry from the extracellular environment through either the NMDAR or VGCCs such as the LTCC; or by Ca^{2+} uptake into intracellular Ca^{2+} stores such as the ER through the sarco-endoplasmic reticulum Ca^{2+}-ATPase (SERCA) pump.[177, 178] Ca^{2+} release from the ER occurs through the inositol-1,4,5-triphosphate receptors (IP_3Rs) or ryanodine receptors (RyRs) *via* IP_3-induced or Ca^{2+}-induced mechanisms.[56, 57, 179] Increased cytoplasmic Ca^{2+} concentrations will also sensitize IP_3Rs to IP_3 and activate CICR.[58-60] Ca^{2+} release *via* the RyRs is mainly triggered by CICR. The RyRs are also regulated by other intraneuronal factors, such as cyclic adenosine diphosphate ribose (cADP-ribose).[4]

It has also been reported that the LTCC are able to directly interact with the RyR to triggering CICR.[180, 181] However, more recently studies have revealed that depolarization in the absence of extracellular Ca^{2+} result in Ca^{2+} release through the RyRs and a global increase in $[Ca^{2+}]_i$.[182, 183] The increased $[Ca^{2+}]_i$ did not involve Ca^{2+} release through the IP_3R.[182] This process was designated as voltage-induced Ca^{2+} release (VICaR), with the voltage sensor being the dihydropyridine receptors which are allosterically linked to type 1 RyRs.[183] This process has been well documented in skeletal muscle.[94, 184, 185] The study by De Crescenzo *et al*., 2006 also describe the ability of the dihydropyrine LTCC blocker nifedipine to interact with both the LTCC and RyR. Nifedipine act on the LTCC by immobilizing the gating charge and not by directly blocking Ca^{2+} influx. According to this study nifedipine also interact with the RyR by means of allosteric modulation.[183] It is important to note that direct blockers of the LTCC will have no effect on VICaR because they do not affect the gating charge which initiates subsequent Ca^{2+} release through the RyR. It is a direct link between the LTCC and RyR that initiate opening or closing of the RyR.[186-188] Thus depolarization in the absence of extracellular Ca^{2+} could also be used as a method to clarify the mechanism by which an LTCC antagonist interacts with the channel e.g. either by blocking Ca^{2+} influx directly or by immobilizing the gating charge. As these compounds may also act by inhibiting the RyR directly, additional studies would have

to be done with caffeine to initiate Ca^{2+} release through the RyR as a direct mechanism.

The ability of compounds to inhibit calcium release from the intracellular stores can also be evaluated by releasing calcium from the ER with thapsigargin (TG), a selective inhibitor of the SERCA pump.[177, 178] TG, will induced Ca^{2+} release by passive depletion of ER Ca^{2+} by increasing the net Ca^{2+} flux through the IP_3Rs and RyRs, resulting in an global increase in $[Ca^{2+}]_i$.[93, 177] The fall in Ca^{2+} concentrations within the ER activates plasma membrane Ca^{2+} channels, which in the presence of extracellular Ca^{2+} will result in an influx of Ca^{2+} from the extracellular environment.[189] This process is known as "capacitative calcium entry" (CCE) or "store-operated calcium entry" (SOCE) and is responsible for the replenishing of Ca^{2+}-storing organelles such as the ER.[189, 190] In excitable cells the subsequent Ca^{2+} entry will occur through plasma membrane Ca^{2+} channels such as the NMDA and VGCC.

Polycyclic compounds such as NGP1-01 have been shown to be able to modulate Ca^{2+} influx through both the NMDAR and LTCC.[38, 40, 42, 43, 95] NGP1-01 (**7a**) has also been established as a multimechanistic neuroprotective drug candidate with the ability to offer protection in animal models of ischemic stroke.[34, 44, 45] In the previous study (Chapter 3) **7a** showed the ability to offer significant protection against H_2O_2-induced cell death in several cell viability assays. Nimodipine, a widely used LTCC blocker,[22] has more recently been investigated as a possible candidate in the treatment regime of neurodegenerative disorders. It has been found particularly useful in the treatment of conditions such as ischemic stroke and found to improve the outcome in animal models of ischemia.[23, 25] However, as mentioned the NMDAR and LTCC are not the only entry points for Ca^{2+} that lead to increased $[Ca^{2+}]_i$ during excitotoxicity and contributions from intracellular stores such as the ER and mitochondria should also be considered.[93] There is another aspect to bear in mind when blocking multiple pathways responsible for regulation of Ca^{2+} homeostasis. Although excessive Ca^{2+} influx result in cell death, the depletion of $[Ca^{2+}]_i$ in turn will also facilitate cell death.[149-151] Therefore, the goal is to maintain an adequate $[Ca^{2+}]_i$ by regulating Ca^{2+}

influx through the pathways involved in excitotoxicity in a use-dependent manner taking care not to induce intracellular Ca^{2+} depletion.

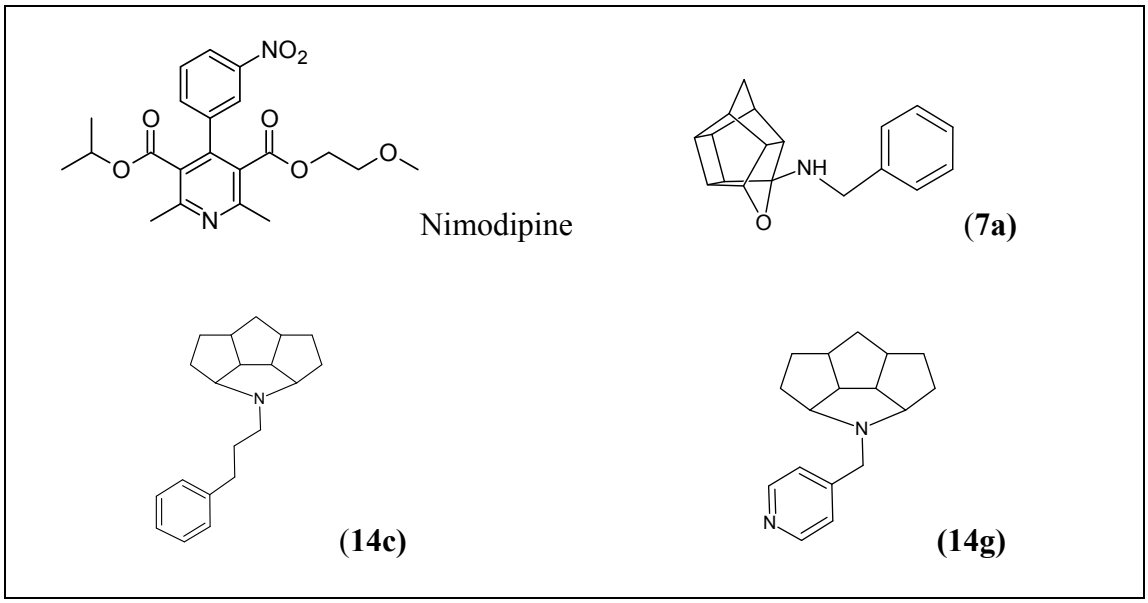

Figure 5.1. Nimodipine and polycyclic compounds evaluated in this study.

5.2 Experimental

5.2.1 Materials

The experimental conditions for fluorescence measurement were done in the same manner as the fluorescence measurements in chapter 3. Loading solutions and test compound stock solutions were also made in the same manner. For more detailed experimental procedures and composition of solutions, refer to chapter 3. Materials were purchased as follow: Undifferentiated rat pheochromocytoma (PC12) cells was obtained from the American Type Culture Collection (ATCC, Manassas, VA, USA); RPMI-1640 media (Hyclone, Fisher Scientific, USA); Fura-2 acetoxymethylethyl ester (AM) from (Invitrogen™, Molecular Probes™, Eugene, OR, USA).

5.2.2 Cell culture

Undifferentiated rat pheochromocytoma (PC12) cells obtained from the American Type Culture Collection (ATCC, Manassas, VA, USA) were used in this study. The cells were cultured in 75 cm^2 tissue-culture treated flasks containing RPMI-1640 media (Hyclone, Fisher Scientific, USA) supplemented with 5% fetal bovine serum, 10% horse serum, 0.5% penicillin/streptomycin/amphotericin B, and 1% (2.05 mM) L-glutamine. The medium was formulated for use with a 5% CO_2 at 37 °C. Culture media were changed every 3 days and cells were sub cultivated twice a week.

5.2.3 Fluorescence calcium measurement protocol

To evaluate whether polycyclic amines have the ability to modulate Ca^{2+} flux through intracellular Ca^{2+} channels, we examined calcium release from the ER by treatment with 1 μM TG in the presence of extracellular Ca^{2+} or 50 mM KCl in the absence of extracellular Ca^{2+}. The induced increase in $[Ca^{2+}]_i$ was measured by means of a 96-well based high through-put fluorescence Ca^{2+} assay, utilizing Fura-2/AM as fluorescent probe. PC12 cells were plated (1×10^5 cells/well) in a black, clear-bottom 96-well tissue culture treated plate (Costar, Corning, NY, USA) 24 h before experiment commenced. Cultures were then washed twice with PBS and loaded with 5 μM Fura-2/AM in Hanks balanced salt solution (HBSS) containing Ca^{2+}, Mg^{2+} and 10% bovine serum albumin (BSA) for 20 min at 37°C. Normal HEPE-buffered HBSS was composed of: 137 mM NaCl; 5 mM KCl; 10 mM $NaHCO_3$; 0.6 mM Na_2HPO_4; 0.6 mM KH_2PO_4; 1.4 mM $CaCl_2$; 0.9 mM $MgSO_4$; 5.5 mM Glucose; 20 mM HEPES. After loading the cells were washed twice with HBSS and then incubated for 10 min with the compounds to be evaluated in HBSS at various concentrations to obtain a dose-response profile. For the experiments done in the absence of extracellular Ca^{2+} HBSS was adjusted to contain: 126 mM NaCl; 3 mM KCl; 26 mM $NaHCO_3$; 1.25 mM Na_2HPO_4; 2 mM $MgCl_2$; 2 mM $MgSO_4$; 10 mM Glucose; 0.5 mM EDTA. For experiments done in the absence of extracellular Ca^{2+} we also had to adjust the high concentration (100 mM) KCl depolarizing solutions by substituting 1.4 mM $CaCl_2$ with 1.4 mM $MgCl_2$, 137 mM NaCl with 43 mM NaCl and 5 mM KCl with 100 mM KCl. In addition Na_2HPO_4 and KH_2PO_4 were omitted from this solution and

1 mM EDTA was added to this solution. The 100 mM KCl solution was diluted to 50 mM KCl when injected by the microplate reader to the wells containing the cells in compound solution. The fluorescence was read on a BioTech Synergy 4 microplate reader (Winooski, VT, USA) with the excitation wavelengths set at 340 and 380 nm, and the emission wavelength set at 510 nm.

5.2.4 Fluorescence measurement of Ca^{2+} release from intracellular stores by thapsigargin

Thapsigargin (TG), an inhibitor of the SERCA pump, can initiate calcium release from the ER through receptors such as the IP_3R and RyR. This will result in an increase in $[Ca^{2+}]_i$ which can be assessed by measuring Fura-2/AM fluorescence as described in text above. After Fura-2/AM loading as described in the fluorescence calcium measurement protocol, the cells were incubated for 10 min with the compounds to be evaluated in HBSS at various concentrations (0.1 μM to 100 μM) to obtain a dose-response profile. These experiments were done in the presence of extracellular Ca^{2+}. After a 10 sec recording period the cells were stimulated by injecting 1 μM thapsigargin and continued recording the time-dependent change in fluorescence. The increase in fluorescence indicating an increase in $[Ca^{2+}]_i$. Measurements were done in triplicate (n = 3) and the EC_{50} values were calculated from the dose-response fluorescence curves.

5.2.5 Fluorescence measurement of Ca^{2+} release from intracellular stores by depolarization in the absence of extracellular Ca^{2+}

As described in the text above by chelating extracellular Ca^{2+} and initiating depolarization with a high concentration of KCl, we can evaluate whether the polycyclic compounds have the ability to modulate Ca^{2+} release through the RyR either by direct inhibition of the RyR receptor or by modulating the gating mechanism of LTCC which will also inhibit subsequent intracellular Ca^{2+} release. The ability of the polycyclic compounds to attenuate this increase in $[Ca^{2+}]_i$ can be assessed by measuring Fura-2/AM fluorescence as described in the fluorescence calcium measurement protocol. After Fura-2/AM loading, the cells were incubated for 10 min

with the compounds to be evaluated in Ca^{2+} free solution at various concentrations (0.0001 μM to 200 μM) to obtain a dose-response profile. These experiments were done in the absence of extracellular Ca^{2+}. After a 10 sec recording period the cells were depolarized by injecting the high concentration KCl (50 mM) solution and continued recording the time-dependent change in fluorescence. The increase in fluorescence indicating an increase in $[Ca^{2+}]_i$. Measurements was done in triplicate (n = 3) and the IC_{50} values were calculated from the dose-response fluorescence curves.

5.2.6 Statistical analysis

For the Ca^{2+} flux assays all experimental results are presented as the mean ± SDEV. Experiments were done in triplicate (n = 3). Analyses were performed and graphs drawn in Excel (Microsoft® Office 2003, USA). For the calculation of IC_{50} and EC_{50} values we calculated the rate of change from the fluorescence dose-response profiles for each concentration evaluated. These values were then fitted to the log concentration-response relationship curve. Sigmoidal dose-response analyses were performed and graphs were drawn in Prism 3.0 (Graph Pad, San Diego, CA); and results presented as the mean ± SDEV.

5.3 Results

5.3.1 Inhibition of thapsigargin-induced Ca^{2+} influx

To evaluate if the polycyclic compounds have any effect on intracellular Ca^{2+} receptors, we used TG to initiate an increase in $[Ca^{2+}]_i$ by inhibiting the SERCA pump. As shown in Figure 5.2 a-d, TG (1 μM) produce a sustained increase in $[Ca^{2+}]_i$, which will result in passive depletion of ER Ca^{2+}. This increase in $[Ca^{2+}]_i$ consists of both Ca^{2+} release from the ER and secondary influx of extracellular Ca^{2+} which in excitable cells such as the PC12 cells is called Ca^{2+}–induced Ca^{2+} release (CICR). Several polycyclic test compounds were pre-incubated for 10 min with increasing concentrations (0.1 μM to 100 μM) before the application of 1 μM TG in the presence of extracellular Ca^{2+}. The fluorescence intensity (ratio of 340/380 nm) was

normalized for each graph to start at 1 and plotted as a function of time (sec). The Ca^{2+} release is characterized by a transient peak (within seconds) followed by a more sustained increase in $[Ca^{2+}]_i$.

As a control, TG was evaluated alone and produced a substantial increase in fluorescence corresponding to a rapid rise in $[Ca^{2+}]_i$. Where the test compounds were pre-incubated we observed an attenuation of the Ca^{2+} release initiated by 1 μM TG, although not in the manner expected. There was a definite concentration dependent reduction of the TG-induced $[Ca^{2+}]_i$ increase, however the largest reduction in $[Ca^{2+}]_i$ was observed at 0.1 μM for each compound evaluated and the smallest attenuation of Ca^{2+} released by TG was observed at 100 μM. For nimodipine and compound (**14c**), 100 μM resulted in an elevation of $[Ca^{2+}]_i$ above the level stimulated with 1 μM TG. It would appear that the compounds evaluated have a stimulatory effect; however it should be noted that this is only observed in the presence of TG and that the compounds showed no increase in fluorescence before the addition of TG. As mentioned this stimulation also demonstrated a dose dependent increase of $[Ca^{2+}]_i$ from 0.1 μM to 100 μM, whilst still showing a reduction from the increased $[Ca^{2+}]_i$ caused by the TG control.

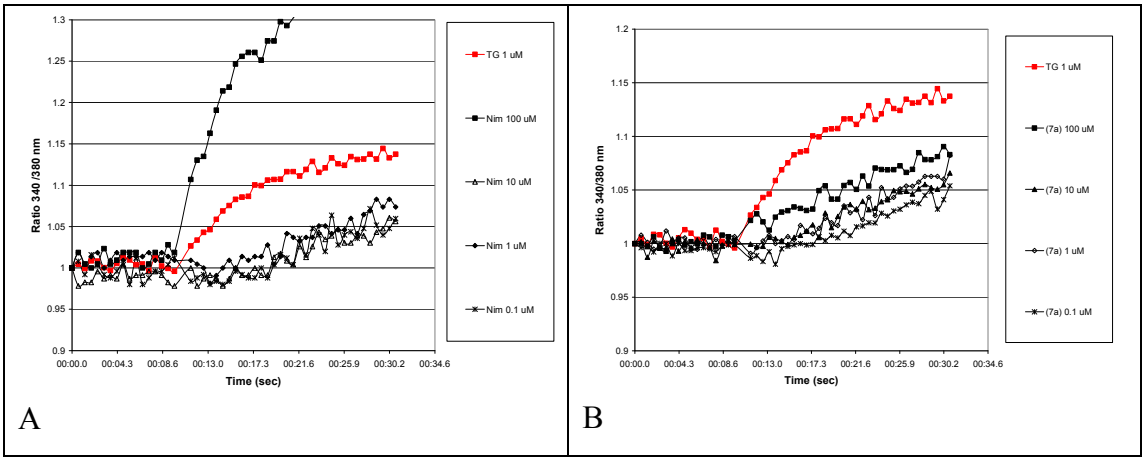

A B

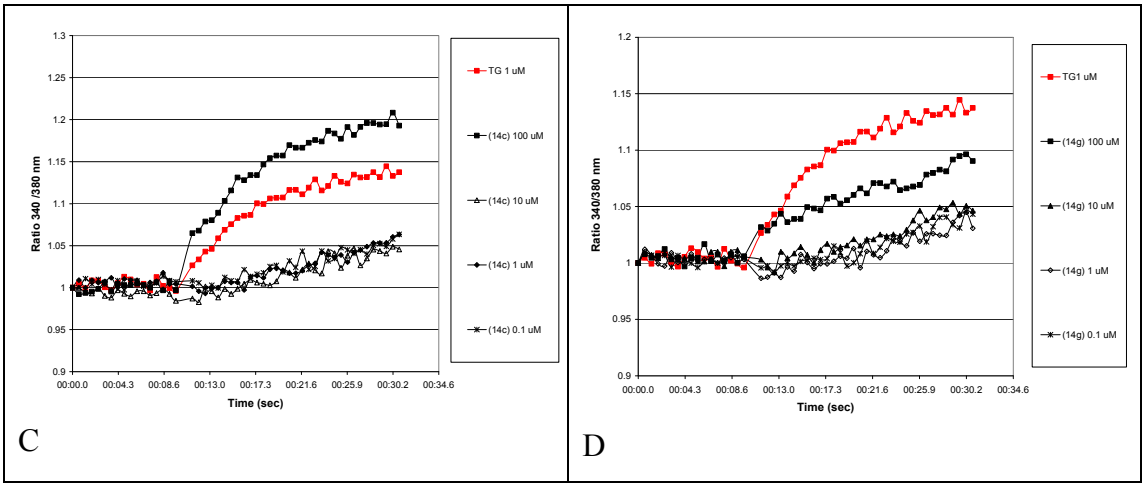

Figure 5.2. Effect of polycyclic compounds on thapsigargin-induced increase in $[Ca^{2+}]_i$. Fluorescence was read at 60 msec intervals for 34.6 sec using Fura-2/AM. The ratiometric (340/380 nm) measurement of the fluorescence intensity was normalized for each graph to start at 1 and plotted as a function of time (sec). Results are presented as the mean (n = 3) for each concentration evaluated. Graphs show an inhibition of TG stimulated maximum effect but also a concentration dependent increase of Ca^{2+} release. Fluorescence graphs are representative of: A, nimodipine; B, compound (**7a**); C, compound (**14c**) and D, compound (**14g**); which were all evaluated at concentrations ranging from 0.1 µM to 100 µM.

From the fluorescence results we calculated the response as the rate of $[Ca^{2+}]_i$ increase for each concentration evaluated and plotted a dose-response curve, from which the EC_{50} values (to evaluate the observed stimulatory effect) could be calculated. The log concentration vs. percentage of control-response graphs are presented in Figure 5.3. The rate of $[Ca^{2+}]_i$ increase, a measure of calcium influx, showed a concentration-dependent increase from 0.1 µM to 100 µM after the addition of 1 µM TG. The calculated EC_{50} values for the test compounds were as follow: compound (**7a**) EC_{50} = 44.56 µM, compound (**14c**) EC_{50} = 22.9 mM and compound (**14g**) EC_{50} = 85.18 µM.

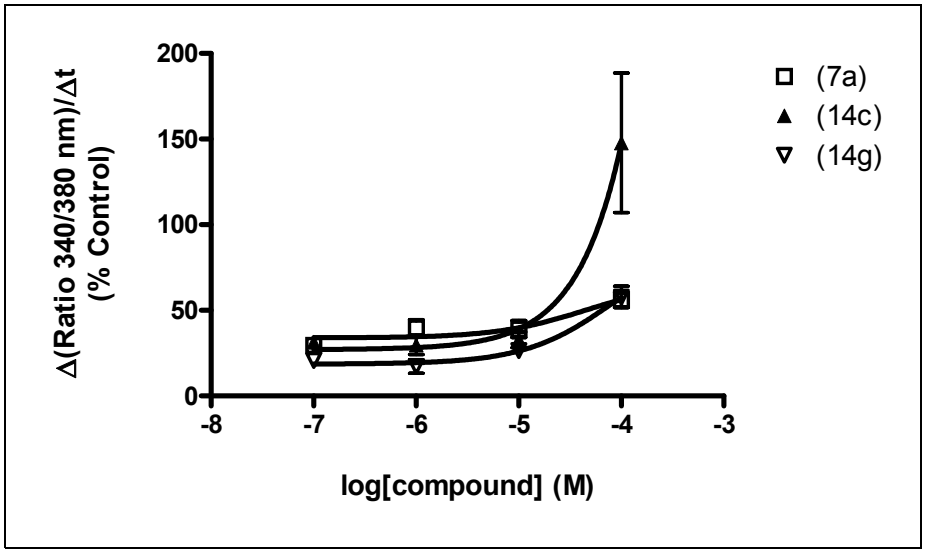

Figure 5.3. The log concentration vs. percentage of control response profile indicating the rate of change for test compounds after 1 μM TG induced increase in $[Ca^{2+}]_i$. Results are presented as the mean ± STDEV (n = 3). Where error bars are not shown, these are covered by the point itself.

5.3.2 Inhibition of KCl-induced Ca^{2+} release through RyR

To evaluate if the polycyclic compounds have the ability to modulate Ca^{2+} flux through the RyR after depolarization, we chelated extracellular Ca^{2+}. RyR will still be activated in the absence of Ca^{2+} influx from the extracellular environment due to allosteric interaction between the LTCC and RyR.[181, 182] Several polycyclic test compounds were pre-incubated for 10 min with increasing concentrations (0.0001 μM to 200 μM) in the absence of extracellular Ca^{2+} before depolarization with 50 mM KCl. We also evaluated nimodipine, a known LTCC blocker for comparison. KCl produce a sustained increase in $[Ca^{2+}]_i$, which in the absence of extracellular Ca^{2+} could be the result of Ca^{2+} influx from the ER through the RyR. The fluorescence intensity (ratio of 340/380 nm) was normalized for each graph to start at 1 and plotted as a function of time (sec) as shown in Figure 5.4 a, c, e and g.

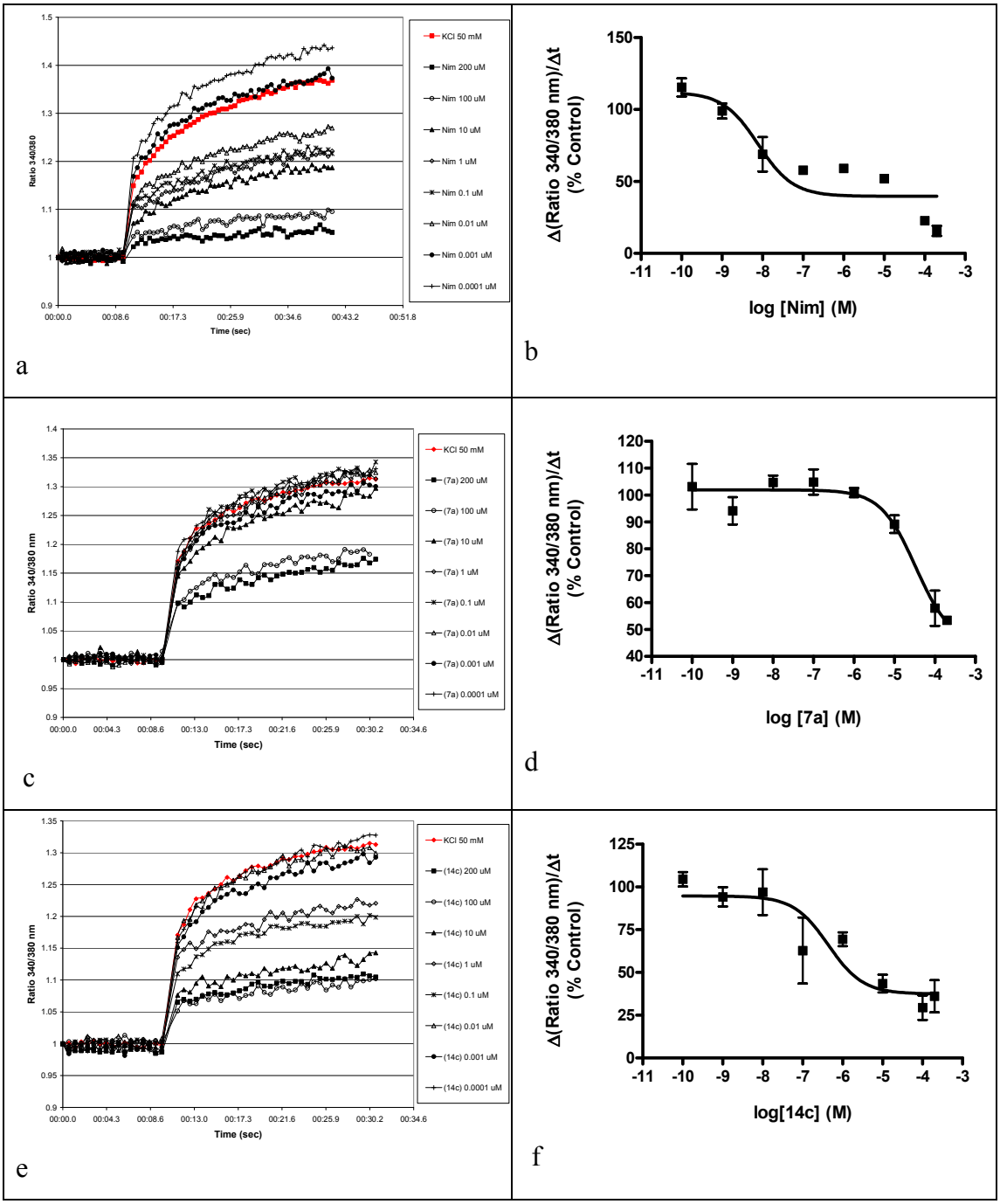
Ratio 340/380
Time (sec)
KCl 50 mM
Nim 200 uM
Nim 100 uM
Nim 10 uM
Nim 1 uM
Nim 0.1 uM
Nim 0.01 uM
Nim 0.001 uM
Nim 0.0001 uM
a
Δ(Ratio 340/380 nm)/Δt (% Control)
log [Nim] (M)
b
Ratio 340/380 nm
Time (sec)
KCl 50 mM
(7a) 200 uM
(7a) 100 uM
(7a) 10 uM
(7a) 1 uM
(7a) 0.1 uM
(7a) 0.01 uM
(7a) 0.001 uM
(7a) 0.0001 uM
c
Δ(Ratio 340/380 nm)/Δt (% Control)
log [7a] (M)
d
Ratio 340/380 nm
Time (sec)
KCl 50 mM
(14c) 200 uM
(14c) 100 uM
(14c) 10 uM
(14c) 1 uM
(14c) 0.1 uM
(14c) 0.01 uM
(14c) 0.001 uM
(14c) 0.0001 uM
e
Δ(Ratio 340/380 nm)/Δt (% Control)
log[14c] (M)
f

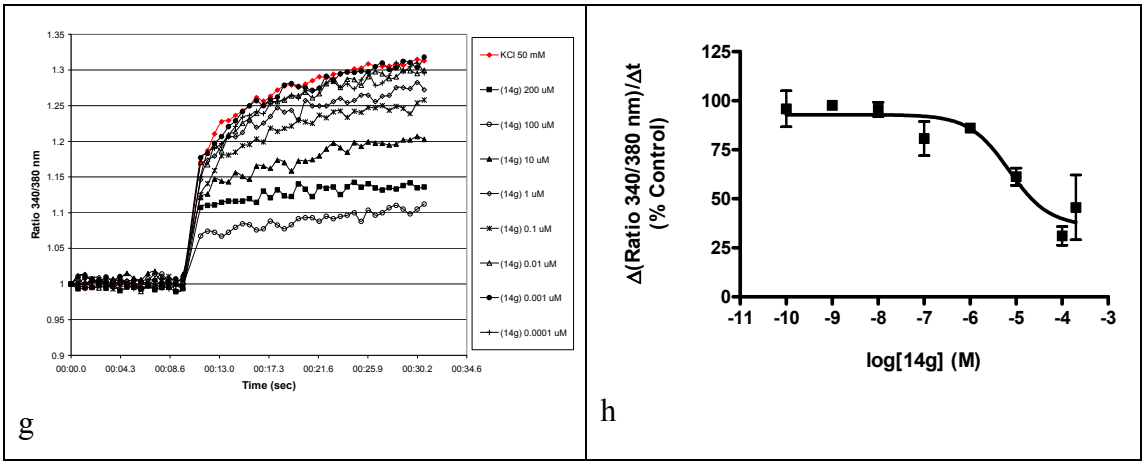

Figure 5.4. Concentration dependent inhibition of KCl-induced increase in $[Ca^{2+}]_i$. Fluorescence graphs are representative of: a, nimodipine; c, compound (**7a**); e, compound (**14c**) and g, compound (**14g**); which were all evaluated at concentrations ranging from 0.0001 μM to 200 μM in the absence of extracellular Ca^{2+}. Fluorescence was read at 60 msec intervals for 34.6 sec using Fura-2/AM. The ratiometric (340/380 nm) measurement of the fluorescence intensity was normalized for each graph to start at 1 and plotted as a function of time (sec). Results are presented as the mean (n = 3) for each concentration evaluated. The log concentration vs. percentage of control response profiles (b, d, f and h) indicating the rate of change for test compounds after depolarization induced increase in $[Ca^{2+}]_i$. Results are presented as the mean ± STDEV (n = 3). Where error bars are not shown, these are covered by the point itself.

As a control, KCl was evaluated alone and produced a substantial increase in fluorescence corresponding to a rapid rise in $[Ca^{2+}]_i$. Where the test compounds were pre-incubated we observed a dose dependent attenuation of the Ca^{2+} release after KCl-initiated depolarization. From the fluorescence results we calculated the response as the rate of $[Ca^{2+}]_i$ increase for each concentration evaluated and plotted a dose-response curve, from which the IC_{50} values could be calculated. The log concentration vs. percentage of control-response graphs are presented in Figure 5.4 b, d, f and h. The rate of $[Ca^{2+}]_i$ increase is a measure of calcium influx and showed a concentration-dependent decrease from 0.0001 μM to 100 μM after depolarization. The calculated IC_{50} values for the test compounds were as follow: nimodipine IC_{50} = 7.74 nM, compound (**7a**) IC_{50} = 433.8 μM, compound (**14c**) IC_{50} = 0.439 μM and

compound (**14g**) IC_{50} = 7.04 μM. It is interesting to note that the most potent LTCC blocker (in the presence of extracellular Ca^{2+}) in the previous study (Chapter 3), compound **14c** with an IC_{50} = 0.398 μM were also the most potent inhibitor in the present study with an IC_{50} = 0.439 μM. Also for compound **14g** did the IC_{50} = 7.04 μM fall within close proximity of that found as LTCC blocker (IC_{50} = 5 μM) in the previous study.

5.4 Discussion

5.4.1 Inhibition of thapsigargin-induced Ca^{2+} influx

To assess whether the polycyclic compounds, both pentacycloundecylamines and triquinylamines, have an effect on intracellular Ca^{2+} receptors; we induced an increase in $[Ca^{2+}]_i$ by two different mechanism utilizing both thapsigargin (TG) and potassium chloride (KCl). For $[Ca^{2+}]_i$ increase initiated with 1 μM TG we observed a dose-dependent increase from 0.1 μM to 100 μM for each of the compounds evaluated, including nimodipine. This stimulatory effect occurred in the presence of TG, but to a lesser extent than $[Ca^{2+}]_i$ increase initiated with TG. Only at 100 μM for compounds **14c** and nimodipine did the $[Ca^{2+}]_i$ increase rise above that stimulated with TG. At the same time the compounds were still able to attenuate the increase in $[Ca^{2+}]_i$ induced by TG. This again occurred in a dose dependent manner from 0.1 μM to 100 μM, with 100 μM having the least effect. Could these compound act on both the SERCA pump and IP_3R, resulting in this duel mechanistic dose-response profile?

The stimulatory effect observed for the test compounds might suggest intracellular mobilization of Ca^{2+}, in a similar manner than TG. This observation was also made by several other authors in the evaluation of the ability of 2-aminoethoxydiphenyl borate (2APB) to block agonist-induced Ca^{2+} mobilization from intracellular stores.[176, 191, 192] In the study by Maruyama *et al*., 1997; the authors suggested that the stimulative effects of 2APB at 100 μM might be due to partial inhibition of Ca^{2+}-ATPase activity, which sequestrates Ca^{2+} into endoplasmic reticulum, similar to the effects of TG. In addition to its inhibition of Ca^{2+}-ATPase activity; 2APB could inhibit Ca^{2+} release from the IP_3R by allosteric modulation of the channel formation or by causing steric

hindrance to Ca^{2+} flow.[176] These proposed mechanism could also explain the dose dependent rise in $[Ca^{2+}]_i$ we saw in our experiments for the polycyclic compounds, whilst reducing TG initiated increase $[Ca^{2+}]_i$. Another possibility would be that these compounds are antagonists on the IP_3R or RyR at lower concentrations and agonists at higher concentrations.

We should also keep in mind that the polycyclic compounds are Ca^{2+} channel blockers on both the NMDAR and LTCC,[38, 40, 42, 43, 95] therefore reducing secondary calcium influx from the extracellular environment. Thus if we are able to modulate Ca^{2+} influx from both the extracellular environment and intracellular Ca^{2+} store, it gives us an greater ability to offer protection against excitotoxicity induced by intracellular Ca^{2+} overload. Preliminary evidence of this concept was seen in cell viability assay performed in a previous study (Chapter 3). We evaluated the ability of several polycyclic compounds to offer protection against induced cell death in LDH and trypan blue staining assays. Interestingly compound **14c**, which was also evaluated in this assay, showed toxicity at 100 μM. At that point we attributed the observed toxicity to the compound being a high-affinity LTCC blocker which might cause $[Ca^{2+}]_i$ depletion. However, results from the present study that show compound **14c** at 100 μM increasing $[Ca^{2+}]_i$ to a level above that of TG suggest that this could be the reason for the observed toxicity in the previous study. The fact that **14c** was still able to offer some protection in the cell viability assays could also affirm the suggestion that this compound is only a partial inhibitor of Ca^{2+}-ATPase activity, increasing the $[Ca^{2+}]_i$ to a lesser extent. In the cell viability assays NGP1-01 (**7a**) had the most favorable pharmacological profile and like wise in the present study we see no excessive increase in $[Ca^{2+}]_i$ at 100 μM, suggesting no toxicity for this compound.

5.4.2 Inhibition of KCl-induced Ca^{2+} release through RyR

For $[Ca^{2+}]_i$ increase initiated by depolarization with 50 mM KCl, in the absence of extracellular Ca^{2+}, we observed a much less complicated fluorescence profile. We saw a dose dependent attenuation of KCl-induce increase in $[Ca^{2+}]_i$ from 0.0001 μM to 200 μM for each of the compounds evaluated including nimodipine, with 200 μM being the most effective. Thus we can conclude that Ca^{2+} release through the RyR

contribute to a proportion of the $[Ca^{2+}]_i$ increase after depolarization and that the polycyclic compounds evaluated in this study are able to attenuate this release. The mechanism by which these compounds inhibit secondary Ca^{2+} release can however be more complicated. As shown in this study and others,[182, 183] Ca^{2+} release still occurred from the ER after depolarization in the absence of extracellular Ca^{2+}. It is often assumed that Ca^{2+}-induced Ca^{2+} release (CICR) are the sole mechanism responsible for secondary Ca^{2+} release from intracellular Ca^{2+} stores such as the ER through receptors such as the RyR.[183] However, as discussed in the introduction section, increase in the $[Ca^{2+}]_i$ after depolarization have an underlying mechanism called voltage-induced Ca^{2+} release (VICaR). The study by De Crescenzo *et al*., 2006 showed that nifedipine were able to attenuate KCl-induced Ca^{2+} release from intracellular Ca^{2+} stores, in the absence of extracellular Ca^{2+}, by modulating the gating charge of dihydropyridine receptors which are linked to RyRs. In the present study we demonstrated that the polycyclic compounds **7a**, **14c** and **14g** as well as nimodipine were also able to attenuate KCl-induced Ca^{2+} release from intracellular Ca^{2+} stores in the absence of extracellular Ca^{2+}. Since the polycyclic compounds and in particular the compounds evaluated in this study have been shown to be LTCC antagonists,[38, 40, 95] it is entirely possible that these compounds would also be able to modulate the gating charge of dihydropyridine receptors such as the LTCC. If these compounds were only physical blockers of the LTCC, they would have had no effect on Ca^{2+} release from intracellular Ca^{2+} stores in the absence of extracellular Ca^{2+}. This could be one mechanism by which these compounds are able to regulate Ca^{2+} flux through the RyR, however we cannot rule out direct interaction or allosteric modulation with the RyR itself. To investigate this possibility in future studies, we would have to directly initiate Ca^{2+} release through the RyR with either caffeine or ryanodine (agonists), and evaluate whether the polycyclic compounds have the ability to attenuate this agonist-initiated Ca^{2+} release.

5.5 Conclusion

The $[Ca^{2+}]_i$ can be regulated by a number of mechanisms, for example: Ca^{2+} entry from the extracellular environment through either the NMDAR or VGCCs such as the LTCC; or by Ca^{2+} uptake into intracellular Ca^{2+} stores such as the ER through the

SERCA pump.[177, 178] Ca^{2+} release from the ER occurs through the IP_3Rs or RyRs.[56, 57, 179] A rise in $[Ca^{2+}]_i$ can also result from Ca^{2+}-induced Ca^{2+} release (CICR) *via* the IP_3Rs and RyRs.[58-60] However, an underlying mechanism for CICR can been seen in the absence of extracellular Ca^{2+} that has been designated as voltage-induced Ca^{2+} release (VICaR), and will initiated Ca^{2+} release through the RyR upon depolarization.

In this study we were able to show that the polycyclic compounds, both the pentacycloundecylamines and triquinylamines, have the ability to modulate Ca^{2+} flux through intracellular Ca^{2+} channels, although not in the manner expected. These compounds showed a dual mechanistic response profile after TG-induced Ca^{2+} release, where they exhibited a dose dependent increase in $[Ca^{2+}]_i$ from 0.1 μM to 100 μM, whilst in the presence of TG and to a lesser extent than stimulated with TG alone. Thus they were still able to reduce the effect TG-induced Ca^{2+} release. We propose that the stimulative effect, especially at higher concentrations, might be due to partial inhibition of Ca^{2+}-ATPase activity, which is responsible for Ca^{2+} uptake into the ER, in a similar manner than TG. In addition to the compounds ability to inhibit Ca^{2+}-ATPase activity; they could possibly also inhibit Ca^{2+} release from the IP_3R, thus explaining the reduction of TG-induced Ca^{2+} release.

In addition to these compounds' ability to modulate Ca^{2+} flux into and from intracellular stores in the presence of extracellular Ca^{2+}, these compounds also displayed the ability to inhibit Ca^{2+} release from intracellular stores in the absence of extracellular Ca^{2+}. As mentioned, depolarization can activate the RyR receptors even in the absence of extracellular Ca^{2+}.[182] This indicates that these compounds are possibly inhibiting Ca^{2+} release from the ER through the RyR by modulating the gating charge of dihydropyridine receptors which are allosterically linked to RyRs. Compounds **7a**, **14c** and **14g** were able to attenuate KCl-induced Ca^{2+} release (in the absence of extracellular Ca^{2+}) in a dose dependent manner from 0.0001 μM to 200 μM. In this study we found that compound **14c** was the most active compound with an IC_{50} = 0.398 μM just as it was the most active compound (IC_{50} = 0.439 μM) in the previous study (Chapter 3), where we evaluated inhibition of KCl-induced Ca^{2+} release in the presence of extracellular Ca^{2+}. This could possibly be additional confirmation that in both studies this compound is acting in the same manner, which

would be by modulating the gating charge of dihydropyridine receptors. In the presence of extracellular Ca^{2+}, this would lead to inhibition of Ca^{2+} influx from the extracellular environment and in the absence of extracellular Ca^{2+}, the effect would be visible in the underlying mechanism (VICaR) of CICR as a attenuation of Ca^{2+} release throught the RyRs.

From this study we gained direct evidence that these compounds exert an effect on intracellular Ca^{2+} channels. Thus these compounds demonstrate potential as multifunctional drugs with the ability to broadly regulate calcium homeostasis through multiple pathways of Ca^{2+} entry. However the mechanisms by which they act on intracellular Ca^{2+} channels still remains unclear. This study was only preliminary to evaluate whether the polycyclic compounds have activity on intracellular Ca^{2+} channels and more will need to be done towards the elucidation of the mechanism by which they exert this effect.

CHAPTER 6

CONCLUSION

6.1 Introduction

Perturbation of Ca^{2+} homeostasis and subsequent Ca^{2+} overload have been implicated in both chronic and acute neurodegenerative disorders.[2-5] Disregulation of Ca^{2+} homeostasis initiates downstream Ca^{2+}-dependent events that lead to apoptotic and/or necrotic cell death.[83] The intracellular Ca^{2+} concentration ($[Ca^{2+}]_i$) can be regulated by a number of mechanisms, for example Ca^{2+} influx from the extracellular environment predominantly through the N-methyl-D-aspartate receptor (NMDAR) or voltage gated Ca^{2+} channels (VGCCs) such as the L-type Ca^{2+} channel (LTCC).[8, 83] To maintain homeostasis Ca^{2+} uptake into intracellular Ca^{2+} stores such as the endoplasmic reticulum (ER) occur through the sarco-endoplasmic reticulum Ca^{2+}-ATPase (SERCA) pump.[177, 178] Ca^{2+} release from the ER occurs through the inositol-1,4,5-triphosphate receptors (IP_3Rs) or ryanodine receptors (RyRs) *via* IP_3-induced or Ca^{2+}-induced mechanisms.[56, 57, 179] Increased $[Ca^{2+}]_i$ will also sensitize IP_3Rs to IP_3 and activate Ca^{2+}-induced Ca^{2+} release (CICR).[58-60] Ca^{2+} release *via* the RyRs is mainly triggered by CICR. There is also an underlying mechanism to CICR which can be seen in the absence of extracellular Ca^{2+}. This has been designated as voltage-induced Ca^{2+} release (VICaR), and will initiated Ca^{2+} release through the RyR upon depolarization. Mitigation of Ca^{2+} overload through these Ca^{2+} channels offers an opportunity for pharmacological interventions that may protect against neuronal death.

Considering that LTCC blockers such as nimodipine are of limited value in a clinical setting due to cardiological effects and that high-affinity NMDAR channel blockers such as MK-801 induce psychotomimetic and neurotoxic effects;[20, 32] it might be of greater value to have a low-affinity multimechanistic drug with the ability to modulate Ca^{2+} flux through several pathways. NGP1-01 (**7a**), a polycyclic amine initially

characterized as an LTCC blocker;[38-41] also have activity as a potent uncompetitive NMDAR channel blocker.[42, 43] This compound was identified as a lead in studies that investigated the ability of both the pentacycloundecylamines and triquinylamines to modulate Ca^{2+} influx through either the NMDA receptor or the LTCC.[39-43] Although much is known about pentacycloundecylamines such as **7a**, the IC_{50} values for LTCC blocking activity has not yet been determined for a series of derivatives. We have also not explored other pathways through which these compounds might be able to modulate Ca^{2+} flux.

In the present study we evaluated the ability of a series of polycyclic compounds, both pentacycloundecylamines and triquinylamines, to regulate Ca^{2+} influx through the LTCC and for the first time calculated their IC_{50} values. We utilized cell viability assays such as the LDH-assay, MTT-assay, Trypan blue staining assay and the Annexin V-FITC staining assay to evaluate the ability of these compounds to offer protection against induced cell death and assess whether these compounds have any inherent toxicity. Base on the observed potentiating effect at lower concentrations (0.0001 μM to 1 μM) for the compounds evaluated as LTCC blockers, we investigated the possibility that the polycyclic compounds might have the ability to modulate Ca^{2+} flux through intracellular Ca^{2+} channels. To this purpose we initiated an increase in $[Ca^{2+}]_i$ by two different mechanism utilizing both thapsigargin (TG) and postasium chloride (KCl).

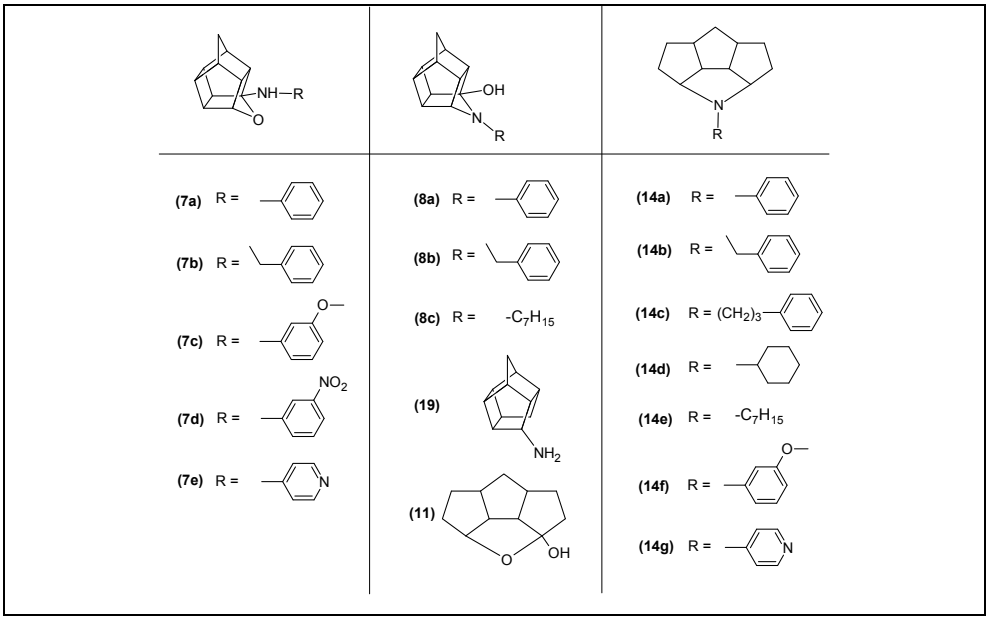

Figure 6.1. Polycyclic compounds evaluated in this study.

6.2 LTCC blockers and anti-apoptotic agents

The series of compounds presented in this study and characterized as LTCC blockers with the ability to offer protection against H_2O_2-induced cell death is part of an ongoing study into the polycyclic compounds and their potential as novel multifunctional drug candidates in the treatment of neurodegenerative disease. In this study we evaluated the pentacycloundecylamines, both the aza- and oxa-brided dervatives; as well as several novel triquinylamine compounds. To gain further understanding of these compounds ability to act as LTCC blockers we determined their IC_{50} values by means of fluorescence Ca^{2+} flux experiments. All three series of compounds had the ability to modulate Ca^{2+} influx through the LTCC after depolarization with 50 mM KCl to a greater extent than the lead compound NGP1-01 (**7a**). However, **7a** had the most favourable pharmacological profile overall with an acceptable IC_{50} value of 86 μM and the ability to attenuated cell death in both the LDH and Trypan blue staining cell viability assays, exhibiting no toxicity. The aza-pentacycloundecylamines (**8a-c**) also showed promise as LTCC blockers and compound **8b** were able to offered protection in cell viability assays. We concluded that it might be worthwhile to further evaluate the aza-pentacycloundecylamines in future studies.

Results from the QSAR study showed that the predicted IC_{50} values correlated well with the experimentally calculated IC_{50} values. This consistency gives us a good indication that *in silico* predictions can be successfully utilized to develop an accurate QSAR model with marginal error. QSAR models such as this will aid us in the design of compounds with improved activity. However, it is important to note that known LTCC blockers are neither structurally nor pharmacologically homogeneous, and so these findings serve only to guide us in the design of a series of compounds. We also applied several cell viability studies to assess the ability of these compounds to offer protection against 200 μM H_2O_2 induced cell death and to assess if these compounds had any inherent toxicity. With the exception of compound **14c** (the most potent LTCC blocker in the series, IC_{50} = 0.398 μM), most compounds were able to afford protection at two or more concentrations evaluated. Compound **14c** displayed inherent toxicity at the highest concentrations evaluated and we visually confirmed that this compound induce apoptotic cell death by means of the Annexin V-FITC assay. We attributed this toxicity to intracellular Ca^{2+} depletion that might be caused by this compound. We found good correlation between the LDH assay and Trypan blue staining assay evaluated in this study and conclude that in future studies these cell viability assays might be valuable tools in screening possible drug candidates before proceeding to more complex *in vivo* studies.

6.3 X-ray crystallography analysis

We were able to obtain crystal structures for the two triquinane scaffolds (**9** and **10**) and a derivative *N*-(3-methoxybenzyl)-3,11-azatricyclo[6.3.0.$0^{2,6}$]undecane (**14f**). The data obtained from the crystallographic analysis confirmed the NMR-data based structural assignments done for these compounds in previous studies.[95, 175] Least squares overlays the two triquinane scaffolds (**9** and **10**) with the tetra- (**15**) and pentacycloundecanes (**4** and **16**) allowed valuable insight into the differences in size and geometric constrains, which are key features for LTCC activity of these compounds. We found that substitution of the bridgehead or sp_2 hybridized C atoms by sp_3 hybridized CH_2 groups in triquinane **10** caused strain release, resulting in an asymmetric compound with greater flexibility and more asymmetric molecular shape.

These features are beneficial and will allow this compound to flex and adopt a possibly more suitable conformation for a better ion-channel fit. We were also able to obtain crystal structure data for derivative (**14f**) that has shown significant activity as an LTCC blocker in this study (Chapter 3). The introduction of the aza-bridge in this compound resulted in some loss of the flexibility gained from its precursor, compound **10**. Compound **14f** had a calculated log *P* value of 3.51 ± 0.39 (ACD log *P*® software), suggesting a more lipophilic compound with a favorable, although not optimal, blood-brain barrier permeability.[156] This can be attributed to the triquinane being a lipophilic carrier (scaffold) with the ability to enhance the compound's pharmacokinetic/pharmacodynamic properties to favorable distribution in the central nervous system (CNS). This is of great benefit when designing drugs for treatment of neurodegenerative disorders. We also explored the photocyclization and cycloreversion reaction mechanisms and computational studies indicate that the cyclization of **3** to **4**, is more likely than from **9b** to **4** due to higher activation energy and more suitable phase alignment of the orbitals.

6.4 Modulators of intracellular Ca^{2+} channels

We investigated the possibility that the polycyclic compounds, both the pentacycloundecylamines and triquinylamines, might also have the ability to modulate Ca^{2+} flux throught intracellular Ca^{2+} channels in addition to their ability to modulate influx from the extracellular environment through Ca^{2+} channels such as the NMDAR and LTCC. This assumption was base on the potentiating effect observed for these compounds during the fluorescence LTCC influx study. We speculated that this could be due to Ca^{2+}-induced Ca^{2+} release (CICR), where these compounds may not have the ability at lower concentrations to block KCl-induced increases in intracellular calcium concentration ($[Ca^{2+}]_i$), which has been shown to induce Ca^{2+} release from intracellular stores.[146, 147]

After initiating an increase in $[Ca^{2+}]_i$ with an inhibitor of the sarco-endoplasmic reticulum Ca^{2+}-ATPase (SERCA) pump, thapsigargin (TG), we observed a dual mechanistic response profile with a dose dependent increase in $[Ca^{2+}]_i$ ranging from 0.1 μM to 100 μM, whilst in the presence of TG but to a lesser extent than stimulated

with TG alone. Compounds **7a**, **14c** and **14g** were still able to reduce the effect TG-induced Ca^{2+} release. We propose that that this stimulative effect could be due to partial inhibition of Ca^{2+}-ATPase activity in a similar manner than TG, resulting in increase in $[Ca^{2+}]_i$. It could also be possible that these compounds are able to inhibit Ca^{2+} release from the IP_3R, thus explaining the reduction of TG-induced Ca^{2+} release.

The polycyclic compounds also displayed the ability to inhibit KCl- induced Ca^{2+} release in the absence of extracellular Ca^{2+}, possibly by inhibiting Ca^{2+} release from the ER through the RyR by modulating the gating charge of dihydropyridine receptors which are allosterically linked to RyRs. In the absence of extracellular Ca^{2+}, compounds **7a**, **14c** and **14g** were able to attenuate KCl-induced Ca^{2+} release from the ER in a dose dependent manner from 0.0001 μM to 200 μM. We found that compound **14c** was the most active compound with an IC_{50} = 0.398 μM, which was comparable to the fluorescence Ca^{2+} influx study (IC_{50} = 0.439 μM) with KCl-induced Ca^{2+} release in the presence of extracellular Ca^{2+}. We concluded that this could possibly be additional confirmation of the mechanism by which these compounds inhibit the LTCC, which would be by modulating the gating charge of dihydropyridine receptors. The same was also found for compound **14g**, with an IC_{50} = 5 μM in the presence of extracellular Ca^{2+} and IC_{50} = 7.04 μM in the absence of extracellular Ca^{2+}.

6.5 Conclusion

The polycyclic amines, both pentacycloundecylamines and triquinylamines, evaluated in this study represent a novel series of compounds that has potential in the treatment of acute neurological disorders such as ischemia, trauma and epilepsy; and chronic neurological disorders such as Alzheimer's disease, Parkinson's disease and Huntington's disease. All of these neurodegenerative conditions share Ca^{2+} as a common key mediator in neuronal death. These compounds exhibited promising activity as LTCC blockers and we were able to determine their IC_{50} values for the first time. Based on the IC_{50} values obtained some compounds had activity comparable to that of known LTCC blockers such as nimodipine. NGP1-01 (**7a**) had and IC_{50} value of 86 μM and had the most favourable pharmacological profile overall with the ability

to attenuated cell death at all concentrations evaluated in both the LDH and trypan blue staining cell viability assays. This compound also exhibited no inherent toxicity which makes this an ideal candidate for a lead compound in further investigations of preventative therapy in neurodegenerative disorders. It is noteworthy to mention that the aza-pentacycloundecylamine series evaluated were overall the most active LTCC blockers, with some compounds evaluated in this series showing the ability to offer protection in the cell viability assays. In addition to their ability to modulate Ca^{2+} influx from the extracellular environment, these compounds also displayed the ability to modulate Ca^{2+} flux through intracellular Ca^{2+} channels. It would appear that these compounds have a multimechanistic role, with the ability to partially inhibiting Ca^{2+}-ATPase activity whilst simultaneously possibly inhibiting the IP_3R. In the absence of extracellular Ca^{2+} these compounds showed the ability in inhibit voltage-induced Ca^{2+} release (VICaR), an underlying mechanism of Ca^{2+}-induced Ca^{2+} release (CICR), possibly by modulating the gating charge of the voltage sensor being the dihydropyridine receptors. This subsequently reduced Ca^{2+} release through the RyRs which are allosterically linked.

These compounds demonstrate potential as multifunctional drugs due to their ability to broadly regulate calcium homeostasis through multiple pathways of Ca^{2+} entry and may prove to be more effective in diseases where perturbed Ca^{2+} homeostasis have devastating effects eventually leading to excitotoxicity and cell death. However, care should be taken when blocking multiple pathways responsible for regulation of Ca^{2+} homeostasis. Even though Ca^{2+} influx may result in cell death, the depletion of $[Ca^{2+}]_i$ in turn will also facilitate cell death.[149-151] Therefore, our aim with the development of multimechanistic drug is to maintain adequate $[Ca^{2+}]_i$ by regulating Ca^{2+} influx through the multiple pathways involved in excitotoxicity in a use-dependent manner taking care not to induce intracellular Ca^{2+} depletion. The polycyclic compounds have been characterized as use-dependent blockers of the both the NMDAR and LTCC,[38, 42] but the mechanisms by which they act on intracellular Ca^{2+} channels still remains unclear.

This was only a preliminary study to evaluate whether the polycyclic compounds have activity on intracellular Ca^{2+} channels and more needs to be done towards the

elucidation of the mechanism by which they exert this effect. However, we now have direct evidence that these compounds do exert an effect on intracellular Ca^{2+} channels. In future studies we need to further explore the mechanisms by which the polycyclic compounds interact with intracellular Ca^{2+} channels by examining the direct interaction with the individual Ca^{2+} channels independently. To evaluate whether these compounds have the ability to inhibit the SERCA pump, Ca^{2+} uptake can be initiated by the addition of ATP. To evaluate whether these compounds inhibit the IP_3R, Ca^{2+} release through this receptor can be initiated by the addition of inositol-1,4,5-triphosphate (IP_3) or to evaluate whether these compounds inhibit the RyR, Ca^{2+} release can be initiated by the addition of caffeine or ryanodine at low concentrations. By individually eliciting Ca^{2+} release from each of these receptors, we can get a clearer picture of which of these receptors are involved and in which manner are the polycyclic compounds able to exert their effect.

In future studies we would also like to expand the series of polycyclic compounds, both pentacycloundecylamines and triquinylamines, in search of the most pharmacologically active structure displaying no inherent toxicity. Base on the good correlation found between the experimental and predicted IC_{50} values, it would be beneficial to do an expanded QSAR study to predict structures that might have improved activity on the desired target site. Based on the IC_{50} values obtained in the current study for the aza-pentacycloundecylamines, these compounds would be the ideal candidates for such a QSAR study. The compounds that obtained the best predicted values could then be evaluated on the desired target sites.

REFERENCES

1. Khachaturian, Z. S., Calcium hypothesis of Alzheimer's disease and brain aging. *Annals of the New York Academy of Science.* **1994,** 747, (1-11).

2. Mattson, M. P., Pathways towards and away from Alzheimer's disease. *Nature.* **2004,** 430, 631-639.

3. Korotzer, A. R.; Whittemore, E. R.; Cotman, C. W., Differential regulation by beta-amyloid peptides of intracellular free Ca^{2+} concentration in cultured rat microglia. *European Journal of Pharmacology.* **1995,** 288, 125-130.

4. Wojda, U.; Salinska, E.; Kuznicki, J., Calcium ions in neuronal degeneration. *Life.* **2008,** 60, (9), 575-590.

5. Sattler, R.; Tymianski, M., Molecular mechanisms of calcium-dependent excitotoxicity. *Journal of Molecular Medicine.* **2000,** 78, 3-13.

6. Arundine, M.; Tymianski, M., Molecular mechanisms of calcium-dependent neurodegeneration in excitotoxicity. *Cell Calcium.* **2003,** 34, 325-337.

7. Tymianski, M.; Tator, C. H., Normal and abnormal calcium homeostasis in neurons: a basis for the pathophysiology of traumatic and ischemic central nervous system injury. *Neurosurgery.* **1996,** 38, 1176-1195.

8. Triggle, D. J., L-type calcium channels. *Current Pharmaceutical Design.* **2006,** 12, 443-457.

9. Pringle, A. K., In, out, shake it all about: elevation of $[Ca^{2+}]_i$ during acute cerebral ischemia. *Cell Calcium.* **2004,** 36, 235-245.

10. Choi, D. W., Calcium-mediated neurotoxicity: relationship to specific channel types and role in ischemic damage. *Trends in Neuroscience.* **1988,** 11, 465-467.

11. Choi, D. W.; Maulucci-Gedde, M.; Kriegstein, A. R., Glutamate neurotoxicity in cortical cell culture. *Journal of Neuroscience.* **1987,** 7, 357-368.

12. Choi, D. W., Ionic dependence of glutamate neurotoxicity. *Journal of Neuroscience.* **1987,** 7, 369-379.

13. Ozyurt, E.; Graham, D. I.; Woodruff, G. N.; McCulloch, J., Protective effect of the glutamate antagonist, MK-801 in focal cerebral ischemia in the cat. *Journal of cerebral blood flow and metabolism.* **1988,** 8, 138-143.

14. Choi, D. W.; Koh, J. Y.; Peters, S., Pharmacology of glutamate neurotoxicity in cortical cell culture: attenuation by NMDA antagonists. *The Journal of Neuroscience.* **1988,** 8, (1), 185-196.

15. Chen, H. S.; Lipton, S. A., The chemical biology of clinically tolerated NMDA receptor antagonists. *Journal of Neurochemistry.* **2006,** 97, (6), 1611-1626.

16. Lipton, S. A., Paradigm shift in NMDA receptor antagonist drug development: Molecular mechanism of uncompetitive inhibition by memantine in the treatment of Alzheimer's disease and other neurologic disorders. *Journal of Alzheimer's Disease.* **2004,** 6, S61-S74.

17. Parsons, C. G.; Danysz, W.; Quack, G., Memantine is a clinically well tolerated N-methyl-D-aspartate (NMDA) receptor antagonist - a review of preclinical data. *Neuropharmacology.* **1999,** 38, 735-767.

18. Reisberg, B.; Doody, R.; Stoffler, A.; Schmitt, F.; Ferris, S.; Mobius, H. J., Memantine study group. Memantine in moderate-to-severe Alzheimer's disease. *New England Journal of Medicine.* **2003,** 348, 1333-1341.

19. Catterall, W. A., Structure and function of voltage-gated ion channels. *Annual review of biochemistry.* **1995,** 64, 493-531.

20. Kobayashi, T.; Mori, Y., Ca^{2+} channel antagonists and protection from cerebral ischemia. *European Journal of Pharmacology.* **1998,** 363, 1-15.

21. Bär, P. R.; Traber, J.; Schuurman, T.; Gispen, W. H., CNS and PNS effects of nimodipine. *Journal of Neural Transmission. Supplementum.* **1990,** 31, 55-71.

22. Triggle, D. J., Calcium, calcium channels, and calcium channel antagonists. *Canadian Journal of Physiology and Pharmacology.* **1990,** 68, 1474-1481.

23. Inzitari, D.; Poggesi, A., Calcium channel blockers and stroke. *Aging Clinical and Experimental Research.* **2006,** 17, (4 Supplement), 16-30.

24. Sobrado, M.; Lopez, M. G.; Carceller, F.; Garcia, A. G.; Roda, J. M., Combined nimodipine and citicoline reduce infarct size, attenuate apoptosis and increase bcl-2 expression after focal cerebral ischemia. *Neuroscience.* **2003,** 118, 107-113.

25. Rasmussen, G.; Bergholdt, B.; Dalh, B.; Sunde, N.; Cold, G.; Voldby, B., Effect of nimodipine on cerebral blood flow and cerebrovascular reactivity after subarachnoid haemorrhage. *Acta Neurological Scandinavica.* **1999,** 99, 182-186.

26. Tomassoni, D.; Lanari, A.; Silvestrelli, G.; Traini, E.; Amenta, F., Nimodipine and its use in cerebrovascular disease: evidence from recent preclinical and controlled clinical studies. *Clinical and Experimental Hypertension.* **2008,** 30, 744-766.

27. Rod, M. R.; Auer, R. N., Combination therapy with nimodipine and dizocilpine in a rat model of transient forebrain ischemia. *Stroke.* **1992,** 23, 725-732.

28. Schurr, A., Neuroprotection against ischemic/hypoxic brain damage: blockers of ionotropic glutamate receptor and voltage sensitive calcium channels. *Current Drug Targets.* **2004,** 5, 603-618.

29. Stuiver, B. T.; Douma, B. R.; Bakker, R.; Nyakas, C.; Luiten, P. G., In vivo protection against NMDA-induced neurodegeneration by MK-801 and nimodipine: combined therapy and temporal course of protection. *Neurodegeneration.* **1996,** 5, 153-159.

30. Uematsu, D.; Araki, N.; Greenberg, J. H.; Sladky, J.; Reivich, M., Combined therapy with MK-801 and nimodipine for protection of ischemic brain damage. *Neurology.* **1991,** 41, 88-94.

31. Zhang, C.; Shen, W.; Zhang, G., *N*-Methyl-$_D$-aspartate receptor and L-type voltage-gated Ca(2+) channel antagonists suppress the release of cytochrome *c* and the expression of procaspase-3 in rat hippocampus after global brain ischemia. *Neuroscience Letters.* **2002,** 328, 265-268.

32. Hoyte, L.; Kaur, J.; Buchan, A. M., Lost in translation: taking neuroprotection from animal models to clinical trials. *Experimental Neurology.* **2004,** 188, 200-204.

33. Youdim, M. B.; Buccafusco, J. J., Multi-functional drugs for various CNS targets in the treatment of neurodegenerative disorders. *Trends Pharmacological Sciences.* **2005,** 26, (1), 27-35.

34. Van der Schyf, C. J.; Geldenhuys, W. J., Polycyclic Compounds: Ideal Drug Scaffolds for the Design of Multiple Mechanism Drugs? *Neurotherapeutics: The Journal of the American Society for Experimental NeuroTherapeutics.* **2009,** 6, 175-186.

35. Van der Schyf, C. J.; Geldenhuys, W. J.; Youdim, M. B. H., Multifunctional drugs with different CNS targets for neuropsychiatric disorders. *Journal of Neurochemistry.* **2006,** 99, (4), 1033-1048.

36. Culmsee, C.; Junker, V.; Kremers, W.; Thal, S.; Plesnila, N.; Krieglstein, J., Combination therapy in ischemic stroke: synergistic neuroprotective effects of memantine and clenbuterol. *Storke.* **2004,** 35, 1197-1202.

37. Kubinyi, H., Drug research: myths, hype and reality. *Nature Reviews. Drug Discovery.* **2003,** 2, 665-668.

38. Van der Schyf, C. J.; Squier, G. J.; Coetzee, W. A., Characterisation of NGP1-01, an aromatic polycyclic compound, as a calcium antagonist. *Pharmacological Research Communications.* **1986,** 18, 407-417.

39. Malan, S. F.; Dockendolf, G.; Van der Walt, J. J.; Van Rooyen, J. M.; Van der Schyf, C. J., Enantiomeric resolution of the calcium channel antagonist 8-benzylamino-8,11-oxapentacyclo[5.4.0.0^{2,6}.0^{3,10}.0^{5,9}]undecane (NGP1-01). *Pharmazie* **1998,** 53, 859-862.

40. Malan, S. F.; Van der Walt, J. J.; Van der Schyf, C. J., Structure-activity relationships of polycyclic aromatic amines with calcium channel blocking activity. *Archiv der Pharmazie. Pharmaceutical and Medicinal Chemistry.* **2000,** 333, 10-16.

41. Liebenberg, W.; Van der Walt, J. J.; Van der Schyf, C. J., Effects of derivatives of NGP1-01, a putative calcium channel antagonist, on electrically stimulated guinea-pig papillary muscle. *Pharmazie.* **2000,** 55, 833-836.

42. Geldenhuys, W. J.; Malan, S. F.; Bloomquist, J. R.; Van der Schyf, C. J., Structure-activity relationships of pentacycloundecylamines at the N-methyl-D-aspartate receptor. *Bioorganic and Medicinal Chemistry.* **2007,** 15, 1525-1532.

43. Kiewert, C.; Hartmann, J.; Stoll, J.; Thekkumkara, T. J.; Van der Schyf, C. J.; Klein, J., NGP1-01 is a brain-permeable dual blocker of neuronal voltage- and ligand-operated calcium channels. *Neurochemistry Research.* **2006,** 31, 395-399.

44. Mdzinarishvili, A.; Geldenhuys, W. J.; Abbruscato, T. J.; Bickel, U.; Klein, J.; Van der Schyf, C. J., NGP1-01 a lipophilic polycyclic cage amine, is neuroprotective in focal ischemia. *Neuroscience Letters.* **2005,** 383, 49-53.

45. Hao, J.; Mdzinarishvili, A.; Abbruscato, T. J.; Klein, J.; Geldenhuys, W. J.; Van der Schyf, C. J.; Bickel, U., Neuroprotection in mice by NGP1-01 after transient focal brain ischemia. *Brain Research.* **2008,** 1196, 113-120.

46. Berridge, M. J.; Bootman, M. D.; Roderick, H. L., Calcium signalling: dynamics, homeostasis and remodeling. *Nature Reviews. Molecular cell biology.* **2003,** 4, 517-529.

47. Ghosh, A.; Greenberg, M. E., Calcium signaling in neurons: molecular mechanisms and cellular consequences. *Science.* **1995,** 268, 239-247.

48. Kornhuber, J.; Weller, M., Psychotogenicity and *N*-methyl-$_D$-aspartate receptor antagonism: Implications for neuroprotective pharmacotherapy. *Biological Psychiatry.* **1997,** 41, 135-144.

49. Michaelis, E. K., Molecular biology of glutamate receptors in the central nervous system and their role in excitotoxicity, oxidative stress and aging. *Progress in Neurology.* **1998,** 54, 369-415.

50. Timin, E. N.; Berjukow, S.; Hering, S., Concepts of state-dependent pharmacology of calcium channels. In *Pharmacology of Calcium Channels.*, 1st ed.; McDonough, S. I., Ed. Kluwer Academic/Plenum Publishing: New York, 2004; Vol. 1, p 418.

51. Haeseleer, F.; Imanishi, Y.; Sokal, I.; Filipek, S.; Palczewski, K., Calcium-binding proteins: intracellular sensors from the calmodulin superfamily. *Biochemical and Biophysical Research Communications.* **2002,** 290, 615-623.

52. Thayer, S. A.; Usachev, Y. M.; Pottorf, W. J., Modulating Ca^{2+} clearance from neurons. *Frontiers in Bioscience: a journal and virtual library.* **2002,** 7, 1255-1279.

53. Kirichok, Y.; Krapivinsky, G.; Clapham, D. E., The mitochondrial calcium uniporter is a highly selective ion channel. *Nature.* **2004,** 427, 360-364.

54. Celsi, F.; Pizzo, P.; Brini, M.; Leo, S.; Fotino, C.; Pinton, P.; Rizzuto, R., Mitochondria, calcium and cell death: a deadly triad in neurodegeneration. *Biochimica et Biophysica Acta.* **2009,** 1787, (5), 335-344.

55. Giacomello, M.; Drago, I.; Pizzo, P.; Pozzan, T., Mitochondrial Ca^{2+} as a key regulator of cell life and health. *Cell Death and Differentiation.* **2007,** 14, 1267 - 1274.

56. Mattson, M. P., Apoptosis in neurodegenerative disorders. *Nature Reviews: Molecular Cell Biology.* **2000,** 1, 120-129.

57. Hajnoczky, G.; Csordas, G.; Madesh, M.; Pacher, P., Control of apoptosis by IP_3 and ryanodine receptor driven calcium signals. *Cell Calcium.* **2000,** 28, 349-363.

58. Berridge, M. J., Elementary and global aspects of calcium signalling. *Journal of Physiology.* **1997,** 499, 291-306.

59. Pozzan, T.; Rizzuto, R.; Volpe, P.; Meldolesi, J., Molecular and cellular physiology of intracellular calcium stores. *Physiological Reviews.* **1994,** 74, 595-636.

60. Marks, A. R., Intracellular calcium-release channels: regulators of cell life and death. *The American Journal of Physiology.* **1997,** 272, H597-H605.

61. Schanne, F. A. X.; Kane, A. B.; Young, E. E.; Farber, J. L., Calcium dependence of toxic cell death: a final common pathway. *Science.* **1979,** 206, 700-702.

62. Nicotera, P.; Orrenius, S., The role of calcium in apoptosis. *Cell Calcium.* **1998,** 23, 173-180.

63. Yu, S. P.; Canzoniero, L. M. T.; Choi, D. W., Ion homeostasis and apoptosis. *Current Opinion in Cell Biology.* **2001,** 13, 405-411.

64. Zipfel, G. J.; Babcock, D. J.; Lee, J.-M.; Choi, D. W., Neuronal apoptosis after CNS injury: the roles of glutamate and calcium. *Journal of Neurotrauma.* **2000,** 17, (10), 857-869.

65. Mattson, M. P., Calcium and neurodegeneration. *Aging Cell.* **2007,** 6, (3), 337-350.

66. Bano, D.; Nicotera, P., Ca^{2+} signals and neuronal death in brain ischemia. *Stroke.* **2007,** 38, 674-676.

67. Choi, D. W., Calcium: still centre-stage in hypoxic-ischemic neuronal death. *Trends in Neuroscience.* **1995,** 18, 58-60.

68. Kass, G. E.; Orrenius, S., Calcium signaling and cytotoxicity. *Environmental Health Perspectives.* **1999,** 107, 25-35.

69. Dypbukt, J. M.; Ankarcrona, M.; Burkitt, M.; Sjoholm, A.; Strom, K.; Orrenius, S.; Nicotera, P., Different prooxidant levels stimulate growth, trigger apoptosis, or produce necrosis of insulin-secreting RINm5F cells. *The Journal of Biological Chemistry.* **1994,** 269, (48), 30553-30560.

70. Ankarcrona, M.; Dypbukt, J. M.; Bonfoco, E.; Zhivotovsky, B.; Orrenius, S.; Lipton, S. A.; Nicotera, P., Glutamate-induced neuronal death: a succession of necrosis or apoptosis depending on mitochondrial function. *Neuron.* **1995,** 15, (4), 961-973.

71. Bonfoco, E.; Krainc, D.; Ankarcrona, M.; Nicotera, P.; Lipton, S. A., Apoptosis and necrosis: two distinct events induced, respectively, by mild and intense insults with N-methyl D-aspartate or nitric oxide/ superoxide in cortical cell cultures. *Proceedings of the National Academy of Sciences of the United States of America.* **1995,** 92, 7162-7166.

72. Sinder, B. J.; Gottron, F. J.; Choi, D. W., Apoptosis and necrosis in cerebrovascular disease. *Annals of the New York Academy of Science.* **1999,** 893, 243-253.

73. Gwag, B. J.; Canzoniero, L. M. T.; Sensi, S. L.; Demaro, J. A.; Koh, J. Y.; Goldberg, M. P.; Jacquin, M.; Choi, D. W., Calcium ionophores can induce either apoptosis or necrosis in cultured cortical neurons. *Neuroscience.* **1999,** 90, (4), 1339-1999.

74. Boxer, P. A.; Bigge, C. F., Mechanisms of neuronal cell injury / death and targets for drug intervention. *Drug Discovery Today.* **1997,** 2, (6), 219-228.

75. Choi, D. W., Calcium and excitotoxic neuronal injury. . *Annals of the New York Academy of science.* **1994,** 747, 162-171.

76. Vanlangenakker, N.; Vanden Berghe, T.; Krysko, D. V.; Festjens, N.; Vandenabeele, P., Molecular mechanisms and pathophysiology of necrotic cell death. *Current Molecular Medicine.* **2008,** 8, 207-220.

77. Salinska, E.; Danysz, W.; Lazarewicz, J. W., The role of excitotoxicity in neurodegeneration. *Folia Neuropathologica.* **2005,** 43, 322-339.

78. Kass, I. S.; Lipton, P., Calcium and long-term transmission damage following anoxia in dentate gyrus and CA1 regions of the rat hippocampal slice. *Jouornal of Physiology.* **1986,** 378, 313-334.

79. Stys, P. K.; Waxman, S. G.; Ransom, B. R., Na^{+}-Ca^{2+} exchanger mediates Ca^{2+} influx during anoxia in mammalian central nervous system white matter. *Annals of Neurology.* **1991,** 30, 375-380.

80. Stys, P. K.; Waxman, S. G.; Ransom, B. R., Ionic mechanisms of anoxic injury in mammalian CNS white matter: role of Na^{+} channels and Na^{+}-Ca^{2+} exchanger. *The Journal of Neuroscience.* **1992,** 12, 430-439.

81. Gunther, T. E.; Pfeiffer, D. R., Mechanisms by which mitochondria transport calcium. *American Journal of Physiology.* **1990,** 258, c755-c786.

82. Bernardi, P.; Petronilli, V., The permeability transition pore as a mitochondrial calcium release channel: a critical appraisal. *Journal of Bioenergetica and Biomembranes.* **1996,** 28, (2), 131-138.

83. Verkhratsky, A., Calcium and cell death. *Sub-cellular Biochemistry.* **2007,** 45, 465-480.

84. Choi, D. W., Glutamate neurotoxicity and disease of the nervous system. *Neuron.* **1988,** 1, 623-634.

85. Dawson, T. M.; Snyder, S. H., Gases as biological messagers: nitric oxide and carbon monoxide in the brain. *Journal of Neuroscience.* **1994,** 14, 5147-5159.

86. Gurwitz, J. H., Polypharmacy: a new paradigm for quality drug therapy in the elderly? *Archives of Internal Medicine.* **2004,** 164, 1957-1959.

87. Kemp, J. A.; McKernan, R. M., NMDA receptor pathways as drug targets. *Nature Neuroscience. Supplement.* **2002,** 5, 1039-1042.

88. Kirby, J.; Green, C.; Loveman, E.; Clegg, A.; Picot, J.; Takeda, A.; Payne, E., A systematic review of the clinical and cost-effectiveness of memantine in patients with moderately severe to severe Alzheimer's disease. *Drugs Aging.* **2006,** 23, 227-240.

89. Horn, J.; De Haan, R. J.; Vermeulen, M.; Luiten, P. G.; Limburg, M., Nimodipine in animal model experiments of focal cerebral ischemia: a systematic review. *Stroke.* **2001,** 32, 2433-2438.

90. Frandsen, A.; Schousboe, A., Dantrolene prevents glutamate cytotoxicity and Ca^{2+} release from intracellular stores in cultured cerebral cortical neurons. *Journal of Neurochemistry.* **1991,** 56, 1075-1078.

91. Li, Y.-H.; Gong, P.-L., Neuroprotective effect of dauricine in cortical neuron culture exposed to hypoxia and hypoglycemia: involvement of correcting perturbed calcium homeostasis. *Canadian Journal of Physiology and Pharmacology.* **2007,** 85, 621-627.

92. Suen, K.-C.; Lin, K.-F.; Elyaman, W.; So, K.-F.; Chang, R. C.-C.; Hugon, J., Reduction of calcium release from the endoplasmic reticulum could only provide partial neuroprotection against beta-amyloid peptide toxicity. *Journal of Neurochemistry.* **2003,** 87, 1413-1426.

93. Mattson, M. P.; LaFerla, F. M.; Chan, S. L.; Leissring, M. A.; Shepel, P. N.; Geiger, J. D., Calcium signaling in the ER: its role in neuronal plasticity and neurodegenerative disorders. *Trends in Neurosciences.* **2000,** 23, 222-229.

94. Malan, S. F.; Van der Heever, I.; Van der Schyf, C. J., Screening of polycyclic amines for calcium channel antagonism. *Journal of Pharmaceutical Medicine.* **1996,** 6, 125-135.

95. Liebenberg, W.; Van Rooyen, P. H.; Van der Schyf, C. J., The biological activity of two symmetric amine derivatives of the cis-syn-cis triquinane system. *Pharmazie.* **1996,** 51, 20-24.

96. Cooksen, R. C.; Grundwell, E.; Hudec, J., Synthesis of cage-like molecules by irradiation of Diels-Alders adducts. *Chemistry and Industry.* **1958**, 1004-1003.

97. Geldenhuys, W. J.; Malan, S. F.; Murugesan, T.; Van der Schyf, C. J.; Bloomquist, J. R., Synthesis and biological evaluation of pentacyclo[5.4.0.$0^{2,6}$.$0^{3,10}$.$0^{5,9}$]undecane derivatives as potential therapeutic agents in Parkinson's disease. *Bioorganic and Medicinal Chemistry.* **2004,** 12, 1799-1806.

98. Mehta, G.; Srikrishna, A.; Reddy, A. V.; Nair, M. S., A novel, versatile synthetic approuch to linearly fused tricyclopentanoids *via* photo-thermal olefin metathesis. *Tetrahedron.* **1981,** 37, 4543-4559.

99. Bezuidenhout, L. M. Triquinylamines as regulators of calcium homeostasis of neuronal cells. North West University, Potchefstroom. (Thesis). 2007, 154p.

100. Brown, R. F. C., *Pyrolytic methods in organic chemistry: Application of flow and flash vacuum pyrolytic techniques.* Academic Press: New York, 1980; Vol. 41, p 347.

101. Dingemans, M. M. L.; Heusinkveld, H. L.; De Groot, A.; Bergman, A.; Van den Berg, M.; Westerink, R. H. S., Hexabromocyclododecane inhibits depolarization-induced increases in intracellular calcium levels and neurotransmitter release in PC12 cells. *Toxicological Sciences.* **2009,** 107, (2), 490-497.

102. Lee, C. S.; Han, J. H.; Jang, Y. Y.; Song, J. H.; Han, E. S., Differential effect of catecholamines and MPP^+ on membrane permeability in brain mitochondria and cell viability in PC12 cells. *Neurochemistry International.* **2002,** 40, 361-369.

103. Greene, L. A.; Tischler, A. S., *PC12 pheochromocytoma cultures in neurobiological research.* Academic Press: New York, 1982; Vol. 3, p 373.

104. Zhang, Y.; Tao, J.; Huang, H.; Ding, G.; Cheng, Y.; Sun, W., Effects of celecoxib on voltage-gated calcium channel currents in rat pheochromacytoma (PC12) cells. *Pharmacological research.* **2007,** 56, (3), 267-274.

105. Dingemans, M. M.; Heusinkveld, H. J.; De Groot, A.; Bergman, A.; Van den Berg, M.; Westerink, R. H., Hexabromocyclododecane inhibits depolarization-induced increase in intracellular calcium levels and neurotransmitter release in PC12 cells. *Toxicological sciences.* **2009,** 107, (2), 490-497.

106. Usowicz, M. M.; Porzig, H.; Becker, C.; Reuter, H., Differential expression by nerve growth factor of two types of Ca^{2+} channels in rat phaeochromocytoma cell lines. *The Journal of Physiology.* **1990,** 426, 95-116.

107. Garcia-Palomero, E.; Renart, J.; Andres-Mateos, E.; Solis-Garrido, L. M.; Matute, C.; Herrero, C. J.; Garcia, A. G.; Montiel, C., Differential expression of

calcium channel subtypes in the bovine adrenal medulla. *Neuroendocrinology.* **2001,** 74, 251-261.

108. Garcia, A. G.; Garcia-De-Diego, A. M.; Gandia, L.; Borges, R.; Garcia-Sancho, J., Calcium signaling and exocytosis in adrenal chromaffin cells. *Physiological Reviews.* **2006,** 86, 1093-1131.

109. Xia, M.; Imredy, J. P.; Koblan, K. S.; Bennett, P.; Connolly, T. M., State-dependent inhibition of L-type calcium channels: cell-based assay in high-throughput format. *Analytical Biochemistry.* **2004,** 327, 74-81.

110. Grynkiewicz, G.; Poenie, M.; Tsien, R. Y., A new generation of Ca^{2+} indicators with greatly improved fluorescence properties. *The Journal of Biological Chemistry.* **1985,** 260, 3440-3450.

111. Takahashi, A.; Camacho, P.; Lechleiter, J. D.; Herman, B., Measurement of intracellular calcium. *Physiological Reviews.* **1999,** 79, (4), 1089-125.

112. Grawley, J. N.; Gerfen, C. R.; Rogawski, M. A.; Sibley, D. R.; Skolnick, P.; Wray, S. Current protocol in neuroscience. [Web] https://catalog.invitrogen.com/index.cfm?fuseaction=iProtocol.home (Date of access: 11 July 2006),

113. Simpson, A. W. M., Fluorescent measurement of $[Ca^{2+}]_c$. Basic practical considerations. In *Methods in molecular biology. Calcium signalling protocols.*, Lambert, D. G., Ed. Humana Press *Inc*.: New Jersey, 1999; Vol. 114, p 355.

114. Lobner, D., Comparison of the LDH and MTT assays for quantifying cell death: validity for neuronal apoptosis. *Journal of Neuroscience Methods.* **2000,** 96, 147-152.

115. Koh, J. Y.; Choi, D. W., Quantitative determination of glutamate mediated cortical neuronal injury in cell culture by lactate dehydrogenase efflux assay. *Journal of Neuroscience Methods.* **1987,** 20, 83-90.

116. Haslam, G.; Wyatt, D.; Kitos, P. A., Estimatimating the number of viable animal cells in multi-well cultures based on their lactate dehydrogenase activities. *Cytotechnology.* **2000,** 32, 63-75.

117. Koh, J.-Y.; Cotman, C. W., Programmed cell death: its possible role in calcium channel antagonist neurotoxicity. *Brain Research.* **1992,** 587, 233-240.

118. Legrand, C.; Bour, J. M.; Jacob, C.; Capiaumont, J.; Martial, A.; Marc, A.; Wudtke, M.; Kretzmer, G.; Demangel, C.; Duval, D.; Hache, J., Lactate dehydrogenase (LDH) activity of the number of dead cells in the medium of cultured eukaryotic cells as marker. *Journal of Biotechnology.* **1992,** 25, 231-243.

119. Berridge, M. V.; Herst, P. M.; Tan, A. S., Tetrazolium dyes as tools in cell biology: new insights into their cellular reduction. *Biotechnology Annual Reviews.* **2005,** 11, 127-152.

120. Slater, T. F.; Sawyer, B.; Struli, U., Studies on succinate-tetrazolium reductase systems III, points of coupling of four different tetrazolium salts. *Biochimica et Biophysica acta.* **1963,** 77, 383-393.

121. Hansen, M. B.; Nielson, S. E.; Berg, K., Re-examination and further development of a precise and rapid dye method for measuring cell growth/cell kill. *Journal of Immunological Methods.* **1989,** 119, 302-310.

122. Tsai, S.-J.; Yin, M.-C., Antioxidative and anti-inflammatory protection of Oleanolic acid and Ursolic acid in PC12 cells. *Journal of Food Science.* **2008,** 73, (7), 174-178.

123. Tolnai, S., A method for viable cell count. *Methods in cell science.* **1975,** 1, 37-38.

124. Bonfoco, E.; Krainc, D.; Ankarcrona, M.; Nicotera, P.; Lipton, S. A., Apoptosis and necrosis: Two distinct events induced, respectively, by mild and intense insult with *N*-methyl-D-aspartate or nitric oxide / superoxide in cortical cell

cultures. *Proceedings of the National Academy of Science of the United States of America.* **1995,** 92, 7162-7166.

125. Van Engeland, M.; Nieland, L. J. W.; Ramaekers, F. C. S.; Shutte, B.; Reurelingsperger, C. P. M., Annexin V-affinity assay: A review on an apoptosis detection system based on phosphatidylserine exposure. *Cytometry.* **1998,** 31, 1-9.

126. Fadok, V. A.; Voelker, D. R.; Campbell, P. A.; Cohen, J. J.; Bratton, D. L.; Henson, P. M., Exposure of phosphatidylserine on the surface of apoptotic lymphocytes triggers specific recognition and removal by macrophages. *Journal of Immunology.* **1992,** 148, (7), 2207-2216.

127. Bossy-Wetzel, E.; Green, D. R., Detection of apoptosis by Annexin V labeling. *Methods in Enzymology.* **2000,** 322, 15-18.

128. Witasp, E.; Gustafsson, A. C.; Cotgreave, I.; Lind, M.; Fadeel, B., Vitamin D fails to prevent serum starvation- or staurosporine-induced apoptosis in human and rat osteosarcoma-derived cell lines. *Biochemical and Biophysical research communications.* **2005,** 330, 891-897.

129. Kabir, J.; Lobo, M.; Zachary, I., Staurosporine induces endothelial cell apoptosis via focal adhesion kinase dephosphorylation and focal adhesion disassembly independent of focal adhesion kinase proteolysis. *The Biochemical Journal.* **2002,** 367, 145-155.

130. Wang, Y.; Zhang, B.; Peng, X.; Perpetua, M.; Harbrecht, B. G., Bcl-x(L) prevents staurosporine-induced hepatocyte apoptosis by restoring protein kinase B/mitogen-activated protein kinase activity and mitochondria integrity. *Journal of cellular Physiology.* **2007,** 215, (3), 676-683.

131. Malone, T. C.; Ortwine, D. F.; Johnson, G.; Probert Jr., A. W., Synthesis and biological activity of conformationally constrained 4_a-phenantreneamine antagonists. *Bioorganic and Medicinal Chemistry Letters.* **1993,** 3, 49-54.

132. Van der Walt, J. J.; Van der Schyf, C. J.; Van Rooyen, J. M.; De Jager, J.; Van Aarde, M. N., Calium current blockade in the cardiac myocytes by NGP1-01, an aromatic polycyclic amine. *South African Journal of Science.* **1988,** 84, 448-450.

133. McNab, H., Chemistry without reagents: Synthetic application of flash vacuum pyrolysis. *Aldrichimica Acta.* **2004,** 37, 19-26.

134. Crawley, J. N., Gerfen, C.R., Rogawski, M.A., Sibley, D.R., Skolnick, P. and Wray, S. Measurement of cation movement in primary cultures using fluorescent dyes. [Web] https://commerce.invitrogen.com/index.cfm?fuseaction=iProtocol. unitSectionTree&treeNodeId=9E663C86A2A3FA409F26D8F850F50254 (Date accessed 3 June 2008),

135. Stout, A. K.; Reynolds, I. J., High-affinity calcium indicators underestimate increases in intracellular calcium concentrations associated with excitotoxic glutamate stimulations. *Neuroscience.* **1999,** 89, (1), 91-100.

136. Lambert, D. G., *Calcium signaling protocols*. First edition ed.; Humana Press: Totowa, New Jersey, 1999; Vol. 114, p 359.

137. Sullivan, E.; Tucker, E. M.; Dale, I. L., Measurement of [Ca^{2+}] using the fluorometric imaging plate reader (FLIPR). In *Methods in molecular biology. Calcium signalling protocols.*, Lambert, D. G., Ed. Humana Press *Inc.*: New Jersey, 1999; Vol. 114, p 355.

138. Robb, S. J.; Robb-Gaspers, L. D.; Scaduto, R. C., Jr.; Thomas, A. P.; Connor, J. R., Influence of calcium and iron on cell death and mitochondrial function in oxidatively stressed astrocytes. *Journal of Neuroscience Research.* **1999,** 55, (6), 674-86.

139. Gleeson, M. P., Generation of a set of simple, interpretable ADMET rules of thumb. *Journal of Medicinal Chemistry.* **2008,** 51, 817-834.

140. Hong, H.; Liu, G.-Q., Protection against hydrogen peroxide-induced cytotoxicity in PC12 cells by scutellarin. *Life Sciences.* **2004,** 74, 2959-2973.

141. Bossy-Wetzel, E.; Green, D., Detection of apoptosis by Annexin V labeling. *Methods in Enzymology.* **2000,** 322, 15-18.

142. Domingo, O. C. Triquinylamines & aza-cage compounds as neuronal calcium flux modulators. North West University, Potchefstroom. (Thesis). 2008, 121p.

143. Mori, Y.; Mikala, G.; Varadi, G.; Kobayashi, T.; Koch, S.; Wakamori, M.; Schwartz, A., Molecular pharmacology of voltage-dependent calcium channels. *Japanese Journal of Pharmacology.* **1996,** 72, (2), 83-109.

144. Opie, L. H., Calcium channel antagonists, Part 1: Fundamental properties: Mechanisms, classifications, sites of action. *Cardiovascular Drugs and Therapy.* **1987,** 1, 411-430.

145. Rampe, D.; Anderson, B.; Rapien-Pryor, V.; Li, T.; Dage, R. C., Comparison of the *in vitro* and *in vivo* cardiovascular effects of two structurally distinct Ca^{2+} channel activators, Bay K8644 and FPL 64176. *The Journal of Pharmacology and Experimental Therapeutics.* **1993,** 265, (3), 1125-1130.

146. Ogden, D., Intracellular calcium release in central neurones. *Seminars in the Neurosciences.* **1996,** 8, 281-291.

147. Verkhratsky, A.; Shmigol, A., Calcium-induced Calcium-release in Neurones. *Cell Calcium.* **1996,** 19, (1), 1-14.

148. Budriesi, R.; Cosimelli, B.; Ioan, P.; Ugenti, M. P.; Carosati, E.; Frosini, M.; Fusi, F.; Spisani, R.; Saponara, S.; Cruciani, G.; Novellino, E.; Spinelli, D.; Chiarini, A., L-type calcium channel blockers: From diltiazem to 1,2,4-oxadiazol-5-ones *via* thiazinooxadiazol-3-one derivatives. *Journal of Medicinal Chemistry.* **2009,** 52, 2352-2362.

149. Koike, T.; Tanaka, S., Evidence that nerve growth factor dependence of sympathetic neurons for survival *in vitro* may be determined by levels of cytoplasmic Ca^{2+}. *Proceedings of the National Academy of Sciences of the United States of America.* **1991,** 88, 3892-3896.

150. Koike, T.; Martin, D. P.; Johnson, J., E. M., Role of Ca^{2+} channels in the ability of membrane depolarization to prevent neuronal death induced by trophic-factor deprivation: evidence that levels of internal Ca^{2+} determine nerve growth factor dependence of sympathetic ganglion cells. *Proceedings of the National Academy of Sciences of the United States of America.* **1989,** 86, 6421-6425.

151. Canzoniero, L. M. T.; Babcock, D. J.; Gottron, F. J.; Grabb, M. C.; Manzerra, P.; Snider, B. J.; Choi, D. W., Raising intracellular calcium attenuates neuronal apoptosis triggered by staurosporine or oxygen-glucose deprivation in the presence of glutamate receptor blockade. *Neurobiology of Disease.* **2004,** 15, 520-528.

152. Van der Schyf, C. J.; Mandel, S.; Geldenhuys, W. J.; Amit, T.; Avramovich, Y.; Zheng, H.; Fridkin, M.; Gal, S.; Weinreb, O.; Bar Am, O.; Sagi, Y.; Youdim, M. B., Novel Multifunctional Anti-Alzheimer Drugs with Various CNS Neurotransmitter Targets and Neuroprotective Moieties. *Current Alzheimer Research.* **2007,** 4, (5), 522-536.

153. Geldenhuys, W. J.; Terre' Blanche, G.; Van der Schyf, C. J.; Malan, S. F., Screening of novel pentacyclo-undecylamines for neuroprotective activity. *European Journal of Pharmacology.* **2003,** 458, 73-79.

154. Young, L. M.; Zeller, M.; Geldenhuys, W. J.; Malan, S. F.; Van der Schyf, C. J., Synthesis and crystal structures of the triquinane scaffold and its derivative, *N*-(3-methoxybenzyl)-3,11-azatricyclo[6.3.0.$0^{2,6}$]undecane. **In preparation**.

155. Hockerman, G. H.; Peterson, B. Z.; Johnson, B. D.; Catterall, W. A., Molecular determinants of drug binding and action on L-type calcium channels. *Annual Review of Pharmacology and Toxicology.* **1997,** 37, 361-396.

156. Zah, J.; Terre' Blanche, G.; Erasmus, E.; Malan, S. F., Physicochemical prediction of a Brain-Blood distribution profile in polycyclic amines. *Bioorganic and Medicinal Chemistry.* **2003,** 11, 3569-3579.

157. Geldenhuys, W. J.; Malan, S. F.; Bloomquist, J. R.; Marchand, A. P.; Van der Schyf, C. J., Pharmacology and structure-activity relationships of bioactive polycyclic cage compounds: A focus on pentacycloundecane derivatives. *Medical Research Reviews.* **2005,** 25, (1), 21-48.

158. Van der Schyf, C. J.; Squier, G. J.; Coetzee, W. A., Characterization of NGP 1-01, an aromatic polycyclic amine, as a calcium antagonist. *Pharmacological Research Communications.* **1986,** 18, (5), 407-17.

159. Malan, S. F.; Van der Walt, J. J.; Van der Schyf, C. J., Structure-activity relationships of polycyclic aromatic amines with calcium channel blocking activity. *Archiv der Pharmazie (Weinheim).* **2000,** 333, (1), 10-6.

160. Kiewert, C.; Hartmann, J.; Stoll, J.; Thekkumkara, T. J.; Van der Schyf, C. J.; Klein, J., NGP1-01 is a brain-permeable dual blocker of neuronal voltage- and ligand-operated calcium channels. *Neurochemistry Research.* **2006,** 31, (3), 395-9.

161. Linden, A.; Romanski, J.; Mloston, G.; Heimgartner, H., Trifluoromethyl derivatives of pentacyclo[5.4.0.$0^{2,6}$.$0^{3,10}$.$0^{5,9}$]undecane. *Acta Crystallographica.* **2005,** C61, o221-o226.

162. Mehta, G.; Reddy, D. S.; Reddy, A. V., Lewis acid catalysed [2+2] cycloreversion of cookson's cage ketones under ambient conditions: model system for light energy conversion. *Tetrahedron Letters.* **1984,** 25, (21), 2275-2278.

163. *Bruker Advanced X-ray Solutions SMART for WNT/2000 (Version 5.628), Bruker AXS Inc., Madison, Wisconsin: USA.* ***1997-2002.***

164. *Bruker Advanced X-ray Solutions SAINT (Version 6.45), Bruker AXS Inc., Madison, Wisconsin: USA.* ***1997-2003.***

165. *Bruker Advanced X-ray Solutions SADABS in SAINT (Version 6.45), Bruker AXS Inc., Madison, Wisconsin: USA.* ***1997-2003.***

166. *Bruker Advanced X-ray Solutions SHELXTL (Version 6.10), Bruker AXS Inc., Madison, Wisconsin: USA.* ***2000.***

167. Shieldrick, G. M., Supporting information. *Acta Crystallographica.* **2008,** A64, 112-122.

168. Mehta, G.; Rao, K. S., Reductive carbon-carbon cleavage in caged systems: a new general synthesis of linearly fused *cis-sys-cis* triquinanes. *Journal of Organic Chemistry.* **1985,** 50, 5537-5543.

169. Mehta, G.; Srikrishna, A., Synthesis of polyquinane natural products: An update. *Chemical Reviews.* **1997,** 97, (3), 671-720.

170. Linden, A.; Romanski, J.; Mloston, G.; Heimgartner, H., Trifluoromethyl derivatives of pentacyclo[5.4.0.0^{2,6}.0^{3,10}.0^{5,9}]undecane. *Acta Crystallographica.* **2005,** C61, o221-o226.

171. Smith, M. B.; March, J., *March's advance organic chemistry*. 5th ed.; Wiley-Interscience Publication: 2001; p 2083.

172. Mehta, G.; Reddy, A. V.; Murthy, A. N.; Reddy, D. S., A total synthesis of (±)-Δ9(12)-capnellene. *Journal of Chemical Society: Chemical Communications.* **1983,** 824.

173. Mehta, G.; Reddy, A. V., Olefin metathesis in polycyclic frames. A total synthesis of hirsutene. *Journal of the Chemical Society Chemical Communications.* **1981,** 756, 756-757.

174. Silva, M. A.; Pellegrinet, S. C.; Goodman, J. M., A DFT study on the regioselectivity of the reaction of dichloropropynylborane with isoprene. *Journal of Organic Chemistry.* **2003,** 68, (10), 4059-66.

175. Bezuidenhout, L. M. Triquinylamines as regulators of calcium homeostasis of neuronal cells. North West University, Potchefstroom. (Thesis). 2007, 154p.

176. Maruyama, T.; Kanaji, T.; Nakade, S.; Kanno, T.; Mikoshiba, K., 2APB, 2-aminoethoxydiphenyl borate, a membrane-penetrable modulator of Ins(1,4,5)P_3-induced Ca^{2+} release. *Journal of Biochemistry.* **1997,** 122, 498-505.

177. Lytton, J.; Westlin, M.; Hanley, M. R., Thapsigargin inhibits the sarcoplasmic or endoplasmic reticulum Ca-ATPase family of calcium pumps. *Journal of Biological Chemistry.* **1991,** 266, 17067-17071.

178. Thastrup, O.; Cullen, P. J.; Drobak, B. K.; Hanley, M. R.; Dawson, A. P., Thapsigargin, a tumor promoter, discharges intracellular Ca^{2+} stores by specific inhibition of the endoplasmic reticulum Ca^{2+}-ATPase. *Proceedings of the National Academy of Sciences of the United States of America.* **1990,** 87, (2466-2470).

179. Berridge, M. J., Neuronal calcium signaling. *Neuron.* **1998,** 21, 13-26.

180. Murchison, D.; Griffith, W. H., Calcium buffering systems and calcium signaling in aged rat basal forebrain neurons. *Aging Cell.* **2007,** 6, 297-305.

181. Chavis, P.; Fagni, L.; Lansman, J. B.; Bockaert, J., Functional coupling between ryanodine receptors and L-type calcium channels in neurons. *Nature.* **1996,** 382, 719-722.

182. De Crescenzo, V.; ZhuGe, R.; Velazquez-Marrero, C.; Lifshitz, L. M.; Custer, E.; Carmichael, J.; Lai, F. A.; Tuft, R. A.; Fogarty, K. E.; Lemos, J. R.; Walsh Jr., J. V., Ca^{2+} syntillas, miniature Ca^{2+} release events in terminals of hypothalamic neurons, are increased in frequency by depolarization in the absence of Ca^{2+} influx. *The Journal of Neuroscience.* **2004,** 24, 1226-1235.

183. De Crescenzo, V.; Fogarty, K. E.; ZhuGe, R.; Tuft, R. A.; Lifshitz, L. M.; Carmichael, J.; Bellvé, K. D.; Baker, S. P.; Zissimopoulos, S.; Lai, F. A.; Lemos, J. R.; Walsh Jr., J. V., Dihydropyridine receptors and type 1 ryanodine receptors

constitute the molecular machinery for voltage-induced Ca^{2+} release in nerve terminals. *The Journal of Neuroscience.* **2006,** 26, 7565-7574.

184. Katoh, H.; Schlotthauer, K.; Bers, D. M., Transmission of information from cardiac dihydropyridine receptor to ryanodine receptor: evidence from BayK8644 effects on resting Ca^{2+} sparks. *Circulation Research.* **2000,** 87, 106-111.

185. Squecco, R.; Bencini, C.; Piperio, C.; Francini, F., L-type Ca^{2+} channels and ryanodine receptor cross-talk in frog skeletal muscle. *The Journal of physiology.* **2004,** 555, 137-152.

186. Rios, E.; Brum, G., Involvement of dihydropyridine receptors in excitation-contraction coupling in skeletal muscle. *Nature.* **1987,** 325, 717-720.

187. Rios, E.; Karhanek, M.; Ma, J.; González, A., An allosteric model of the molecular interactions of excitation-contraction coupling in skeletal muscle. *The Journal of General Physiology.* **1993,** 102, 449-481.

188. Proenza, C.; O'Brien, J.; Nakai, J.; Mukherjee, S.; Allen, P. D.; Beam, K. G., Identification of a region of RyR1 that participates in allosteric coupling with the α_{1S} ($Ca_v1.1$) II - III loop. *The Journal of Biological Chemistry.* **2002,** 227, 6530-6535.

189. Putney, J. W. J., A model of receptor-regulated calcium entry. *Cell Calcium.* **1986,** 7, 1-12.

190. Putney, J. W. J., *Capacitative Calcium entry.* Landes Biomedical Publishing: Austing, Texas, 1997.

191. Giambelluca, M. S.; Gende, O. A., Selective inhibition of calcium influx by 2-aminoethoxydiphenyl borate. *European Journal of Pharmacology.* **2007,** 565, 1-6.

192. Dobrydneva, Y.; Blackmore, P., 2-Aminoethoxydiphenyl borate directly inhibits store-operated calcium entry channels in human platelets. *Molecular Pharmacology.* **2001,** 3, 541-552.

ACKNOWLEDGEMENTS

COVENANT CARE OF MY GOD

He was better to me than all my hopes;
He was better than all my fears;
He made a bridge of my broken works,
And a rainbow of my tears.

The billows that guarded my sea-girt path,
But carried my Lord on their crest;
When I dwell on the days of my wilderness march
I can lean on His love for the rest.

He emptied my hands of my treasured store,
And His covenant love revealed,
There was not a wound in my aching heart,
But the balm of His breath hath healed.

Oh, tender and true was the chastening sore,
In wisdom, that taught and tried,
Till the soul that He sought was trusting in Him,
And nothing on earth beside.

He guided by paths that I could not see,
By ways that I have not known;
The crooked was straight, and the rough was plain
As I followed the Lord alone.

I praise Him still for the pleasant palms,
And the water-springs by the way,
For the glowing pillar of flame by night,
And the sheltering cloud by day.

Never a watch on the dreariest halt,
But some promise of love endears;
I read from the past, that my future shall be
Far better than all my fears.

Like the golden pot, of the wilderness bread,
Laid up with the blossoming rod,
All safe in the ark, with the law of the Lord,
Is the, covenant care of my God."

~ Author Unknown ~

I would like to express my gratitude to the following people for their assistance and contributions:

- Prof. C.J. van der Schyf, my supervisor, for all the opportunities you have given me, your guidance and support.
- Dr. W.J. Geldenhuys, my co-supervisor, an overwhelming thank you for your generous help, sharing your expertise, support, friendship and guidance.
- Prof. S.F. Malan, my co-supervisor, for your guidance and support.
- Dr. M. Zeller for performing the X-ray analysis and Youngstown State University (USA), for allowing the use of their facilities.
- All the personnel at the College of Pharmacy and the department of Pharmaceutical Sciences at the Northeast Ohio Medical University, USA.
- The personnel at the department of Pharmaceutical Chemistry at the Northwest University, Potchefstroom, South Africa.

- Special thanks to my parents, Piet and Mercia Bezuidenhout for raising me to be a confidant young woman with lots of vigour for life, a positive spirit and a humble soul. You both have set such great examples: my dad with your practical approach to life; you can make anything work, never got discouraged and never gave up. My mom who always gave so much of herself, thank you for teaching me what it is to love and give generously.
- My sisters, Mercia and Cornia Bezuidenhout. You guys are such a joy in my live and I love you dearly.
- To my wonderful husband, Chris Young. You are such an amazing man and have taught me so much about life and love. You inspire me with your wisdom, compassion, calm and gentle nature. I have never had so much respect for a man as I have for you and I love you with all that I have.

I also want to give thanks to:

- Dr. R. Carroll for support and encouragement.
- Megan Storey-Workley for always being willing to help and share your knowledge and experience.
- Dr. J.Y-L. Chiang for allowing us the use of your equipment and laboratory.

ANNEXURE A

Abbreviations and Acronyms

Aβ	amyloid beta
AC	adenyl cyclase
ACN	acetonitrile
AD	Alzheimer's disease
AM	acetoxymethyl ester
AMPA	α-amino-3-hydroxy-5-methylisoxazole-4-propionic acid
AMPAR	α-amino-3-hydroxy-5-methylisoxazole-4-propionic acid receptor (also known as the quisqualate receptor)
ANOVA	analysis-of-variance
AP	action potential
2APB	2-aminoethoxydiphenyl borate
ATP	adenyl triphosphate
cAMP	cyclic adenosine-monophosphate
cADP-ribose	cyclic adenosine diphosphate ribose
BSA	bovine serum albumin
BTZ	bensothiazepine
Ca^{2+}	calcium
$[Ca^{2+}]_i$	intracellular calcium concentration
$[Ca^{2+}]_e$	extracellular calcium concentration
$CaSO_4$	calcium sulfate
CCE	capacitative calcium entry
$CDCl_3$	chloroform
CICR	calcium-induced calcium release
CNS	central nervous system
DCM	dichloromethane
DEPT	distorsionless enhancement by polarisation transfer
DFT	density functional theory

DPH	1,4-dihydropyridine
DSC	differential scanning calorimetry
EAA	excitatory amino acid
EC_{50}	half maximal stimulatory concentration
ER	endoplasmic reticulum
EtOH	ethanol
Et_2O	diethyl ether
EtOAc	ethyl acetate
FITC	fluorescein isothiocyanate
FVP	flash vacuum pyrolysis
GTP	guanosine triphosphate
Glu	glutamate
Gly	glycine
HBSS	Hanks balanced salt solution
HD	Huntington's disease
HOAc	acetic acid
H_2O_2	hydrogen peroxide
HS-MS	high resolution mass spectrometry
IC_{50}	half maximal inhibitory concentration
INT	iodonitrotetrazolium
IP_3	inositol-1,4,5-triphosphate
IP_3R	inositol-1,4,5-triphosphate receptor
IR	infrared spectrometry
KA	kainite
KCl	potassium chloride
$[K^+]_0$	extracellular concentration of potassium
LDH	lactate dehydrogenase
LTCC	L-type calcium channel
MCU	mitochondrial Ca^{2+}-uniporter
MeOH	methanol
$MgSO_4$	magnesium sulfate
MK-801	dizocilpine
MTT	3-(4,5-dimethylthiazol-2-yl)-2,5-diphenyltetrazolium bromide

mNCX	mitochondrial Na^+/Ca^{2+} exchanger
MP	melting point
mPTP	mitochondrial permeability transition pore
MS	mass spectrometry
NAD^+	nicotinamide adenine dinucleotide
NADH	reduced form of nicotinamide adenine dinucleotide
$NaBH_4$	sodium borohydride
$NaBH_3CN$	sodium cyanoborohydride
$NaHCO_3$	sodium bicarbonate
NCX	Na^+/Ca^{2+} exchanger
NGP1-01	8-benzylamino-8,11-oxapentacyclo[5.4.0.$0^{2,6}$.$0^{3,10}$.$0^{5,9}$]undecane
NMDA	*N*-methyl-D-aspartate
NMDAR	*N*-methyl-D-aspartate receptor
NMR	nuclear magnetic resonance
NOS	nitric oxide synthases
PAA	phenylalkylamine
PCD	programmed cell death
PC12 cells	undifferentiated rat pheochromocytoma cells
PCP	phencyclidine
PCU	pentacyclo[5.4.0.$0^{2,6}$.$0^{3,10}$.$0^{5,9}$]undecane-8,11-dione
PD	Parkinson's disease
PE	petroleum ether
PKC	protein kinase-C
PLC	phospholipase-C
PMCA	plasma membrane Ca^{2+} ATPase
ppm	parts per million
PS	phosphatidylserine
QSAR	quantitative structure-activity relationship
ROCC	receptor-operated Ca^{2+} channel
ROS	reactive oxygen species
RyR	ryanodine receptor
SAR	structure-activity relationship
SDEV	standard deviation

SEM standard error of mean

SERCA sarco-endoplasmic reticulum Ca^{2+}-ATPase pump

SiO_2 silica

SOCE store-operated calcium entry

TBI traumatic brain injury

TG thapsigargin

THF tetrahydrofuran

TMS tetramethylsilane

VGCC voltage gated calcium channels

VICaR voltage-induced Ca^{2+} release

ANNEXURE B

Supplemental Information

X-ray Crystallography Analysis Data

Table 4.1. ^{13}C-NMR data (δ, ppm) of compound **14f**

Carbon atoms	δ_C
C-15	159.38 (s)
C-13	142.99 (s)
C-17	128.75 (d)
C-18	120.92 (d)
C-14	114.05 (d)
C-16	111.93 (d)
C-3, 11	73.73 (d)
C-12	58.56 (t)
C-19	55.10 (q)
C-1, 2	54.49 (d)
C-6, 8	47.34 (d)
C-7	37.45 (t)
C-4, 10	34.51 (t)
C-5, 9	32.79 (t)

Table 4.2. Crystal data and refinement details for Tricyclo[6.3.0.0^{2,6}]undecane-4,9-diene-3,11-dione (**9**) and tricyclo[6.3.0.0^{2,6}]undecane-3,11-dione (**10**)

Compound	**9**	**10**
Chemical formula	$C_{11}H_{10}O_2$	$C_{11}H_{14}O_2$
Formula weight	174.19 g/mol	178.22 g/mol
Crystal shape, colour	Block, colorless	Block, colorless
Crystal size	0.44 × 0.39 × 0.24 mm	0.61 × 0.39 × 0.34 mm
Crystal system	Monoclinic	Monoclinic
Space group	$P2_1/n$	$P2_1/c$
Unit cell dimensions	a = 6.5876 (12) Å	a = 7.5992 (7) Å
	b = 10.4204 (19) Å	b = 10.7294 (10) Å
	c = 12.074 (2) Å	c = 10.8664 (10) Å
	α = 90º	α = 90º
	β = 95.201 (4) º	β = 93.805 (2) º
	γ = 90º	γ = 90º
Volume	825.4 (3) Å^3	884.04 (14) Å^3
Formula units (Z)	4	4
Density (D*x*, calculated)	1.402 Mg/m^3	1.339 Mg/m^3
μ (MoKα)	0.096 mm^{-1}	0.091 mm^{-1}
F (000)	368	384
Temperature	100 (2) K	100 (2) K
Theta (θ) range for data collection	2.59 – 28.25º	2.67 – 28.28º
Reflections measured	4762	7138
Unique reflections	2013	2168
R_{int}	0.0187	0.0208

Observed data ($I > 2\sigma(I)$)	1754	1949
R_1, wR_2, goodness-of-fit (S)	0.0508, 0.1215, 1.065	0.0477, 0.1229, 1.050
$R[F^2 > 2\sigma(F^2)]$	0.0451	0.0440
$(\Delta/\sigma)_{max}$	0.000	0.000
$\Delta\rho_{min}$, $\Delta\rho_{max}$	-0.212, 0.370 e Å^{-3}	-0.195, 0.416 e Å^{-3}
T_{min}	0.977	0.970
T_{max}	0.876	0.886
h	-8 → 6	-10 → 10
k	-13 → 13	-14 → 14
l	-15 → 14	-14 → 12
parameters	118	118

Table 4.3. Selected geometric parameter (Å, º) for tricyclo[6.3.0.0^{2,6}]undecane-4,9-diene-3,11-dione (**9**)

C1-O1	1.2160 (15)	C6-C7	1.5069 (16)
C1-C2	1.4748 (17)	C6-C10	1.5464 (17)
C1-C11	1.5291 (16)	C7-C8	1.3349 (17)
C2-C3	1.3348 (17)	C8-C9	1.4681 (17)
C3-C4	1.5111 (16)	C9-02	1.2213 (15)
C4-C5	1.5266 (17)	C9-C10	1.5344 (16)
C4-C11	1.5460 (16)	C10-C11	1.5758 (17)
C5-C6	1.5331 (16)		
C2-C3-C4-C11	14.53 (14)	C2-C1-C11-C4	20.67 (12)
C8-C9-C10-C6	-9.27 (12)	C10-C6-C7-C8	-9.70 (14)

Table 4.4. Selected geometric parameter (Å, º) for tricyclo[6.3.0.0^{2,6}]undecane-3,11-dione (**10**).

C1-O1	1.2143 (14)	C6-O2	1.2119 (14)
C1-C2	1.5169 (15)	C6-C7	1.5205 (16)
C1-C5	1.5260 (15)	C6-C10	1.5237 (15)
C2-C3	1.5303 (16)	C7-C8	1.5319 (16)
C3-C4	1.5380 (15)	C8-C9	1.5485 (16)
C4-C5	1.5415 (15)	C9-C10	1.5430 (15)
C4-C11	1.5544 (15)	C9-C11	1.5477 (15)
C5-C10	1.5400 (14)		
C2-C3-C4-C5	36.26 (11)	C2-C1-C5-C4	14.40 (11)
C8-C9-C10-C6	-27.43 (11)	C10-C6-C7-C8	11.80 (12)

Table 4.5. Crystal data and refinement details for *N*-(3-methoxybenzyl)-3,11-azatricyclo[6.3.0.0^{2,6}]undecane (**14f**)

Chemical formula	$C_{19}H_{25}NO$
Formula weight	283.40 g/mol
Crystal shape, colour	Block, colorless
Crystal size	0.52 × 0.49 × 0.41 mm
Crystal system	Triclinic
Space group	P-1
Unit cell dimensions	a = 7.6714 (7) Å
	b = 9.0100 (9) Å
	c = 11.2539 (11) Å
	α = 103.892 (2) º
	β = 92.749 (2) º
	γ = 97.663 (2) º

Volume	745.78 (12) $Å^3$
Formula units (Z)	2
Density (D*x*, calculated)	1.262 Mg/m^3
μ (MoKα)	0.077 mm^{-1}
F (000)	308
Temperature	100 (2) K
Theta (θ) range for data collection	1.87 – 28.28º
Reflections measured	7817
Unique reflections	3687
R_{int}	0.0181
Observed data ($I > 2\sigma(I)$)	3265
R_1, wR_2, goodness-of-fit (S)	0.0509, 0.1284, 1.052
$R[F^2 > 2\sigma(F^2)]$	0.0462
$(\Delta/\sigma)_{max}$	0.000
$\Delta\rho_{min}$, $\Delta\rho_{max}$	-0.210, 0.396 e $Å^{-3}$
T_{min}	0.969
T_{max}	0.925
h	-10 → 10
k	-12 → 12
l	-14 → 14
parameters	265

Table 4.6. Selected geometric parameter (Å, º) for *N*-(3-methoxybenzyl)-3,11-azatricyclo[6.3.0.0^{2,6}]undecane (**14f**).

N1-C3	1.4690 (14)	O1-C15	1.3711 (13)
N1-C11	1.4722 (13)	O1-C19	1.4279 (13)
N1-C12	1.4588 (13)		
C13-C12-N1-C3	92.88 (11)	C14-C15-O1-C19	178.94 (9)
N1-C12-C13-C18	44.95 (14)	C16-C15-O1-C19	-0.14 (16)
C13-C12-N1-C11	-138.38 (10)		

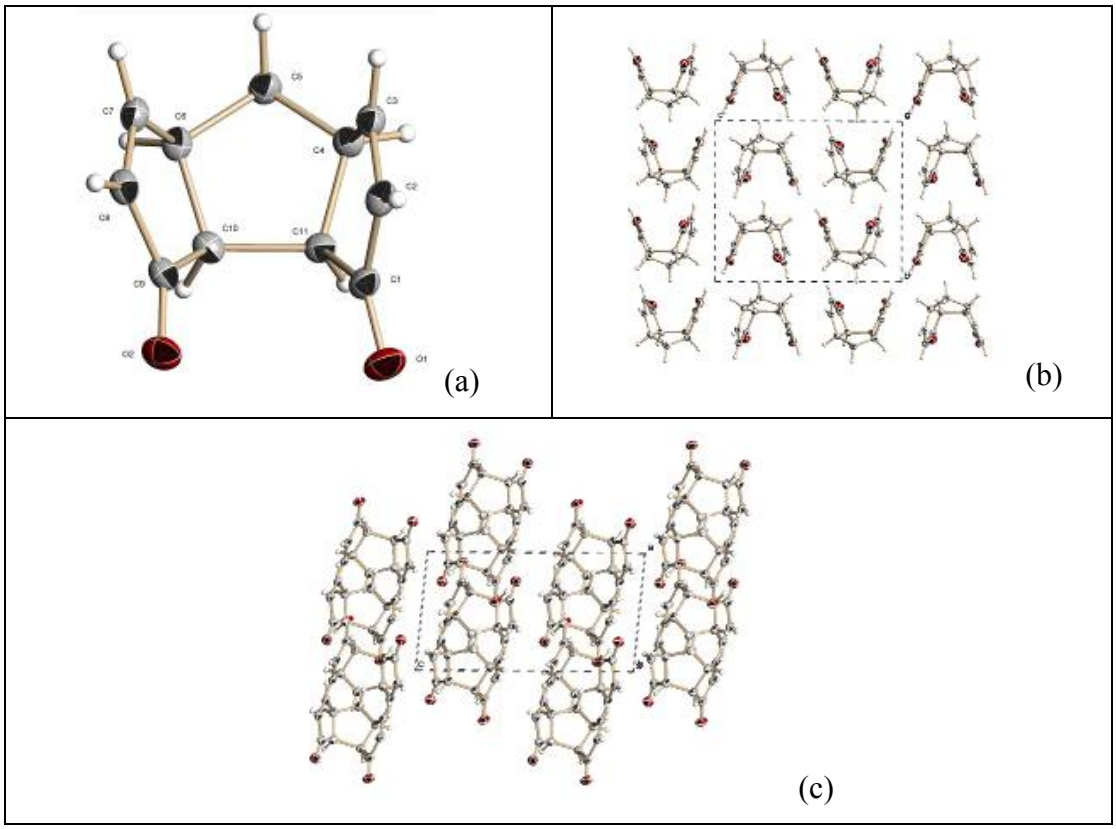

Figure 4.1. The molecular conformation (a) of tricyclo[6.3.0.0^{2,6}]undecane-4,9-diene-3,11-dione (**9**), showing the atomic numbering scheme and displacement ellipsoids at the 50% probability level as well as the crystal packing (b) and (c).

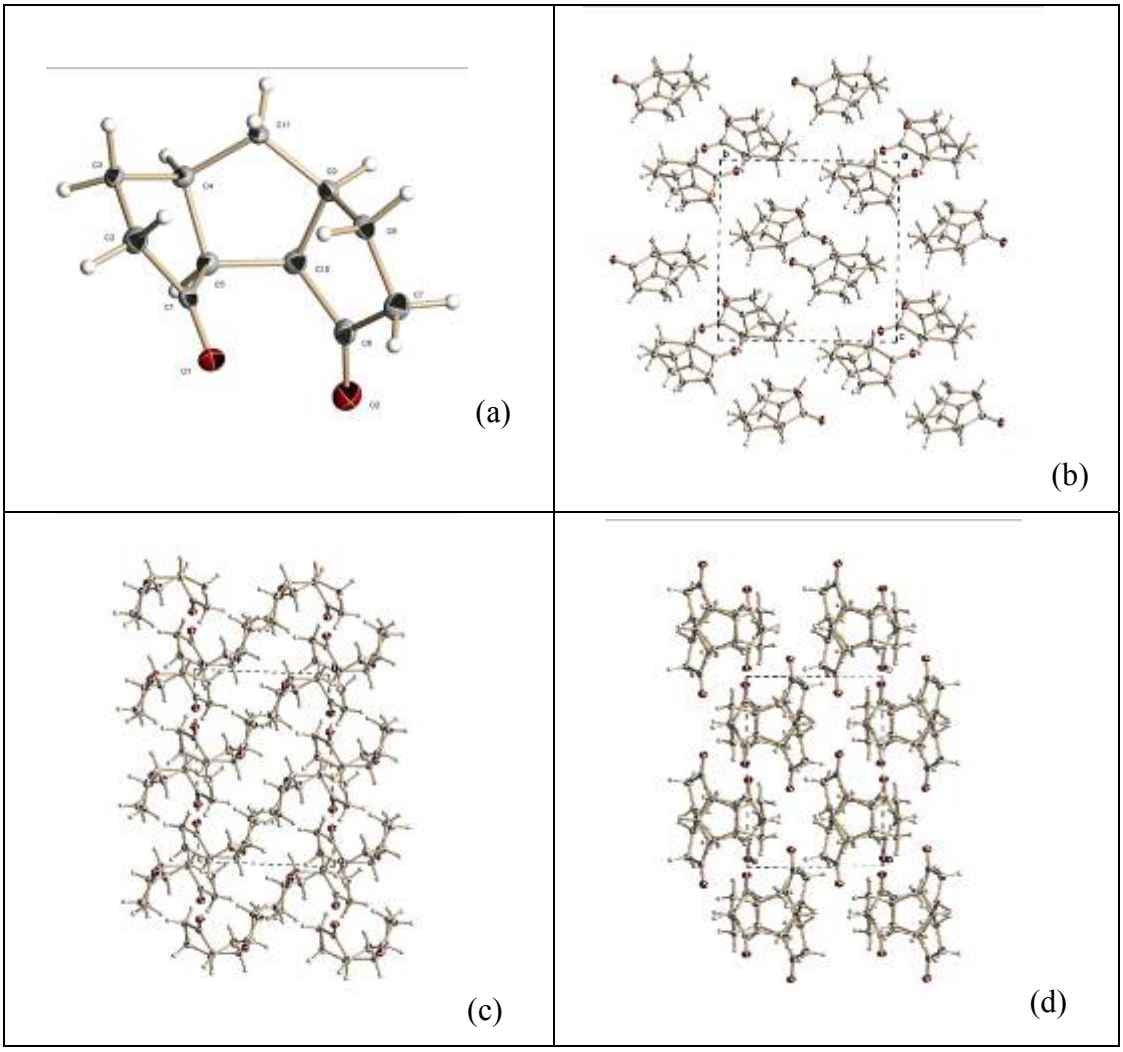

Figure 4.2. The molecular conformation (a) of tricyclo[6.3.0.0^{2,6}]undecane-3,11-dione (**10**), showing the atomic numbering scheme and displacement ellipsoids at the 50% probability level as well as the crystal packing (b), (c) and (d).